AC ARC FLASH LIGHT INTENSITY ESTIMATOR AND MHD BASED DC ARC MODEL

by

SHIUAN-HAU RAU

Presented to the Faculty of the Graduate School of

The University of Texas at Arlington in Partial Fulfillment

of the Requirements

for the Degree of

DOCTOR OF PHILOSOPHY

THE UNIVERSITY OF TEXAS AT ARLINGTON

August 2016

Acknowledgements

I would like to express sincerest gratitude to my supervising professor, Dr. Wei-Jen Lee for his patience, guidance and support throughout my entire doctoral program at University of Texas at Arlington. It is my honor to have the perfect adviser like him. He is not only an academic advisor but also a life-time mentor for me.

I would like to extend my gratitude to my doctoral dissertation committee members: Dr. William E. Dillon, Dr. Rasool Kenarangui, Dr. David A. Wetz, and Dr. Zhen Xue Han. Thanks for their valuable instructions and suggestions. Besides, I want to say great thanks to Mr. Lydon Lee helping me improve the quality of this dissertation.

Meanwhile, I would like to express my thanks for all the members of Energy Systems Research Center at University of Texas at Arlington.

Finally, I would like to dedicate my dissertation to my parents and my family. Without their enduring trust and love, this work will never have been accomplished.

.

April 11, 2016

Abstract

AC ARC FLASH LIGHT INTENSITY ESTIMATOR AND MHD BASED DC ARC MODEL

Shiuan-Hau Rau, PhD

The University of Texas at Arlington, 2016

Supervising Professor: Wei-Jen Lee

Since the light emitted by arc flash is significantly brighter than the normal lighting background, the light sensors have been applied to the arc flash detection. Currently, the optically based arc flash relaying has been considered as the fastest available protection for arc flash hazard reduction. Although it is well known that high intensity light will be emitted during arc flash event and the human delicate eye structures, such as retina or cornea, can be damaged by the sudden bright light, there are limited research providing the quantitative light intensity estimation during different arcing incidents. This dissertation proposes an arc flash visible light intensity estimation model as perceived by the human eyes based on the measured results from arc flash tests in the high power laboratories. The proposed light intensity estimation model can be used to evaluate the potential impact of an arc flash on the human eyes. In addition, the auto darkening welding lens is used in the arc flash testing to evaluate its effectiveness in attenuating the light intensity and mitigating the light hazard during arc flash event.

DC arc flash hazard assessment is a mounting concern with the growth of applications for large-scale photovoltaic arrays and DC buses. The IEEE Std. 1584-2002 pertains to arc flashes originating in only AC systems. Little research has been conducted to investigate the DC arcs. Currently, there are few methods available to model DC arcs and are largely based on theoretical or semi-empirical methods. The theoretical method,

based on the maximum power transfer theorem, overall produces the estimations on the conservative side; the semi-empirical methods are limited by the experiment scale, which cannot provide comprehensive DC arc prediction to the industry. In order to provide a suitable method to predict DC arc flash properties in power systems, new DC arc model development is necessary. This dissertation presents a magnetohydrodynamic (MHD) model of DC arcs. The MHD equations are solved by using computational fluid dynamic (CFD) software *Code Saturne*®, which is based on collocated finite volume. The simulation results are compatible with the lab testing. The proposed MHD modeling provides an innovative approach to study DC arc phenomena.

Table of Contents

List of Illustrations

List of Tables

Chapter 1

Introduction

1.1 Arc Flash Phenomenon

Electric arc is a luminous bridge formed in a gap between two electrodes, which will occur where it coexists with sufficient voltage in an electrical system and a path to ground or lower voltage. The extremely large amount of fatal energy will be expelled during an arc flash event. In an energized power system, any failures or human error can initiate an arc flash event that may injure or even kill personnel and bystanders. After the electric arc is established, the air will be ionized by the arcing current, and the massive heat will be released after the ionization process. The excessive high temperature in an arc flash event may also vaporize the vicinal metals, such as aluminum or copper conductors, the molten metals will be ejected along with the explosion. Figure 1-1 shows the three phase arc flash event in the enclosure, and the schematic diagram in the Figure 1-2 illustrates the flash behaviors.

Figure 1-1 Three Phase Arc Flash Event in the Enclosure

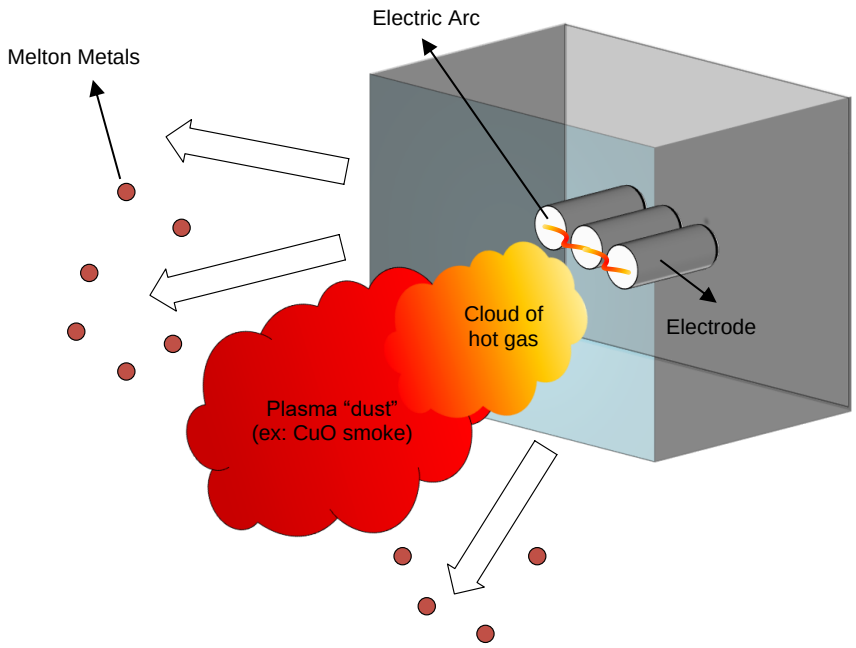

Figure 1-2 Schematic Diagram of Arc Flash Behaviors

1.2 Arc Flash Hazard

On average, 5 to 10 arc flash explosions occur on the job every day in the United States. Annually, more than 2,000 workers suffer extensive injuries caused by arc flash accidents, which can be extremely debilitating or fatal. Also, electrical accidents are the fifth-leading cause of death in the work place [1].

As shown in Figure 1-3, Census of Fatal Occupational Injuries (CFOI) indicated that there were total 5587 fatal electrical injuries happened between 1992 through 2013. The number of fatal injuries has fallen steadily along with the decreasing number of the electrical events due the increasing awareness of the electrical safety. An average 327 fatal electrical injuries happened each year from 1992 to 1996, and the average number had fallen to 161 per year from 2009 through 2013 [1]. Occupational Safety and Health Administration (OSHA) reported that there were total 110 electrical fatalities happened

during calendar year 2014 (January 1, 2014 through December 31, 2014), and 70% of the electrical fatalities were from non-electrical workers [2].

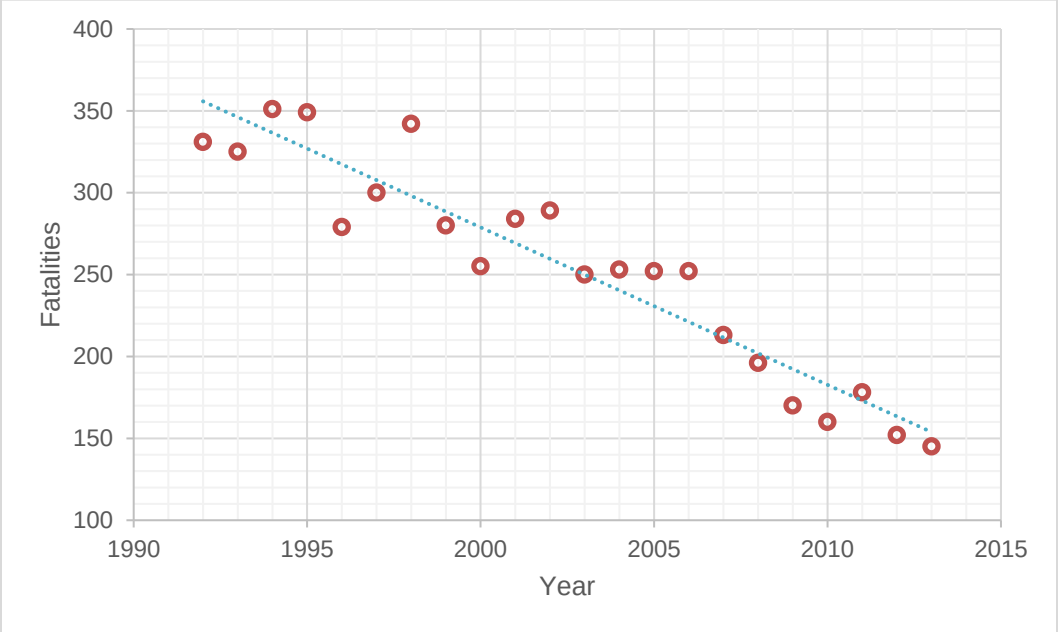

Figure 1-3 Fatal Work-Related Electrical Injuries in the United States, 1992 – 2013

An arc flash event contributes several personnel hazards due to the extremely high energy released rapidly, generally, the arc flash hazards can be categorized as follows.

1.2.1 Burn Injuries

The major arc flash hazard is burn injuries, the immense high temperature levels of gas and plasma are established during an arc flash event, which may cause burn injuries. The electrical burns have been considered as the second most costly injury, and the disability and medical costs for electric injuries may be astronomical [3-5]. The approximate direct costs range of an electrical injury are $150,000 to $370,000 a year, and the total costs may exceed $12 million for one case [6]. Although the electrical injuries only represented lower than 2% of total number of injuries in the electrical worker population, the electrical injuries contributed 26 to 52% of the total worker injury costs for the utility

involved [6]. According to the research provided by Washington State Department of Labor and Industries, there were approximate 10% severe burn injuries happened in the work place contributed by the electric arc and blast explosion [7]. Figure 1-4 shows the burn hazards caused by an arc flash event.

(a) (b)

Figure 1-4 Arc Flash Burning Hazards. (a) is on personnel (b) is on equipment [73]

1.2.2 Ejected Materials Injuries

During an arc flash event, the ejected materials, such as the metal particles, may shot to workers directly along with the explosion. The materials expelled due to the explosion produced by arc flash may produce the penetrating injuries for the weak parts of human body [8]. Figure 1-5 shows the ejection of metal particles during an arc flash test.

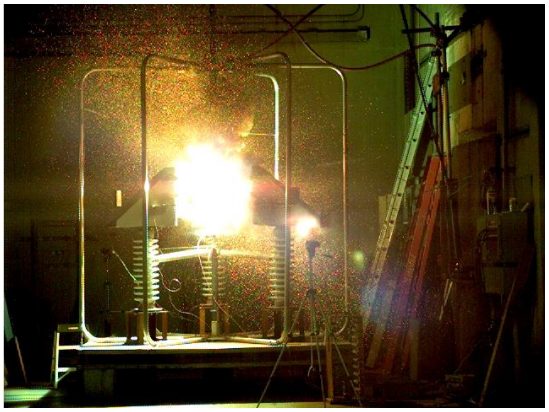

Figure 1-5 Ejection of Metal Particles in an Arc Flash Test

1.2.3 Arc Blast and Pressure Wave

An arc blast is associated with intense pressure and rapid pressure buildup, the blast pressure produced during an arc flash event may result severe hazard for a person positioning directly in front of the event, whose organs, such as lung or brain may be damaged by the high pressure impinging. Additionally, the pressure waves with propel force may knock workers off their feet or even wound human body with projectile parts [9]. Figure 1-6 illustrates the arc blast during an arc flash test.

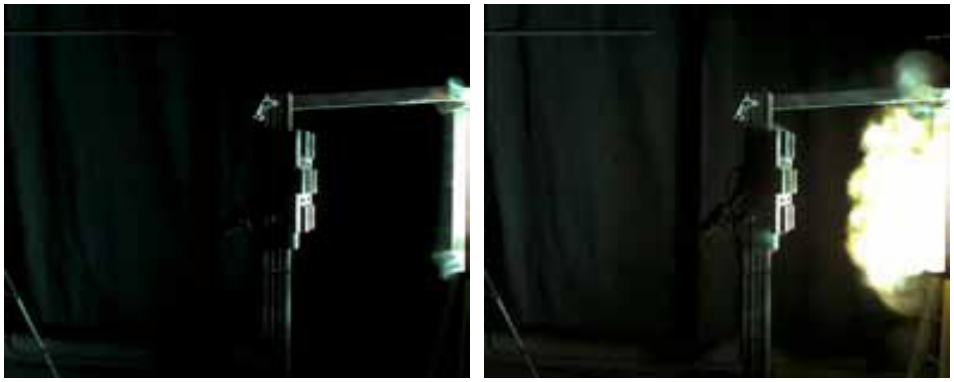

Figure 1-6 Arc Blast in an Arc Flash Test

1.2.4 Intense Light

The excessively high intensity light produced by arc flash can cause temporary or even permanent blindness and damage human delicate eye structures. Once the system voltage is greater than 200 volts, the arc flash event can cause damage to the eyes [10]. According to the record, the eye injuries represents about 4.2% of all arc flash related injuries [11-12]. The Occupational Safety and Health Administration (OSHA) reports that the workplace eye injuries cost estimated $300 million per year for medical treatment, worker compensation, and the lost productivity time [13].

1.2.5 Intense Sound

The intense sound will be produced during an arc flash event, which may contribute temporal or even permanent hearing loss. Figure 1-7 shows the average arcing current versus the peak sound pressure at 1.8m away from the measurement point [14]. Once the peak sound level exceed 140dB, the human without appropriate hearing protection may suffer traumatic damage even eardrum rupture [15].

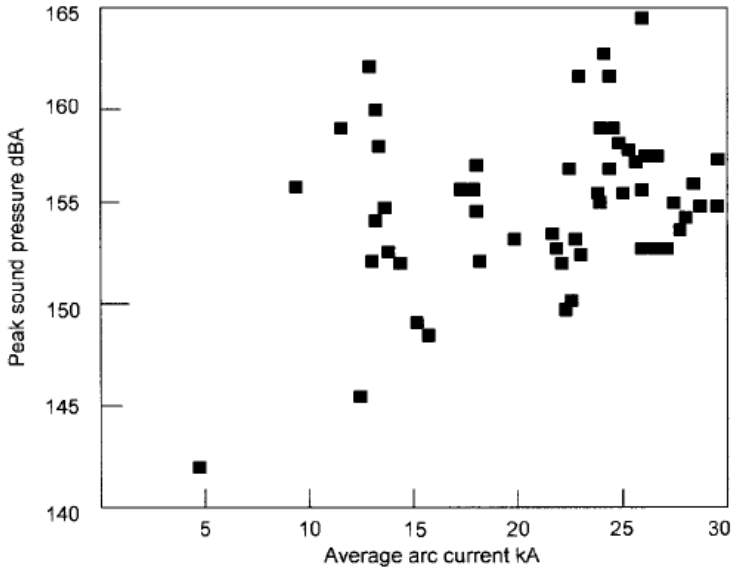

Figure 1-7 Average Arcing Current versus the Peak Sound Pressure

1.3 Research Motivation and Objective

1.3.1 Model for Light Intensity Estimation

Regarding the safety issues in the workplace, the National Fire Protection Association (NFPA) published 70E, the standard for electrical safety in the workplace [16]. NFPA 70E provides the guidance for hazard identification and risk assessments of the workplace. It reduces the exposure of the personnel to major electrical hazards with appropriate personal protective equipment (PPE).

Considering the eye protection in the latest version of NFPA 70E, employees are required to wear the proper PPE such as safety glasses or goggles while locating in the potential arc flash hazards areas. However, the eye shields or glasses can only block ultraviolet (UV) spectrums, the extremely high intensity visible light may still damage the delicate human eye structures such as cornea or retina. In order to establish the appropriate PPE for high intense light emitted in an arc flash event, the first and critical step is to estimate the light intensity of an arc flash event accurately. In order to address this issue, the first part of this dissertation is the AC arc flash light intensity estimation model, which is based upon the measurement of approximately 1500 recording data from three phase arc flash tests.

1.3.2 DC Arc model

In order to estimate potential arc flash hazards, in 2002, IEEE published the standard 1584 “IEEE Guide for Performing Arc Flash Hazard Calculations” to provide arcing current calculation and incident energy estimation based upon 300 laboratory testing data set [17]. Currently, the IEEE 1584-2002 has been considered as the predominant method in industry for performing arc flash calculation studies.

However, the empirically derived equations in IEEE 1584 can only be applied to AC power systems. With the rise of large-scale photovoltaic arrays and DC buses in power system, DC arc hazards have raised great concerns. Currently, there are only limited research addressing to DC arc models, and most of them were done in the early 1900s, which may not be suitable to predict the DC arc hazards of large-scale DC applications lately. Thus, the second and third parts of this dissertation address the DC electric arc simulation and DC arc modeling respectively to provide foundation for DC arc hazard analysis and industry standards development.

1.4 Synopsis of Chapters

The organizational structure of this dissertation is as follows:

Chapter 1 presents the arc flash phenomenon, general arc flash hazards, research motivation and objectives.

Chapter 2 introduces the model development for three phase AC arc flash light intensity estimation model, which is developed based upon the measurement results from approximately 1500 recording data from three phase arc flash tests.

Chapter 3 presents the DC electric arc simulation through magnetohydrodynamic (MHD) approach, including electric arc physics, modeling assumption, numerical models, and etc. Currently, MHD approach has been considered as one of the best approaches to simulate the electric arc burning in the open air, which makes it possible to predict the 3D and time dependent interaction between the air flow and the electric arc.

Chapter 4 discusses the DC arc model based on 3D DC arc simulation presented in Chapter 3. The new DC arc model provides foundations for future DC arc hazard analysis and industry standard development.

Chapter 2

AC Arc Flash Light Intensity Model

2.1 Literature Review

Human's delicate eye structures, such as retina and cornea can be damage if it is exposed in a high light intensity environment without wearing proper eye protective equipment. For example, the retinal damage will be produced by 6,830,000 lux for 0.1 second [18]. Arc flash produces a significantly brighter light than the normal lighting background. Generally, the intensity of normal substation lighting is around 200 to 300 lux. High intensity LED flash light can produce 28,000 lux, and a camera flash can produce 234,000 lux at 18 inches; direct sunlight at any distance is around 100,000 lux. The light emitted during arc flash event can easily reach over 1,000,000 lux depended on the fault conditions [9]. Table 2-1 provides some typical illumination levels [9].

Table 2-1 Typical Ambient Illumination Levels

Light Level	***Description***
50 lux	Living room
80 lux	Brightly lit room
500 lux	Brightly lit office
1000 lux	TV studio
100,000 lux	Direct sunlight
> 234,000 lux	Camera flash at 18 inches
> 1,000,000 lux	Arc Flash event

Figure 2-1 to Figure 2-3 show the bright light emitted for an arc flash test, where the fault conditions are 610 volts, 5.21kA, 2 inches gap, and arc duration is 12 cycle. Apparently, the extremely high intensity light, above 1 million lux, as measured at 3 meters from the arcing point was emitted during this arc flash event.

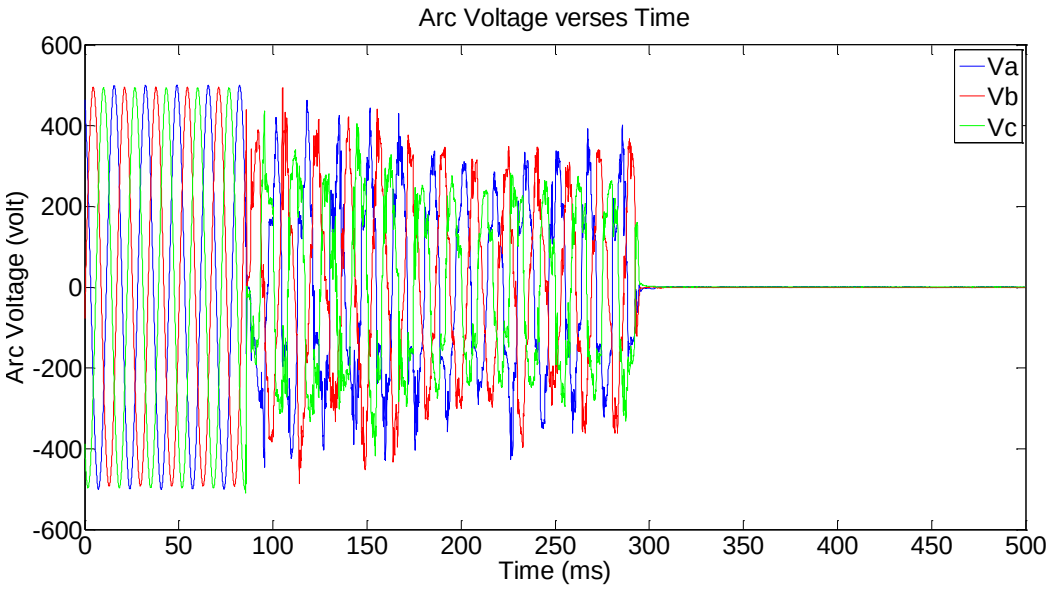

Figure 2-1 Three Phase Arc Flash Test (Voltage)

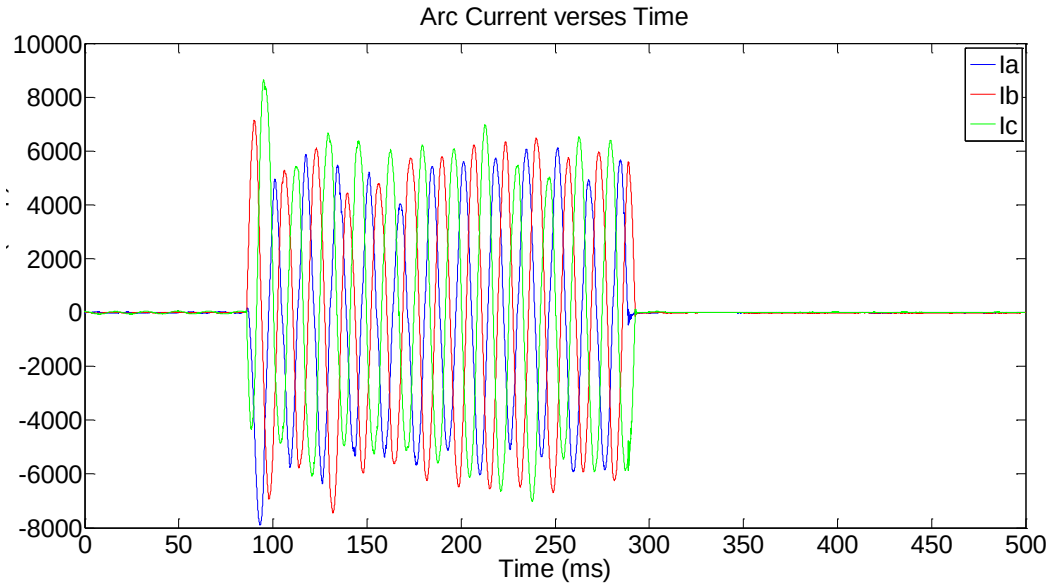

Figure 2-2 Three Phase Arc Flash Test (Current)

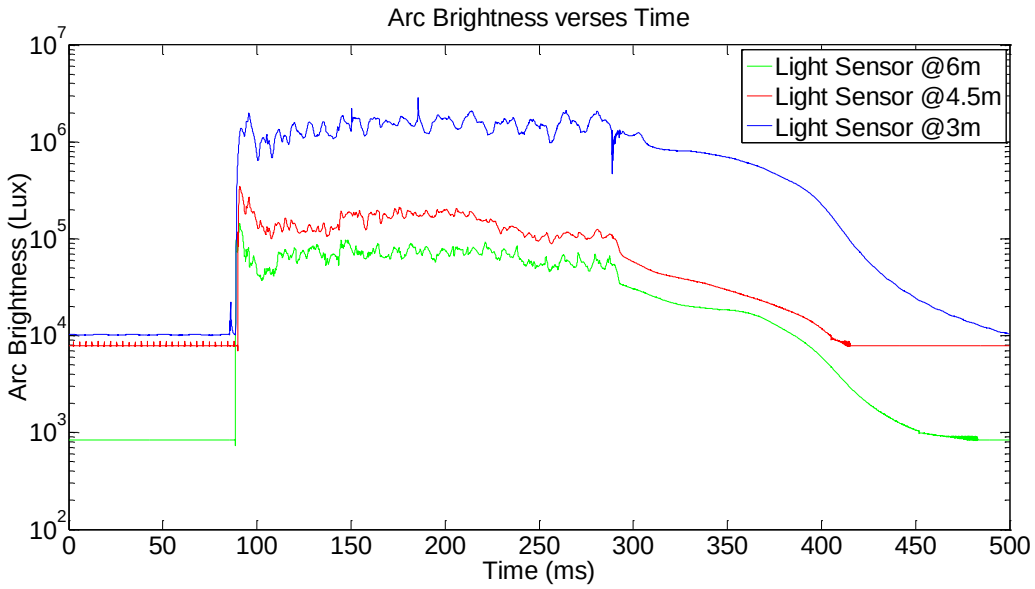

Figure 2-3 Three Phase Arc Flash Test (Light Intensity)

In order to protect people from hazards in the workplace, the OSHA and National Fire Protection Association (NFPA) require workers to wear appropriate personal protective equipment (PPE) when electrical hazards are present [16]. A UV-blocking shield, safety glasses or safety goggles are required for the eye protection. However, the eye shield or glasses can only block UV radiation, which cannot provide the protection of human eyes from the high intensity visible light emitted during arc flash event.

Accurate estimation of light intensity of arc flash is a critical milestone in establishing the PPE requirements on visible light protection. Currently, there are limited researches addressing to the light intensity during arc flash event, and the prediction of light intensity during arc flash event have not been discussed before. To fill the gap, this dissertation proposes an arc flash light intensity estimation model based on more than 1500 measurements from three phase arc flash tests. The light intensity data were recorded by the ambient light sensor that can match the spectral sensitivity response of

the human eyes. Figure 2-4 compares the traditional light sensor (Si photo sensor) and the selected ambient light sensor with the spectral sensitivity response of the human eyes [19].

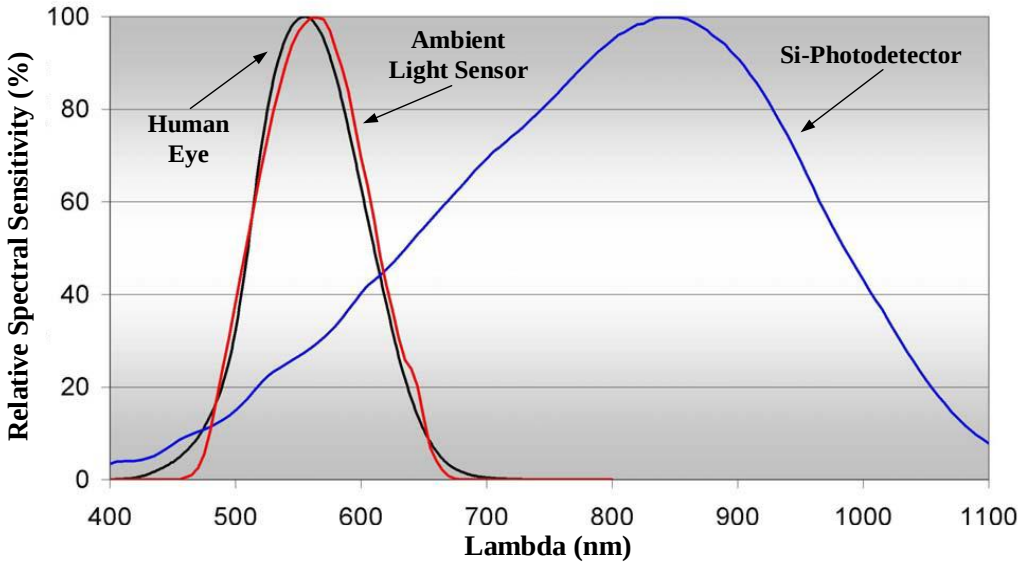

Figure 2-4 Relative Spectral Sensitivity of a Standard Si-Photodector (Blue) Ambient Light Sensor (Red) Compared to the Human Eye (Black)

2.2 Arc Flash Fault Configurations

Regarding most of arc flash occurrence situation in industry, extensive arc flash tests have been performed in five different configurations, which considers not only the electrode orientations but also the arc flash in the enclosure or in the open air. This section attempts to give an introduction of all the tests configurations, and provide some examples about the configuration determination.

2.2.1 Test Configurations

The electrodes of the examples provided in this section are formed by 0.75 inch diameter hard draw cooper, and the enclosure is 20”x20”x20” for 600V, 26”x26”x26” for 2700V, and 36”x36”x36” for 14300V three phase arc flash tests. Figure 2-5 to Figure 2-7

show the arc flash tests in the enclosure with different electrode orientations, and Figure 2-8 and Figure 2-9 present the arc flash tests in the open air with vertical and horizontal electrodes respectively. Table 2-2 provides a typical reference to determine the configurations.

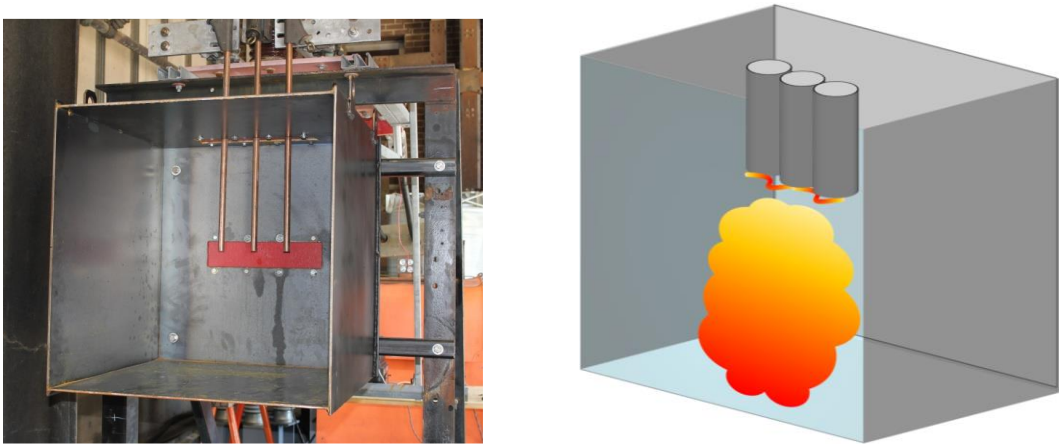

Figure 2-5 Vertical Electrodes in the Cubic Box (VCB), Electrodes are Terminated in the Middle of the Box

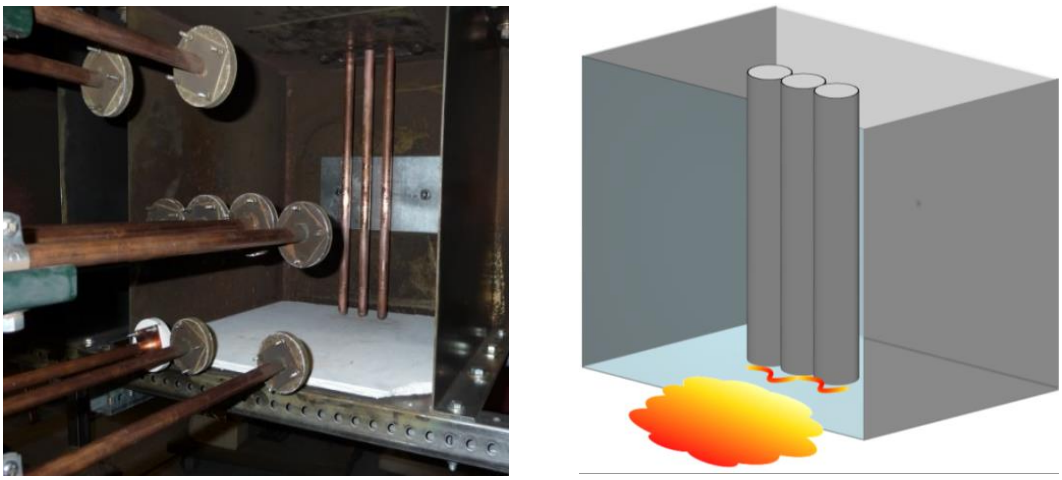

Figure 2-6 Vertical Electrodes in the Cubic Box (VCBB), Electrodes are Terminated at the Bottom of the Box

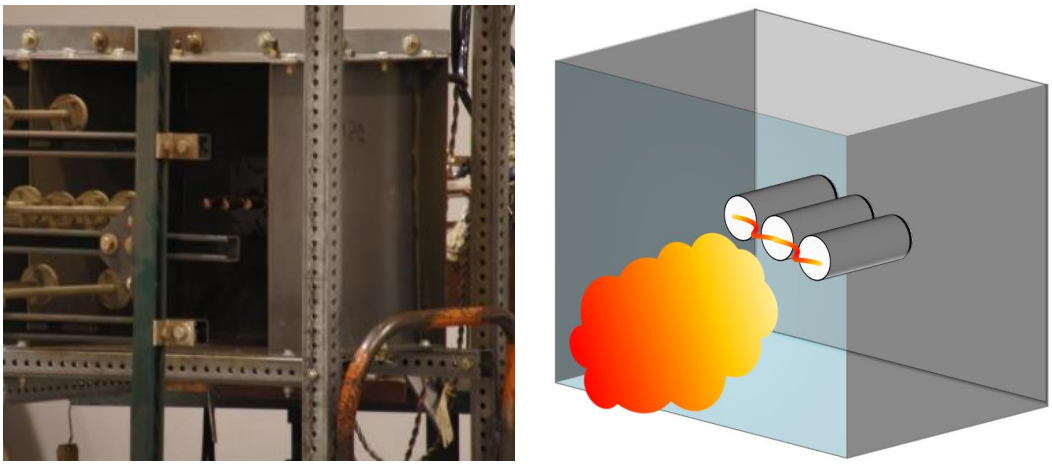

Figure 2-7 Horizontal Electrodes in the Cubic Box (HCB)

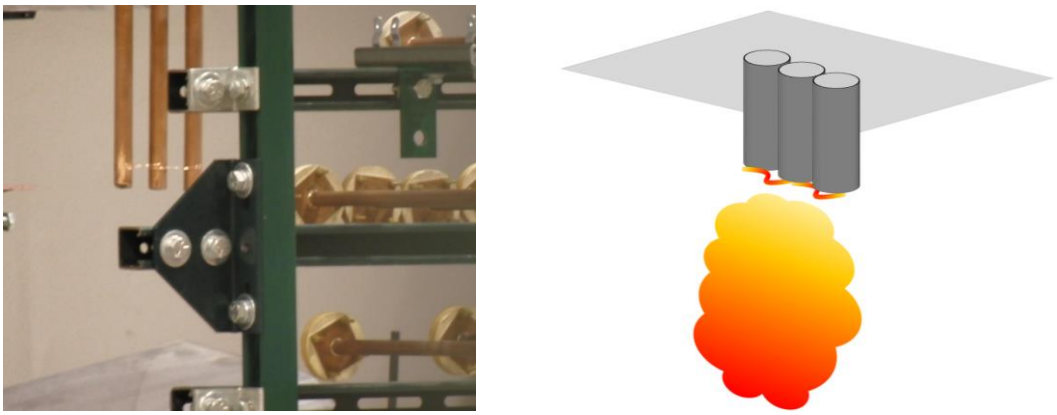

Figure 2-8 Vertical Electrodes in the Open Air (VOA)

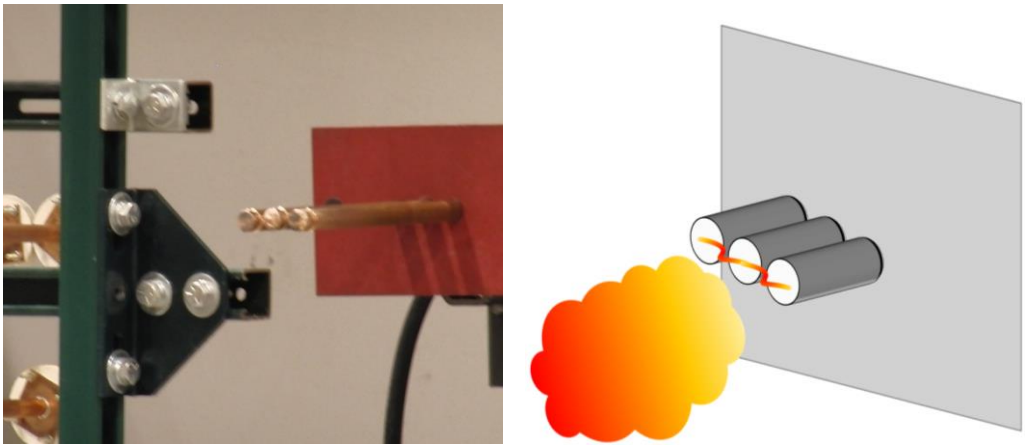

Figure 2-9 Horizontal Electrodes in the Open Air (HOA)

Table 2-2 Typical Equipment Configuration and Electrodes Orientation

Configuration	***Electrode Orientation***	***Enclosure***	***Electrode Termination***
Vertical Electrodes in the Cubic Box (VCB)	Vertical	Enclosed	None, or a top in a bus, arcing will initiated at the end of bus
Vertical Electrodes in the Cubic Box with Bottom Insulated Barrier (VCBB)	Vertical	Enclosed	Terminated in a barrier, arcing is remaining at barrier
Horizontal Electrodes in the Cubic Box (HCB)	Horizontal	Enclosed	None, conductors extend toward in front locations
Vertical Electrodes in the Open Air (VOA)	Vertical	Open air	Same as VCB
Horizontal Electrodes in the Open Air (HOA)	Horizontal	Open air	Same as HCB

2.2.2 Configuration Identification

Practically, various combination of different configurations may exist. Figure 2-10 to Figure 2-14 provide the typical equipment configuration when performing hazard analysis.

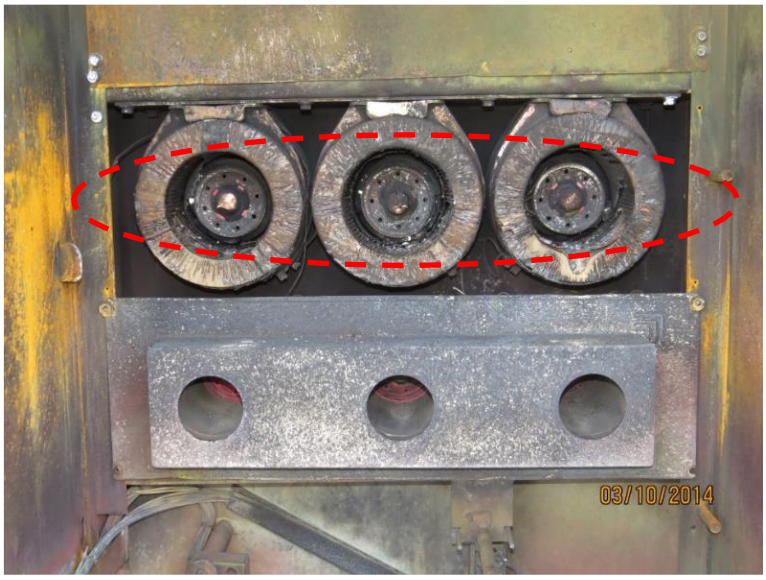

Figure 2-10 HCB/HOA Configuration on Switchgear

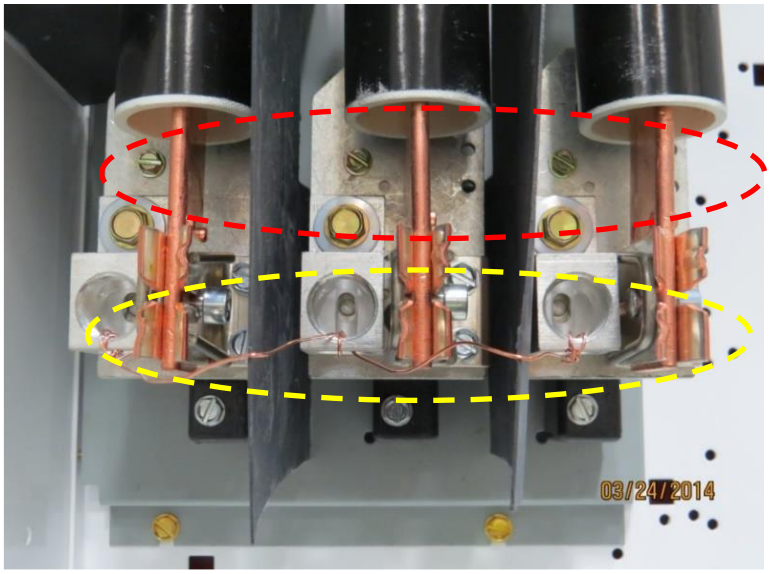

Figure 2-11 VCB (upper circle) and HCB/HOA (low circle) Configuration on Current Limit Fuse

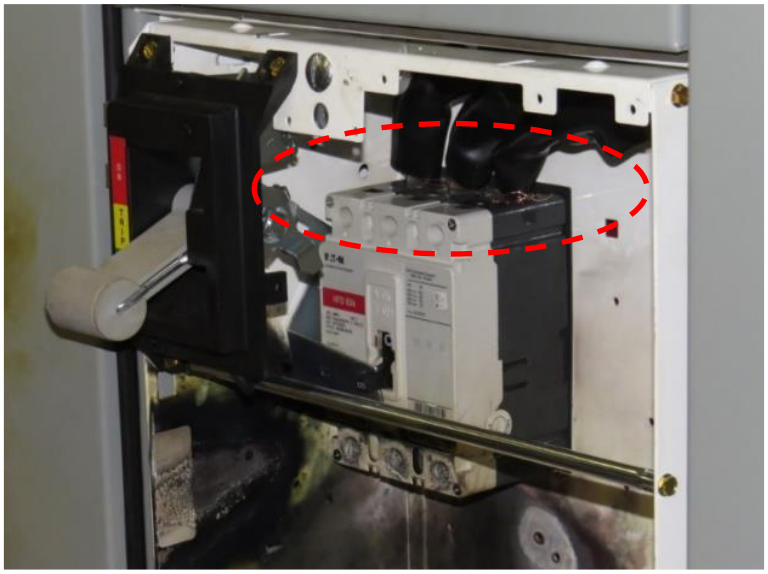

Figure 2-12 VCBB Configuration on Switchgear

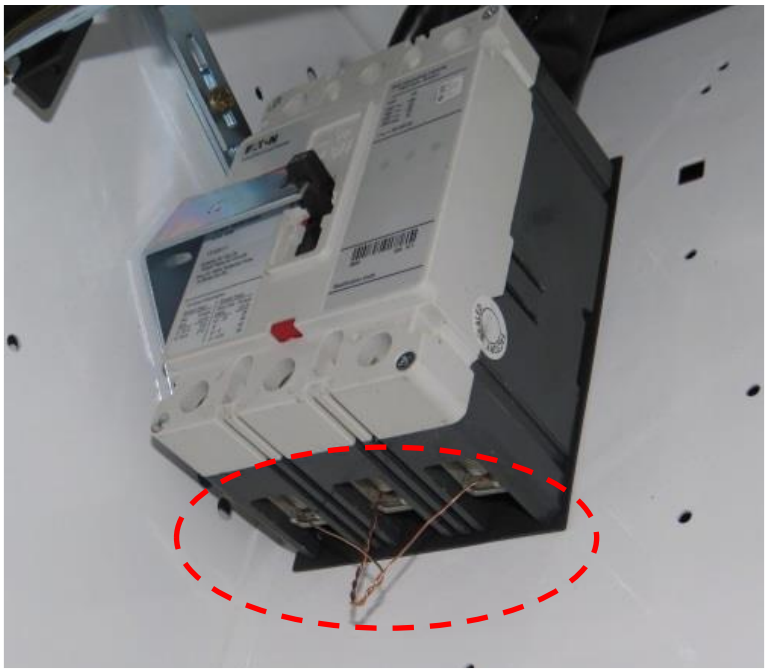

Figure 2-13 VCB Configuration on Switchgear

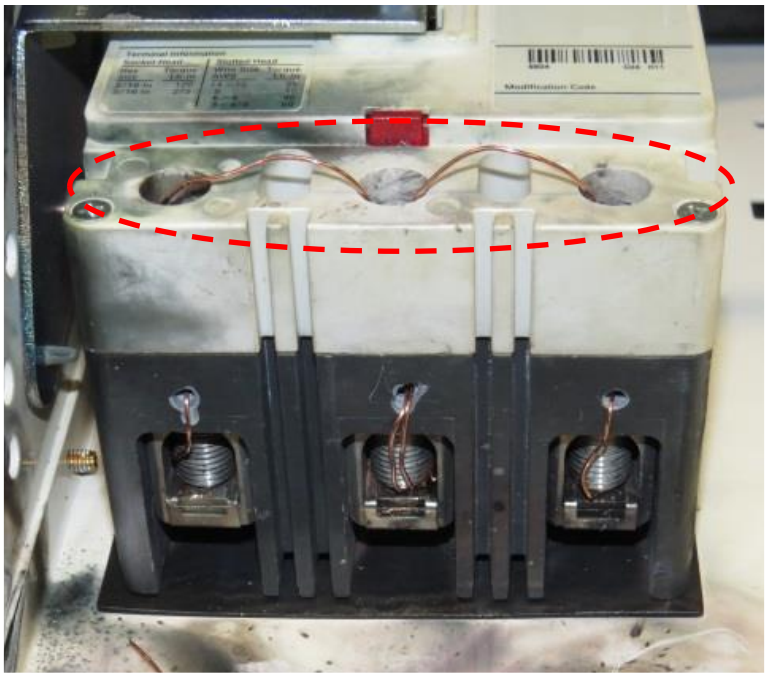

Figure 2-14 HCB Configuration on Switchgear

2.3 Arc Flash Light Intensity Estimation Model Development

In order to mitigate the arc flash hazard caused by the high intensity light, the accurate light intensity estimation is the first and critical step of establishing proper PPE requirements. This section proposes an arc flash light intensity model based on considerable amount of three phase arc tests.

2.3.1 Arc Flash Light Intensity Measurement System

Trying to mimic the arcing light intensity perceived by the human eyes, the arc flash light intensity measurement system was applied to the three phase arc flash tests. The detail information about the arc flash light intensity measurement system is given in [19].

Since the intensity of the light emitted during arc flash can be higher than 1 million lux, the Neutral density (ND) filters, owning characteristic that can equally reduce the intensity of the visible light but without changing the hue of color rendition, have been used in the measurement system. Table 2-3 lists the theoretical attenuation rating of ND filters [20], and the light measurement device with ND filter is shown as Figure 2-15.

Table 2-3 Theoretical Attenuation Rating of ND Filters

ND Number Notation	***Optical Density***	***Transmittance %***
ND2	0.3	50%
ND4	0.6	25%
ND8	0.9	12.5%
ND16	1.2	6.25%
ND32	1.5	3.125%
ND64	1.8	1.563%
ND128	2.1	0.781%

Figure 2-15 Light Measurement Device with ND Filter

The light measurement devices with ND filters were set at three different distance from the arcing point. Generally, the distances are around 3m, 4.5m, and 6m respectively, however, the precise distances are affected by other factors, such as the enclosure size, the placement of calorimeters sensors, and laboratory environment. Figure 2-16 shows the layout scheme of the light intensity measurement.

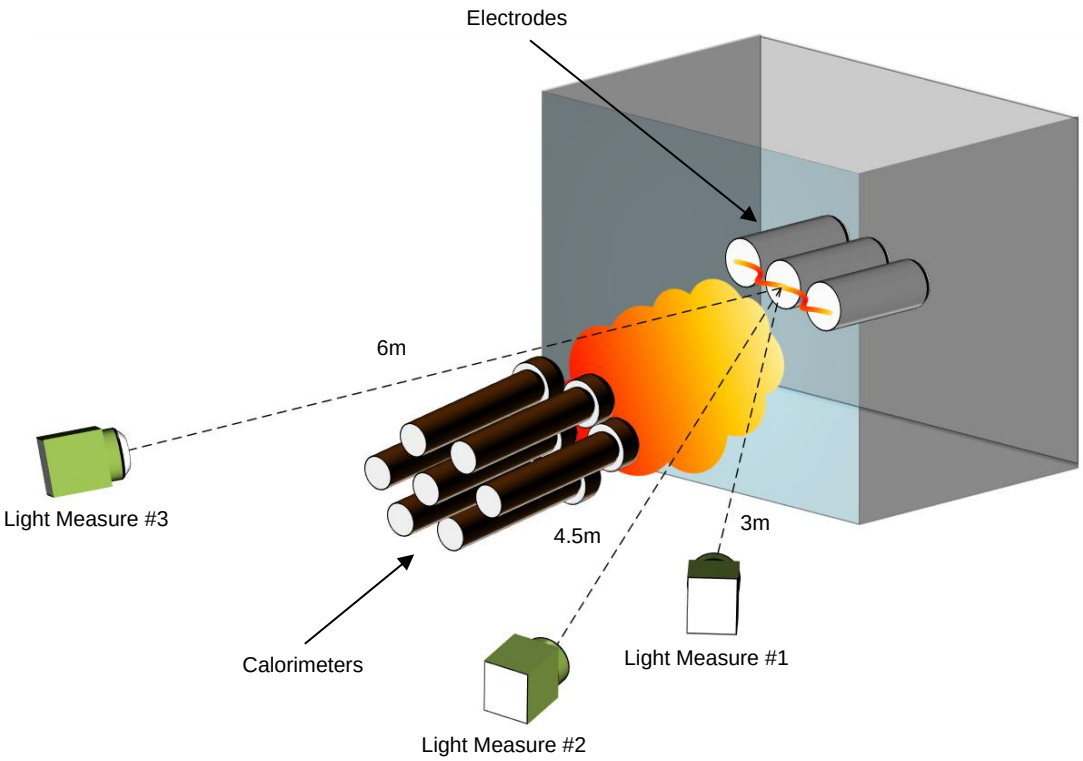

Figure 2-16 Light Measurement Device Layout Scheme in Arc Flash Testing (HCB)

Since the placement of the light sensors affect the measurement results, alignment of the light sensor is important for the measurement accuracy. To ensure the accuracy of the light intensity recording, the light sensors should aim at the center of the arcing point. An improper alignment may result an unsynchronized response among three light sensors, which may impact on the accuracy of measurement. Figure 2-17 illustrates the unsynchronized response problem. The difference of the initial readings among light sensors before the arc flash event are caused by the ambient light in the laboratory.

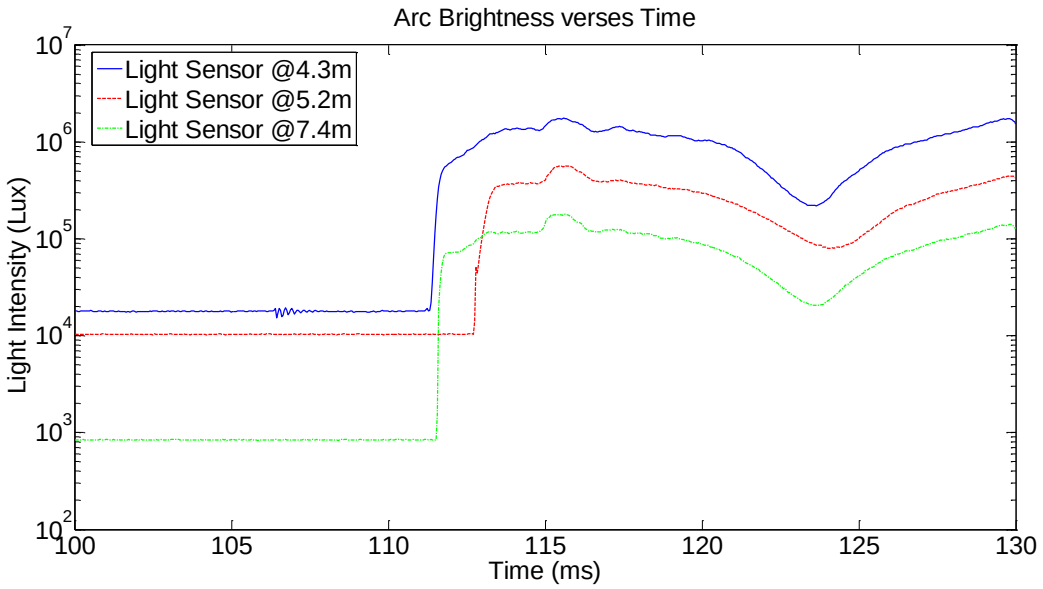

Figure 2-17 Misalignment of Light Measurement

A laser pointer is applied to eliminate the potential misalignment errors. Figure 2-18 and Figure 2-19 show the test result after the alignment improvement and light sensor with laser pointer adjustment respectively.

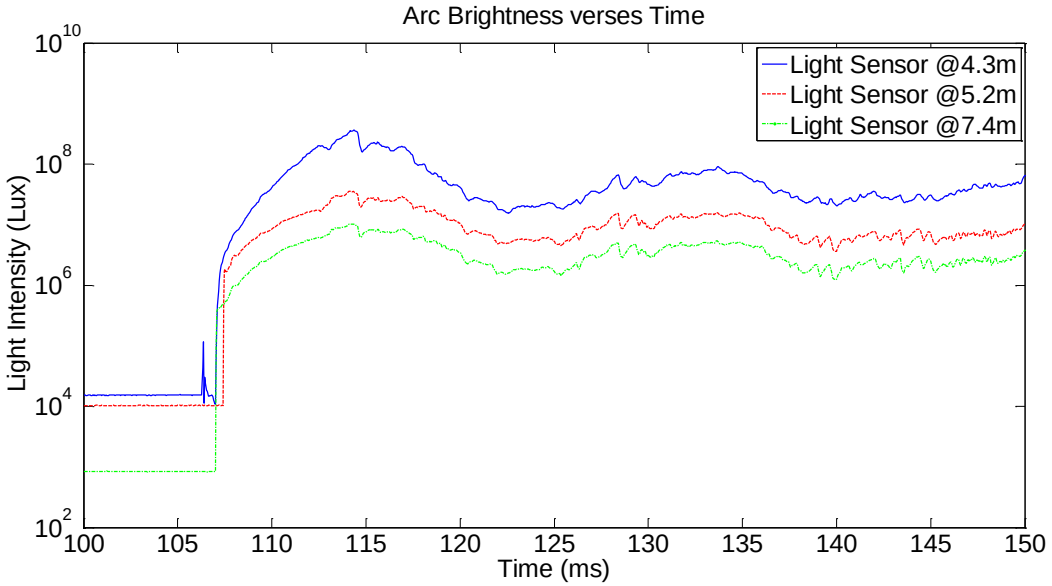

Figure 2-18 Light Measurement Results after Alignment Improvement

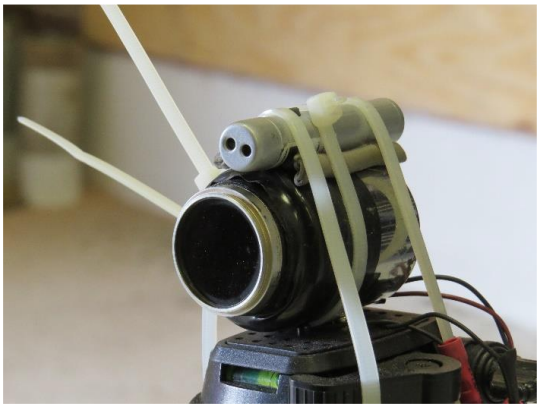

Figure 2-19 Light Sensor with Laser Pointer Adjustment

To ensure the measurement accuracy, the frequency response and transmittance characteristic of each ND filter was characterized before utilizing in light measurement system. The different combination of ND filters have been proven can measure the high intensity light emitted by the arc flash at desired level. For example, stacking two ND8 and one ND128 together is capable of measuring the light intensity up to 1 billion lux [19]. Table 2-4 provides the information about the light measurement devices utilized in arc flash testing including the distance between the measurement devices and arcing point and the transmittance data of each measurement devices.

Table 2-4 Light Measurement Device Data

Voltage (kV)	***Light Near***		***Light Near***		***Light Near***	
	Dist.[a]	***Tran.[b]***	***Dist.***	***Tran.***	***Dist.***	***Tran.***
0.208[c]	4.50	0.121	6.75	0.012	7.50	0.010
0.48[d]	3.00	0.010	4.50	0.013	6.00	0.121
0.60[d]	3.00	0.010	4.50	0.013	6.00	0.121
2.7 (I)[d]	3.00	0.010	4.50	0.013	6.00	0.093
2.7 (II)[e]	3.40	0.013	4.26	0.010	5.39	0.121
14.3 (I)[e]	3.98	0.013	4.86	0.010	5.95	0.121
14.3 (II)[e]	3.78	0.013	5.36	0.010	6.60	0.121
14.3 (III)[e]	4.30	0.013	5.20	0.010	7.40	0.121

[a] Distance between Light Measurement Device and arcing point (m)

[b] Transmittance of Light Measurement Device (%)

[c] *Light Near:* ND8*3; *Light Middle*: ND4*3+ND128; *Light Far:* ND8*2+ND128

[d] *Light Near:* ND8*2+ND128; *Light Middle*: ND4*3+ND128; *Light Far*: ND8*3

[e] *Light Near:* ND4*3+ND128; *Light Middle:* ND8*2+ND128; *Light Far*: ND8*3

2.3.2 Arc Flash Light Intensity Measurement Results

Generally, the maximum intensity of light should be considered in the light intensity model development as the worst case scenario. However, the noise in arc flash test may generate the spike in the test record, which is shown as Figure 2-20. Thus, in order to ensure the accurate of the light model, all the recording data are pre-processed before using for the model development. All unreasonable spike data are excluded from the light estimation model development.

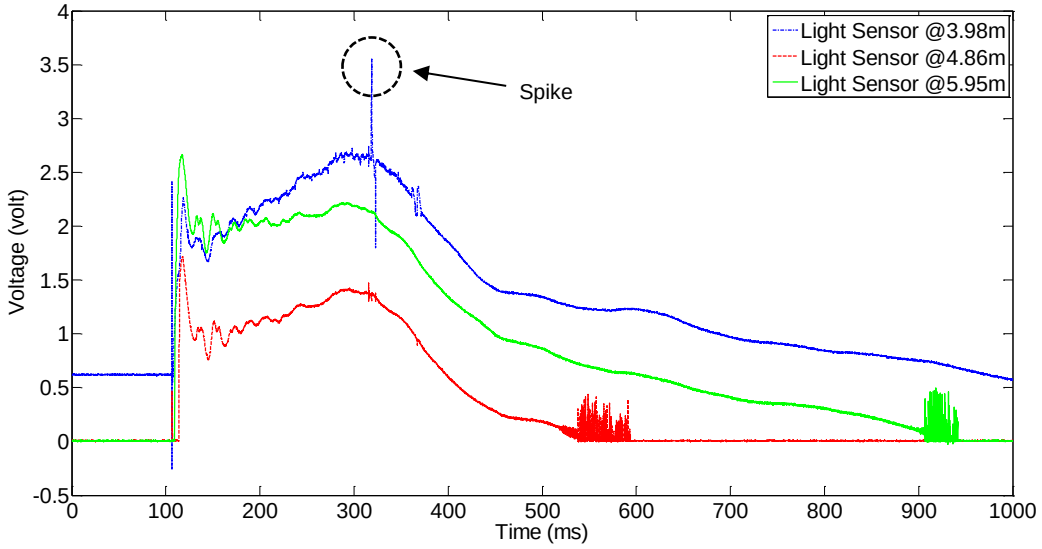

Figure 2-20 Example of the Test Record with Spike Data (VCBB, 14.83kV, 20.4kA, 3" Gaps, 200ms, 36" Box)

The essential parameters (arcing current, gap width, the distance between light measurement device and arcing point) for light intensity modeling could be obtained after data processing. Table 2-5 lists some light intensity data to be used in the modeling process.

Table 2-5 Light Intensity Modeling Data

Config.	***Voc (kV)***	***Ibf (kA)***	***Gap (inch)***	***Dist. (m)***	***Light Intensity (Lux)***
VCB	0.61	20.02	2	3	2.6E+06
VCBB	0.61	5.21	1.25	4.5	5.7E+04
HCB	2.73	9.62	4.5	6	1.3E+05
…	…	…	…	…	…
…	…	…	…	…	…
VOA	14.32	20.08	3	4.86	6.7E+06
HOA	14.07	42	6	5.2	1.7E+07

Approximately 1500 individual recording data from three phase arc flash tests were used for arc flash light intensity modeling, which covered open circuit voltage from 0.208 to 15 kV. The extensive test were performed on 0.6, 2.7, and 14.3 kV, and the selective test on 0.208 and 0.48 kV were used to validate the estimation results of the model. The test parameters are listed in Table 2-6, which includes the combination of bolted fault current and electrode gap width in different size of enclosure.

Table 2-6 Three Phase Arc Flash Tests Range

Voltage (kV)	***Bolted Fault Current (kA)***	***Gap (inch)***	***Enclosure Size***
0.208	2.5 – 100	0.25 – 1	20” x 20” x 20”
0.48	0.5 – 100	0.4 – 3	20” x 20” x 20”
0.60	0.5 – 100	0.5 – 3	20” x 20” x 20”
2.70	0.5 – 63	1.5 – 4.5	26” x 26” x 26”
2.70	20 – 40	1.5 – 4.5	36” x 36” x 36”
14.30	0.5 – 42	3 – 6	36” x 36” x 36”

2.3.3 Parameters Sensitivity Analysis

Important parameters identification are the first step to recognize the correlation between dependent variable and independent variables. Figure 2-21 to Figure 2-23 provide the side by side comparison on some 2.7kV three phase arc flash tests results. Figure 2-21 shows that the light intensity decrease severely along with the increase of the distance from measurement device to arcing point. It means that the measurement distance is an important parameter on light intensity estimation model.

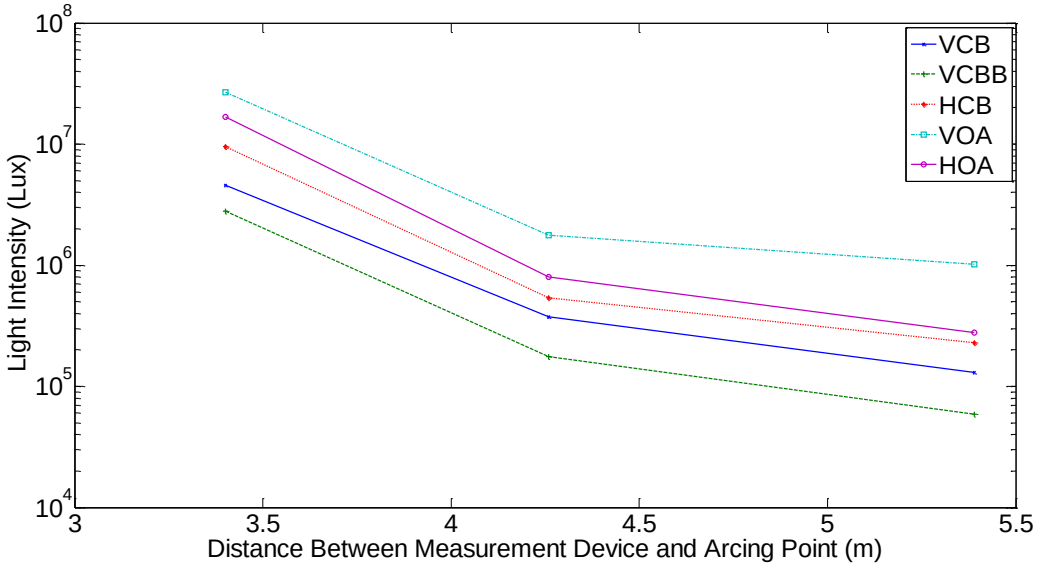

Figure 2-21 Arc Flash Test – Light Intensity vs. Distance (2.73kV, 20.85kA, 1.5" Gaps)

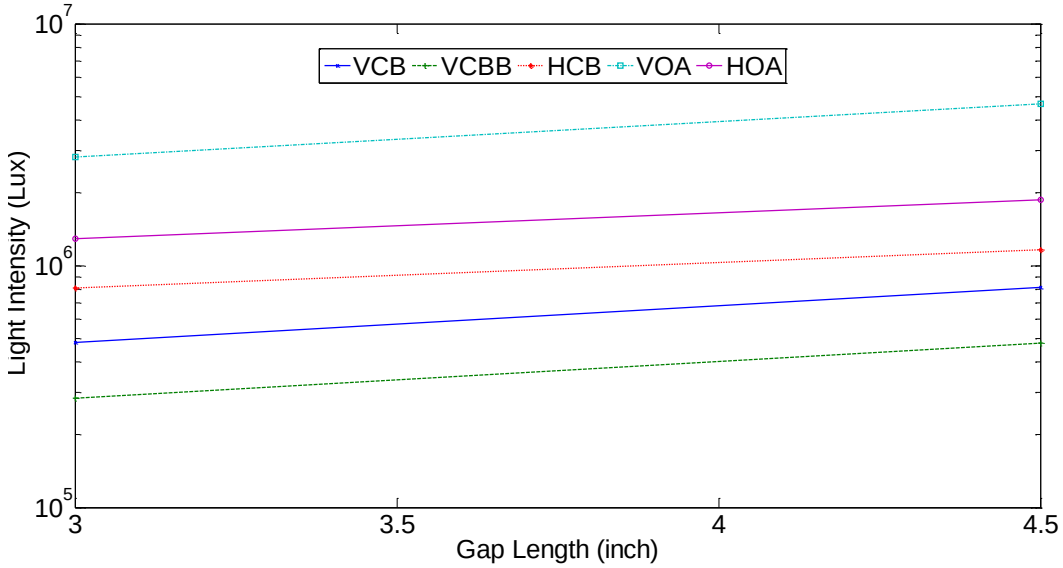

Figure 2-22 Arc Flash Test – Light Intensity vs. Gap Width (2.71kV, 10kA, 4.5m far from Arcing Point)

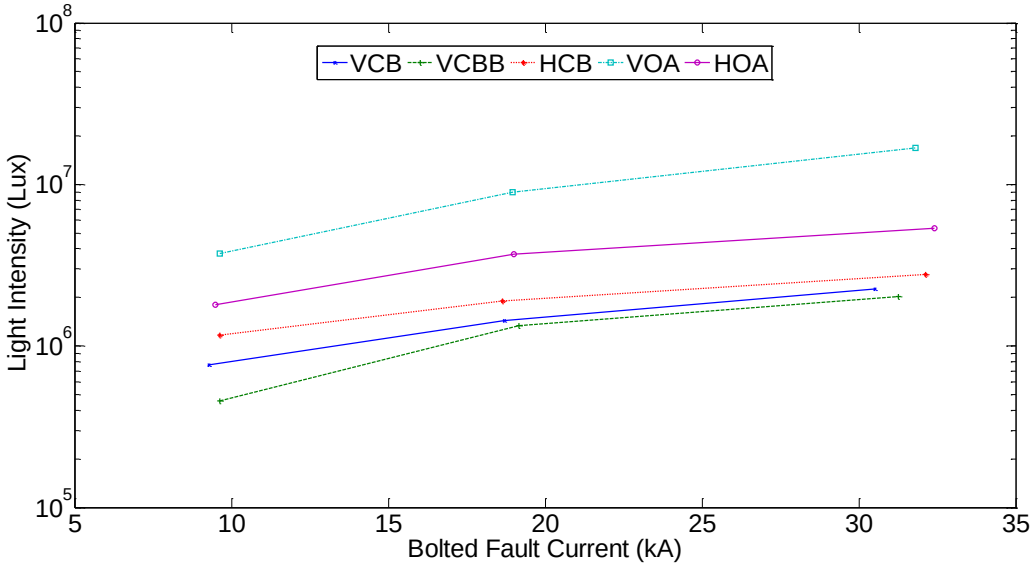

Figure 2-23 Arc Flash Test – Light Intensity vs. Bolted Fault Current (2.71kV, 4.5" Gaps, 4.5m far from Arcing Point)

Figure 2-22 and Figure 2-23 reveal that both gap width and bolted fault current contribute positive correlation with light intensity, and the varying of the bolted fault current provides more significant influence on light intensity than the change of gap width.

This dissertation utilizes statistical approaches to analyze parameter sensitivity of light intensity. Partial regression analysis is applied in this dissertation to study the dependence between independent variables with dependent variable in the model. Partial regression analysis is an approach to show the impact of adding a variable on a model already having one or more independent variables, which also considers the effect among the other independent variables in the model [21].

Figure 2-24 to Figure 2-26 show the partial regression plots on light intensity and independent variables. The results show good linearization performance between

independent variables (Distance, Gap, Bolted fault current) and dependent variable (Light Intensity).

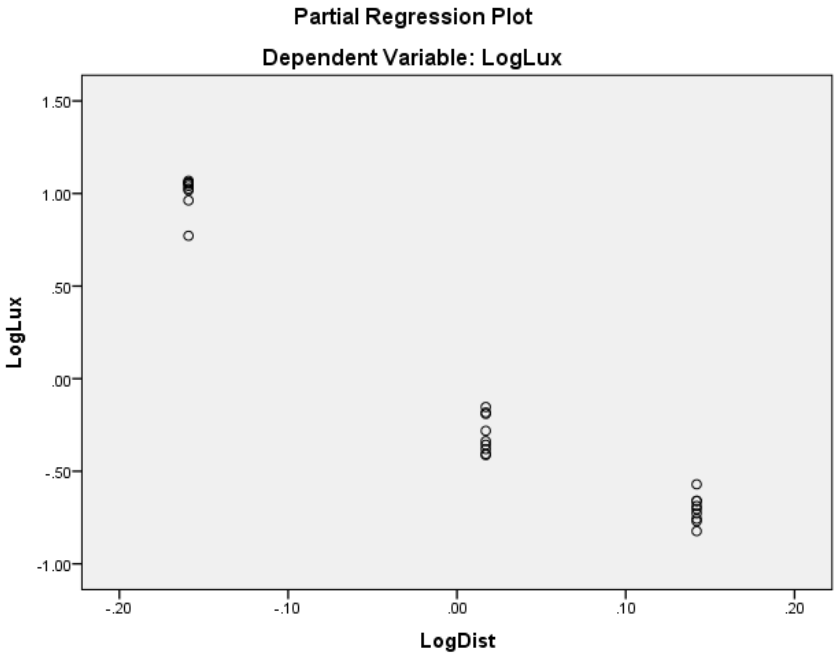

Figure 2-24 Partial Regression Plot (*Lux* vs. *Distance*)

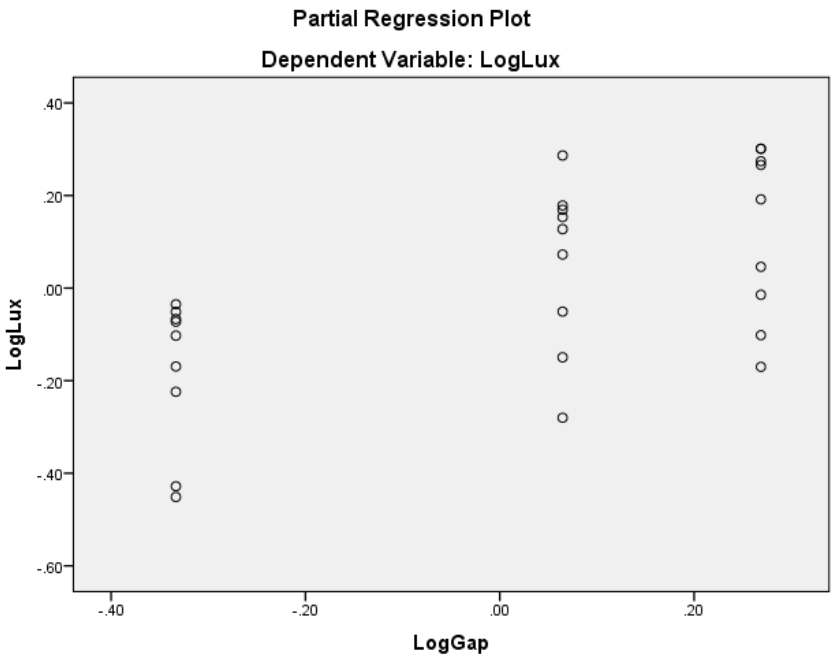

Figure 2-25 Partial Regression Plot (*Lux* vs. *Gap*)

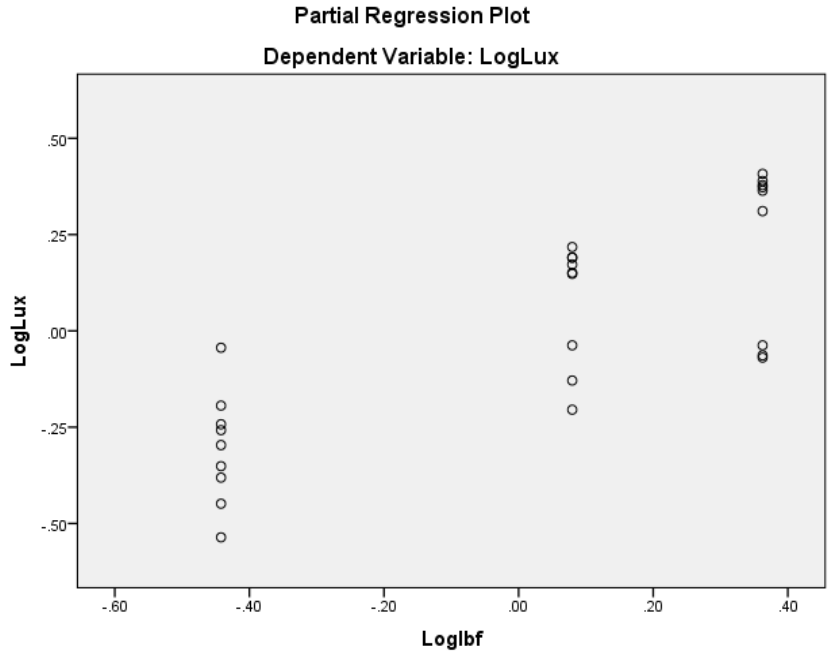

Figure 2-26 Partial Regression Plot (*Lux* vs. *Bolted Fault Current*)

The decreasing trend in Figure 2-24 indicates the negative correlation between distance and light intensity, whereas, the increasing trend in Figure 2-25 and Figure 2-26 present the positive correlation between dependent variable (*Light Intensity*) and independent variables (*Gap width, Bolted Fault Current*). As shown in Figure 2-25 and Figure 2-26, one can see that the bolted fault current contributes stronger positive correlation with light intensity than gap width.

2.3.4 Observation of the Arc Flash Test Results

According to the test results from Figure 2-21 to Figure 2-23, one can see that the intensity of visible light emitted during open air arc flash tests are stronger than the enclosure arc flash tests. This is because the visible light may be blocked by the smoke generated during the arc flash test. Additionally, the smoke contributes the less influence on the VOA test configuration because of the smoke generated in VOA test will be forced toward to the perpendicular direction of the light measurement device. The schematic diagrams and snap shots of arc flash test from high speed video are given in Figure 2-27 to Figure 2-29.

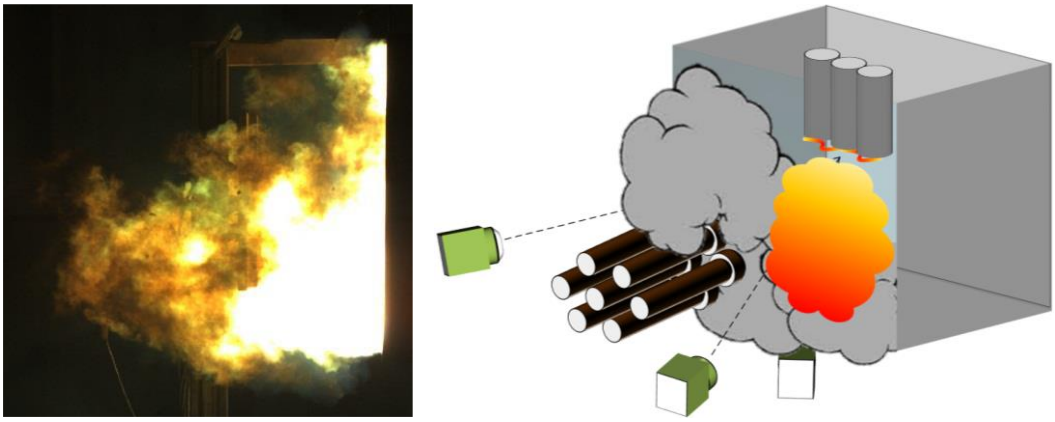

Figure 2-27 Smoke Influence on Vertical Electrodes with Enclosure (VCB)

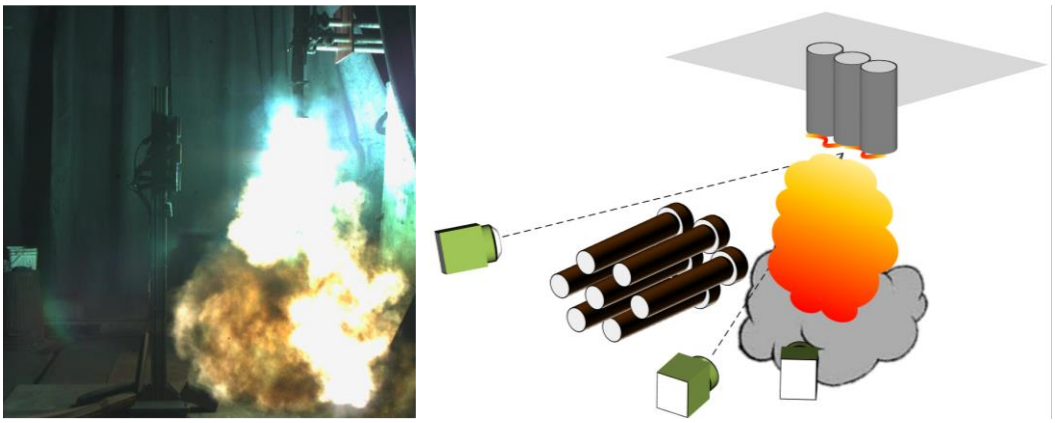

Figure 2-28 Smoke Influence on Vertical Electrodes in Open Air (VOA)

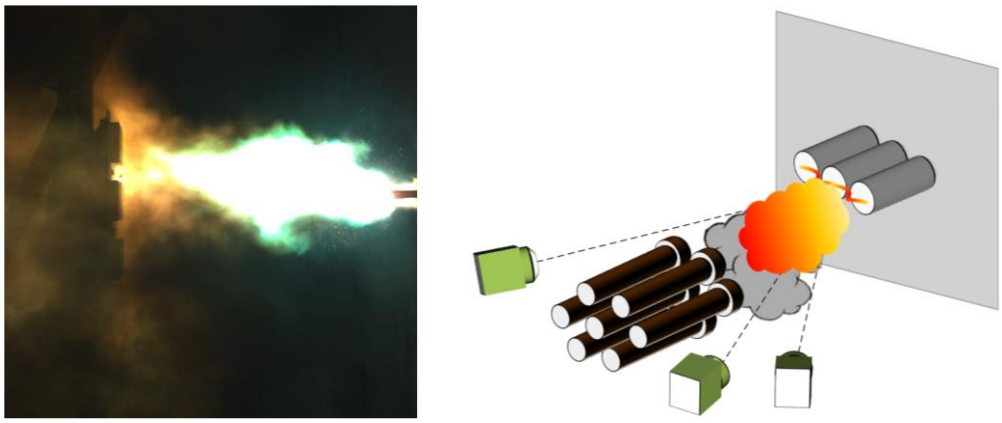

Figure 2-29 Smoke Influence on Horizontal Electrodes in Open Air (HOA)

2.3.5 Correlation Factor for Enclosure Size

Regarding the influence on the light intensity contributed by the enclosure size, curve fitting process was performed to estimate the correction factor. This dissertation establish the correction factor for different enclosure by comparing the light intensity emitted in different enclosure dimensions under the similar arc flash fault conditions. Table 2-7 lists the sample light intensity data for different enclosure dimension at 2.7kV arc flash tests. The enclosure correction equation will be applied to the light intensity model for all

enclosure configurations, the light intensity will be normalized to 20” x 20” x 20” enclosure due to consider effect of enclosure dimension.

Table 2-7 Three Phase Arc Flash Tests Range

Config.	***Voc (kV)***	***Ibf (kA)***	***Enclosure Dimension***	***Light Intensity (Lux)***
HCB	2.73	20.44	26” x 26” x 26”	5.80E+06
HCB	2.73	21.83	36” x 36” x 36”	6.57E+06
VCB	2.73	20.44	26” x 26” x 26”	2.11E+06
VCB	2.97	40.21	26” x 26” x 26”	3.92E+06
VCB	2.73	20.85	36” x 36” x 36”	4.58E+06
VCB	2.97	41.21	36” x 36” x 36”	8.89E+06
VCBB	2.73	20.44	26” x 26” x 26”	1.90E+06
VCBB	2.97	40.21	26” x 26” x 26”	4.48E+06
VCBB	2.73	20.85	36” x 36” x 36”	2.79E+06
VCBB	2.97	41.20	36” x 36” x 36”	1.90E+07

2.3.6 Arc Flash Light Intensity Model

According to the test results and parameter sensitivity analysis, bolted fault current level, open circuit voltage level, gap width between electrodes, and the distance from arcing point to light measurement device will affect the level of light intensity. In statistic, regression analysis focuses on the relationship between a dependent variable and other independent variables, which is widely applied on prediction and forecasting in the aid of

data analysis [22-23]. This dissertation utilizes multiple regression on light intensity modeling for five different configurations.

The arc flash light intensity modeling is based on three reference voltage data points, 0.6kV, 2.7kV, and 14.3kV. A multiple regression can be applied on non-linearized independent parameters to perform curve fitting. In addition, the interpolation and extrapolation techniques have been used to extend the modeling range from three reference voltages to the voltage from 0.208kV to 15kV. Also, the enclosure size has been taken account into light intensity modeling through the enclosure correction equation to consider the light intensity affected by the enclosure dimension. The enclosure correction equation are provided as in Eq. (2-1) and Table 2-8 where *box_size* is the average of the enclosure width and height in inch. The enclosure correction equation is only applied on the enclosure configurations, for the open air configuration, the *bxcf* is equal to 1.

$$bxcf = K1 \bullet e^{(K2 \bullet box\_size)} \tag{2-1}$$

Table 2-8 Coefficients for Enclosure Correction Equation

Coefficients	***VCB***	***VCBB***	***HCB***
K1	0.0939	0.0999	0.8224
K2	0.0896	0.0893	0.0081

The proposed light intensity model for three reference voltage are given as Table 2-9 and Eq. (2-2), where *Ibf* is the bolted fault current in kilo-amperes, *Gap* and the *Dist* are the gap width and distance from the arcing point in millimeters.

$$Lux(V_{ref}) = 10\,\wedge\,(K3 + K4 \bullet \log(I_{bf}) + K5 \bullet \log(Gap) + K6 \bullet \log(Dist)) \bullet bxcf \tag{2-2}$$

Table 2-9 Coefficients for Arc Flash Light Intensity Models

600				
Config.	***K3***	***K4***	***K5***	***K6***
VCB	22.472	0.350	0.384	-4.935
VCBB	23.677	0.750	0.177	-5.399
HCB	23.744	0.676	0.257	-5.301
VOA	23.630	1.146	0.138	-5.210
HOA	25.373	0.672	0.510	-5.804
2700				
Config.	***K3***	***K4***	***K5***	***K6***
VCB	24.857	0.916	1.304	-6.172
VCBB	26.377	1.270	1.292	-6.741
HCB	28.634	0.894	0.879	-6.919
VOA	27.897	1.123	1.245	-6.820
HOA	25.564	0.834	0.920	-6.028
14300				
Config.	***K3***	***K4***	***K5***	***K6***
VCB	18.996	1.034	0.849	-4.313
VCBB	17.073	0.854	1.400	-4.035
HCB	19.826	1.376	1.287	-4.789
HOA	19.869	1.194	1.438	-4.694
VOA	20.325	1.094	1.004	-4.589

This dissertation uses interpolation to estimation the system between 2.7kV and 14.3kV. According to the interpolation approximation, the light intensity can be estimated for the specific voltage V between 2.7kV and 14.3kV as in Eq. (2-3), where V is the voltage in volts, V_{2700} and V_{14300} are two adjacent reference points. Similarly, the system between 0.6kV and 2.7kV can be obtained through the same procedure as in (2-4).

$$Lux(V) = Lux(V_{2700}) + \frac{Lux(V_{14300}) - Lux(V_{2700})}{V_{14300} - V_{2700}}(V - V_{2700}) \quad (2\text{-}3)$$

$$Lux(V) = Lux(V_{600}) + \frac{Lux(V_{2700}) - Lux(V_{600})}{V_{2700} - V_{600}}(V - V_{600}) \quad (2\text{-}4)$$

The extrapolation technique is applied to the system between 14.3kV and 15kV as in (2-5).

$$Lux(V) = Lux(V_{14300}) + \frac{Lux(V_{14300}) - Lux(V_{2700})}{V_{14300} - V_{2700}}(V - V_{14300}) \quad (2\text{-}5)$$

Below 0.6kV light intensity model is derived from 0.6kV model directly because the arc flash at low voltage is more dynamic and unstable, equation (2-6) provides the light intensity model below 0.6kV system.

$$Lux(V) = Lux(V_{600}) \bullet (V / 600)^{0.5} \quad (2\text{-}6)$$

The flow chart of arc flash light intensity model application is illustrated in Figure 2-30.

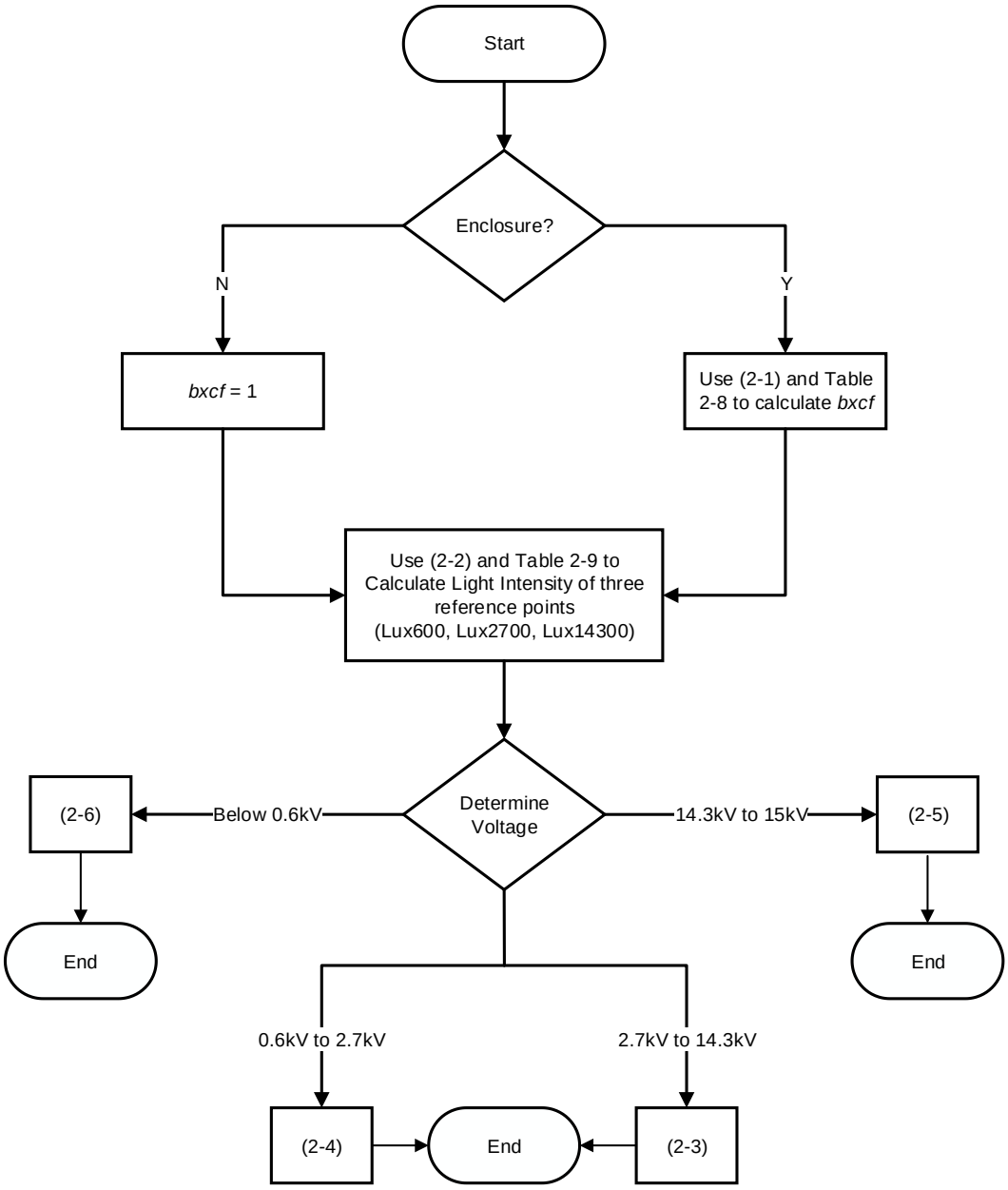

Figure 2-30 Arc Flash Light Intensity Model Flow Chart

The proposed arc flash light intensity model cover system open circuit voltage in the range of 0.208kV to 15kV; bolted fault current from 0.5kA to 100kA and 0.2kA to 65kA

for 0.208kV to 0.6kV and 0.601kV to 15kV respectively; electrodes gap between 0.25inch to 10 inches, where 0.25inch to 3 inches for the system voltage below 0.6kV, 0.75 inch to 10 inches above 0.6kV; the maximum enclosure size is considered as 50 inches in the model, and the width of enclosure must be larger than four times of the gap width. Figure 2-31 through 2-35 and Table 2-10 show the comparison results between model estimations and real arc flash tests.

Table 2-10 Arc Flash Light Intensity Estimation Results

Config.	*Voc (kV)*	*Ibf (kA)*	*Gap (inch)*	*Dist (m)*	*Light Intensity from Test (Lux)*	*Light Intensity from Model (Lux)*
VCBB	0.215	2.50	0.75	4.5	1.14E+04	1.07E+04
HOA	0.61	5.75	0.50	6	3.30E+04	3.29E+04
HOA	2.73	11.10	1.50	5.39	2.50E+05	2.51E+05
VCBB	2.97	41.20	1.50	4.26	1.03E+06	1.03E+06
HCB	2.73	32.01	3.00	6	3.17E+05	3.19E+05
VOA	14.32	40.00	3.75	6.604	4.91E+06	4.99E+06
VCB	2.71	30.51	4.50	6	3.83E+05	3.69E+05
VCB	0.483	2.67	0.39	4.5	5.00E+04	4.79E+04

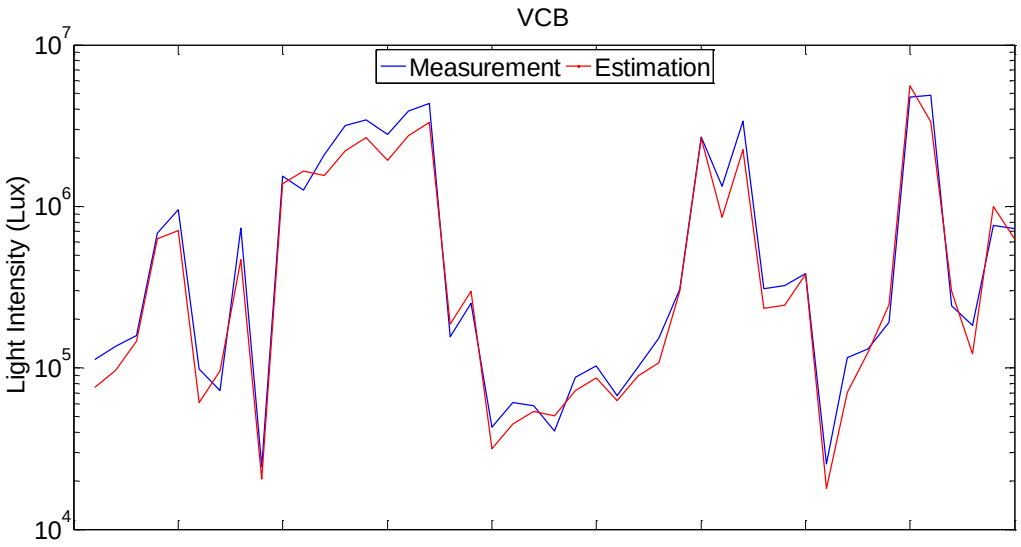

Figure 2-31 Model Estimation Comparison (VCB)

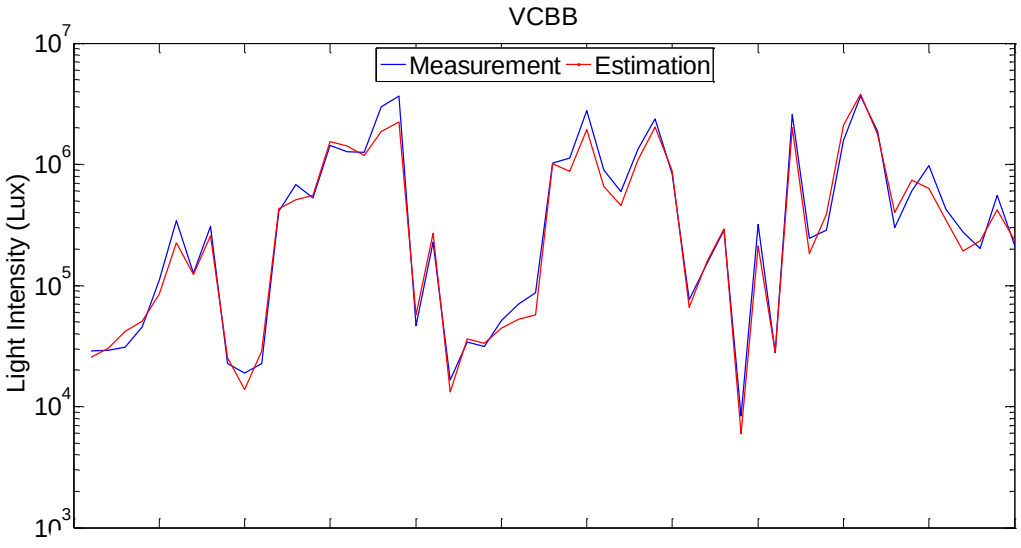

Figure 2-32 Model Estimation Comparison (VCBB)

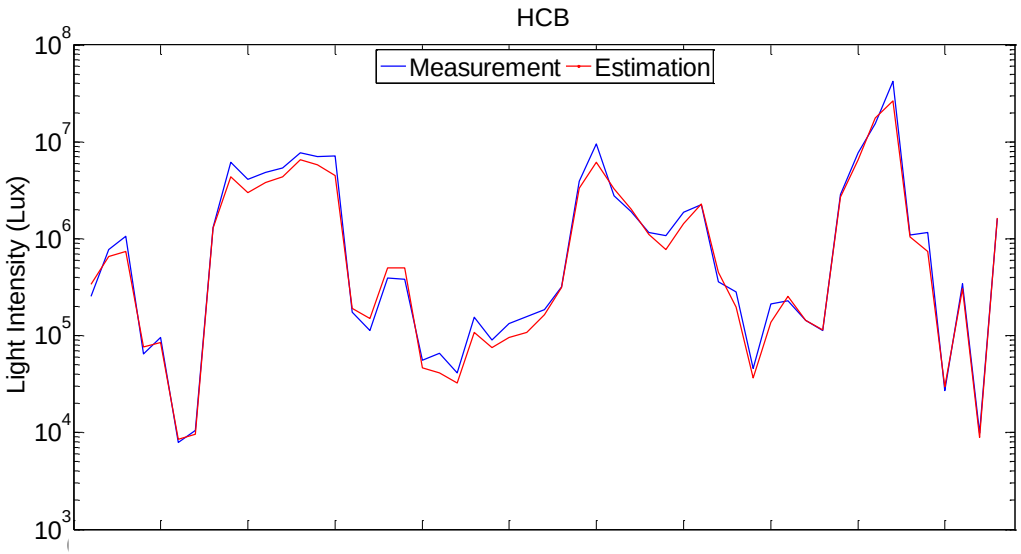

Figure 2-33 Model Estimation Comparison (HCB)

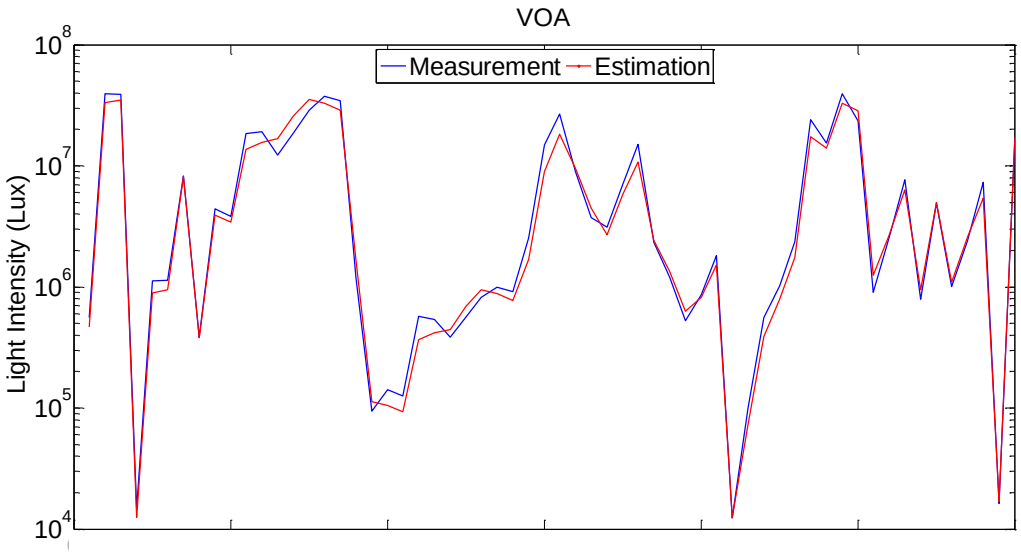

Figure 2-34 Model Estimation Comparison (VOA)

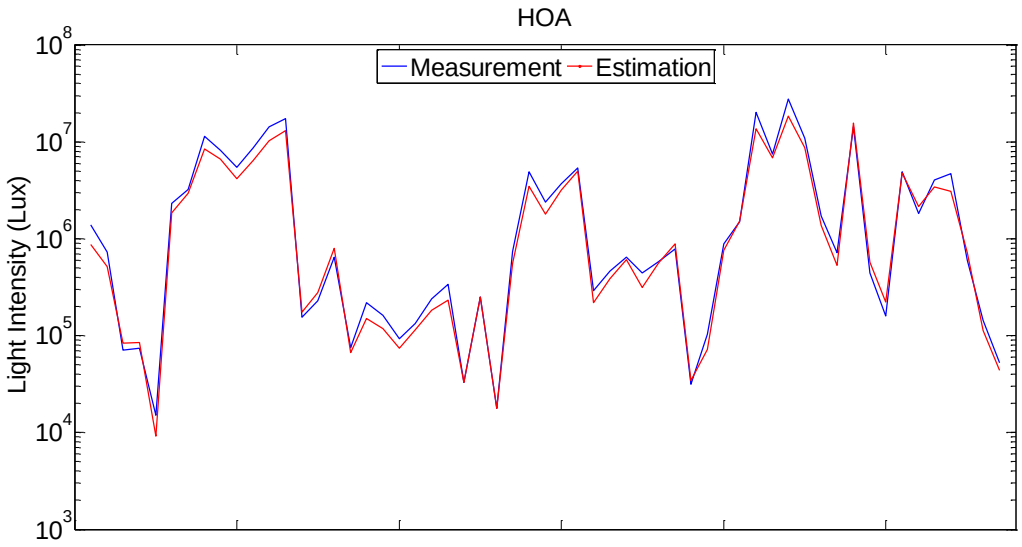

Figure 2-35 Model Estimation Comparison (HOA)

2.3.7 Auto Darkening Welding Lens

Exploring a possible mitigation for extremely high intensity light hazard, the auto darkening welding lens is used to attenuate the light intensity in the arc flash tests. Figure 2-36 shows the auto darkening welding lens utilized in the arc flash test. Figure 2-37 indicates the auto darkening welding lens influence on an arc flash test. The light intensity was around 4.58E+06 lux, after applying auto darkening into the test, the light intensity was decreased as 4.01E+04 lux, attenuated more than 100 times.

Figure 2-36 Auto Darkening Welding Lens

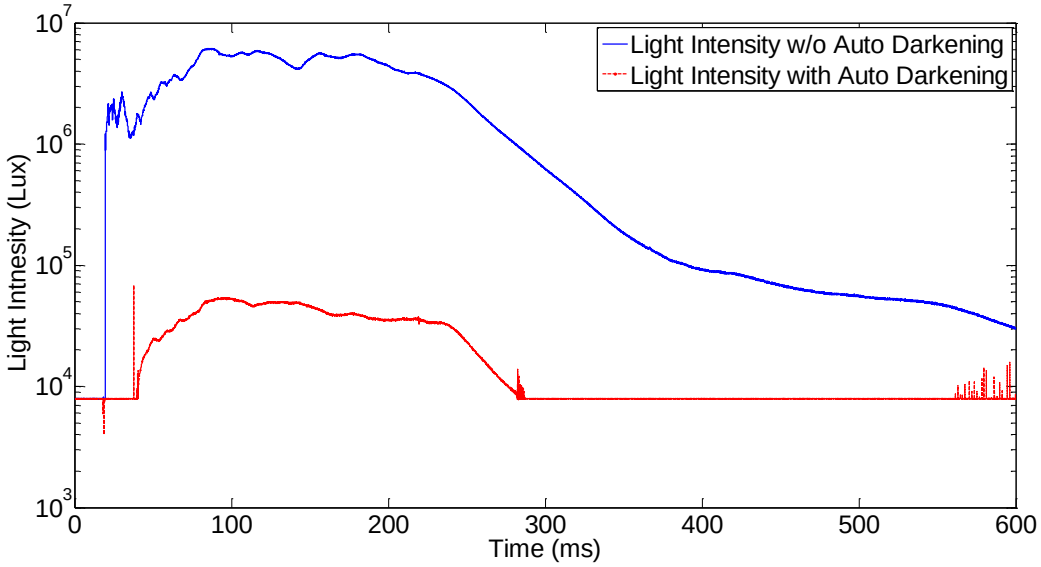

Figure 2-37 Auto Darkening Influence on Arc Flash Test (VCBB, 0.6kV, 30kA, 1" Gap, 200ms, 3m from Arcing Point)

2.4 Summary

In order to estimate the potential arc flash hazard due to the high intensity light during an arc flash event, this dissertation develops an arc flash light intensity estimation model based on approximate 1500 recording data from arc flash tests. To mimic the response of the human eyes, an ambient light sensor was utilized in the light measurement system to record the light intensity perceived by human eyes. In addition, different combinations of ND filters is applied on the measurement to adapt different light intensity level in arc flash tests.

Statistic approaches, such as partial regression and multiple regression are used in the model development process. Considering not only in regression but also in physics, the effect of enclosure size is considered through the enclosure correction equation in the model. Additionally, the interpolation and extrapolation techniques have been applied to the modeling due to extend the modeling range. Compared with the test results, it reveals

that the proposed light intensity model can provide the compatible results with the lab testing.

The auto darkening welding lens is used in the testing to attenuate the light intensity. The light intensity was attenuated more than 100 times after applying the auto darkening welding lens in the testing, which provides a possible method to mitigate the light hazard during arc flash event, and more tests are needed to validate its applicability for light hazard mitigation.

Chapter 3

3D Magnetohydrodynamic Modeling of DC Arc in Power System

3.1 Literature Review

The concern on DC arc flash hazards are increased since photovoltaic (PV) arrays and DC buses in power systems are more broadly used. Recently, large-scale PV arrays have been deployed, which may connect hundreds or even thousands of PV modules together. The combined DC output capacity at aggregation points, such as combiner boxers or inverter-input combiner compartments, may be higher than 1MW, the voltage may reach 1000V, and the current may exceed 1000A. Any equipment failure or human blunder may cause arc flash events in the energized power system, which can cause destruction of equipment, fires, and injury not only the workers but also bystanders [24, 66, 78-79].

For proper system protection and potential hazard estimation/mitigation, accurate estimation of arcing current is essential, as it determines the operating time of the protective device. Furthermore, the incident energy is proportion to the arcing current. Therefore, an accurate arcing current estimation is the first and the most critical step to understand the potential hazards of an arc flash event.

Since 1902, several DC arc models were presented. However, the early works were focused on the theoretical approaches and only had limited test results. Arcings are very dynamic phenomena and the arcing voltage and resistance are dependent on multiple factors, such as the gap width between two electrodes and the arcing current magnitude. Though comprehensive laboratory testing are the best way to develop DC arc flash model, performing rigorous testing is not only time-consuming but also limited by the scale of the laboratories. Currently, several semi-empirical DC arc models were developed from statistical relationships recorded through limited arc testing designed to simulate real arcing

currents and arcing voltage; they are only valid within the range of measured data. Moreover, statistical analysis is not truly based on physical observation, and it may introduce incorrect relationships obscure fundamental phenomena. The commercial software package is mainly applied to analysis AC arc [65, 68], which assumes that it exists 1D temperature field inside the electric arc and using finite difference method to solve electric field and temperature. In contrast to traditional semi-empirical methods to estimate DC arcs, this dissertation presents a DC arc MHD model as an innovative method to understand DC arc behavior and to predict the potential arc flash hazards in a DC power system. It provides sound theoretical base for future model validation and possible range expansion in the cases that the capabilities of the laboratories are limited.

3.1.1 Electric Arc Physics

The arcing phenomenon is a dynamic process. Poisson's formula can express the random nature of the arc lifetime [25]. An electric arc, an electrical breakdown of the resistance of medium (gas or air), can be generated in an electrical system with sufficient voltage through a path to ground or lower voltage. Two separated electrodes in a gas will conduct electric charge under certain conditions. This section attempts to give a brief account of the physical processes that operate to allow the passage of large electric currents through a gaseous medium and across the junctions between gases and metallic conductors.

3.1.1.1 Arc Discharge

The phenomena associated with the passage of the current, which is called '*discharge'* through the gas, depend markedly on the nature and pressure of the gas, the electrode materials, the geometry of the electrodes and its containing vessel, and the magnitude of the flowing current. There are several ways to initiate electric arcs. Arcs can be made through glow to arc transitions in power system. In the cathode region, the glow

state is described by a low current flow and large voltage drop. The transition from the glow to arc in the cathode region can be characterized by a larger current flow and smaller voltage drop, is caused by the electrons released from cathode. Figure 3-1 illustrates the shape of the static voltage-current characteristic for transitions through several discharges until an arc is formed, and the specific voltage and current magnitudes differ with conditions [26].

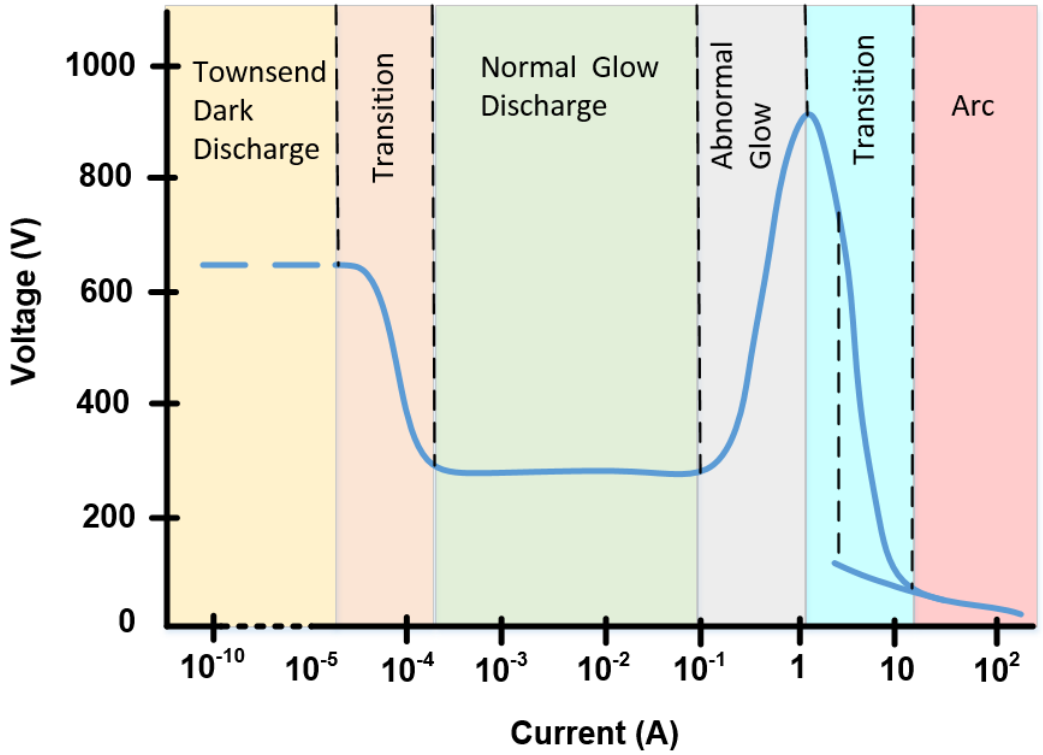

Figure 3-1 Static voltage-current diagram of a discharge at low pressure (at 1 mm Hg)

In addition, an electric arc can be formed through spark discharge. This discharge will occur once the voltage between two electrodes is high enough to breakdown the medium (gas or air) in the environment. The shape of voltage and current for spark discharge is illustrated in Figure 3-2, where the point A represents the beginning of the

sudden voltage collapse. There may be a relatively long time interval between the initial breakdown and the point A. The un-stable discharge, beginning at A, is called a '*spark*' [26].

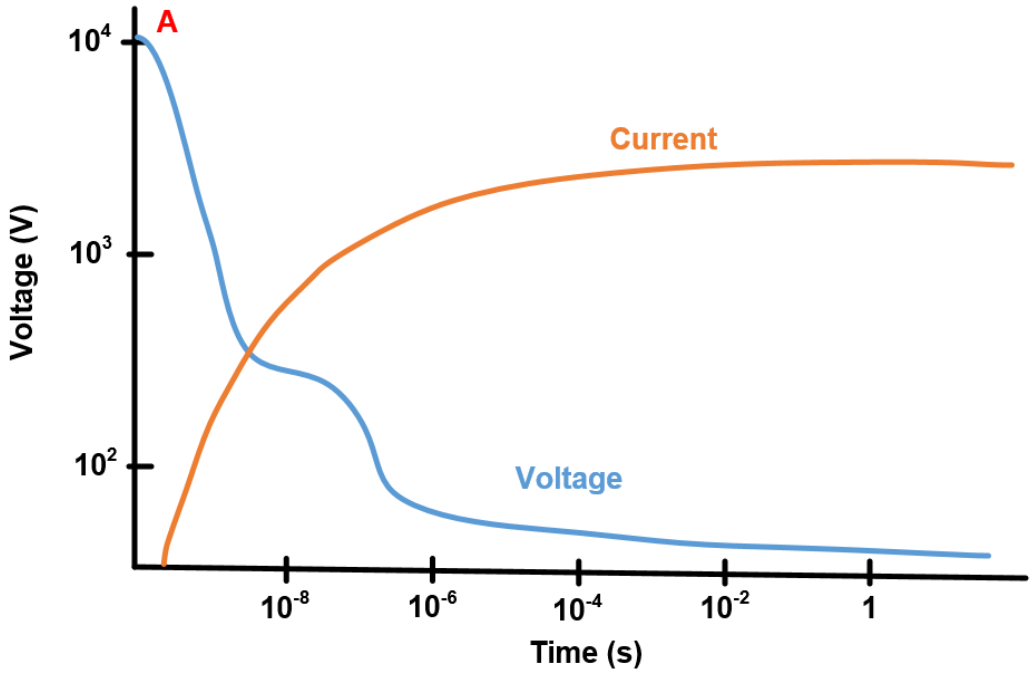

Figure 3-2 Arc Formation from Spark Discharge (at 1 Atm)

Sometimes, sparks may cause arcing on old transmission and distribution systems, whose voltage is greater than 4kV. The 4kV may generate a spark across a 0.762mm (0.03 inch) gap at 1 Atm. Figure 3-3 is the plot of the necessary electric field and minimum voltage to produce a spark [27].

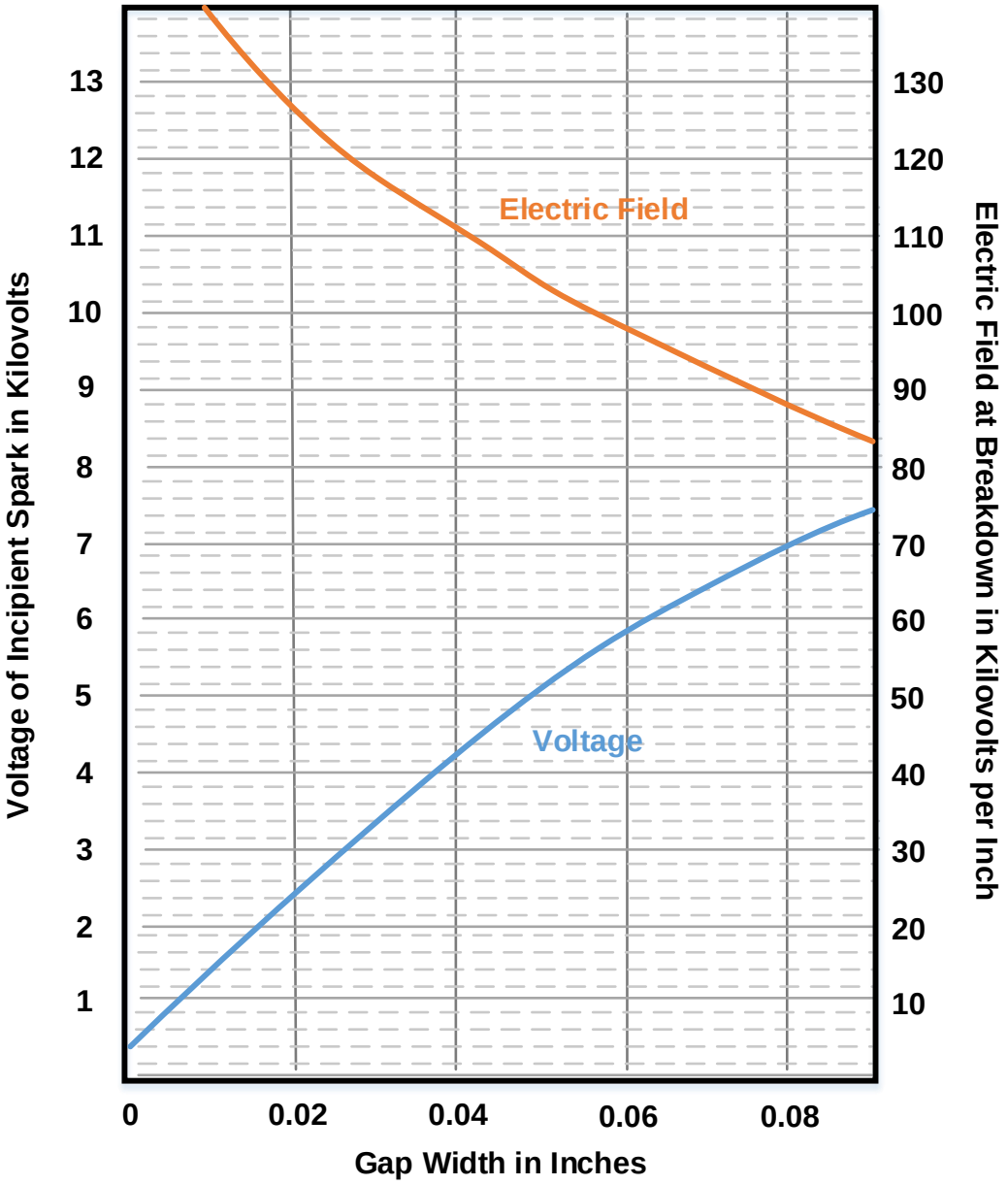

Figure 3-3 Voltage and Electric Field Needed for Sparking (at 1 Atm)

Generally, the electrode material type has no measurable influence on the breakdown voltages [27]. Ionization lower the breakdown or restrike voltage below than the breakdown voltage of a spark gap [29].

Besides, an arc may be formed by drawing apart two current-carrying electrodes initially in contact. An arc formed in this way is said to be '*drawn'*.

In 1889, Friedrich Paschen stated that the breakdown voltage of a gas between parallel plates can be represented as a function of pressure and gap distance [30], as shown in (3-1), where *V* is voltage in volts, *P* is pressure in atmospheres, *Gap* is the gap distance in meters, *a* and *b* is 43.6×10^6 and 12.8 respectively under 1 atmosphere.

$$V_{breakdown} = \frac{a(P \bullet Gap)}{\ln(P \bullet Gap) + b} \tag{3-1}$$

3.1.1.2 Arc Types

Typically, the types of electric arc can be divided into two classes, "high-pressure" arc and "low-pressure or vacuum" arc. The arc burning in air or gasses of significant pressures is usually considered to be a high-pressure arc. The plasma column of a high-pressure arc is collision dominated. Therefore, the plasma properties of high-pressure arc should be described by continuum dynamic theory. On the other hand, the plasma column of low-pressure or vacuum arc is more dominated by electrode region effects [31].

High-pressure arcs can be further subdivided into axisymmetric and non-axisymmetric arcs. An axisymmetric arc burns symmetrically along the electrode axis, and non-axisymmetric arc is either in a state of dynamic equilibrium or continuous motion [31]. Figure 3-4 illustrates a free burning axisymmetric arc. Most studies of arcs prior to the 1990s, which will be presented in Section 3.1.2, were involved in single phase arcing between series electrodes. In industrial applications, most of the arcing faults are free-burning arcs in open air. To validate the simulation results and make it applicable for industry purposes, this dissertation will perform the simulation based upon this configuration.

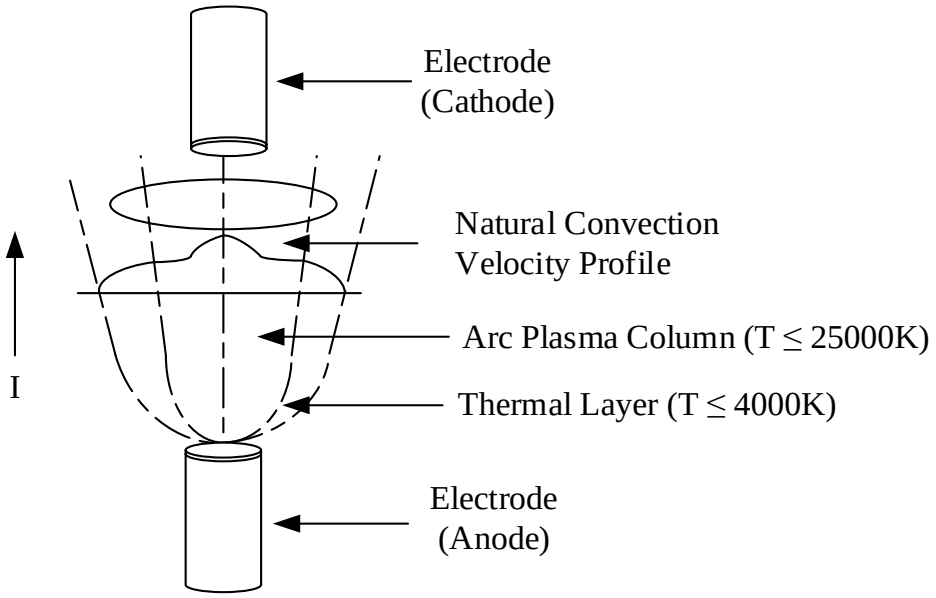

Figure 3-4 Axisymmetric – Free Burning, Vertical Arc [31]

3.1.1.3 Arc Regions and Voltage Distribution

An electric arc can be characterized as three regions: the plasma column regions, anode (positive electrode) region, and cathode (negative electrode) region. An electric arc is an electrical discharge flowing between two electrodes through a medium (vapor or gas), and the voltage drop across the cathode region must be higher than the minimum ionizing potential of the medium [32]. The electrode (anode or cathode) voltage drop is comprised of the electrode fall and the drop in the electrode boundary layer. Mostly, the cathode fall is between 10 to 20V over a region of 1 to 10μm, and the anode fall is between 0 to 5V over a region of 1μm [33]. The boundary regions for electrode can be a few millimeters thick [34]. The voltage gradient across the plasma column has been described as being fairly uniform [35], but is somewhat dependent on the length of the arc and the arc current magnitude. The arc regions and the distribution of arc voltage are shown as Figure 3-5.

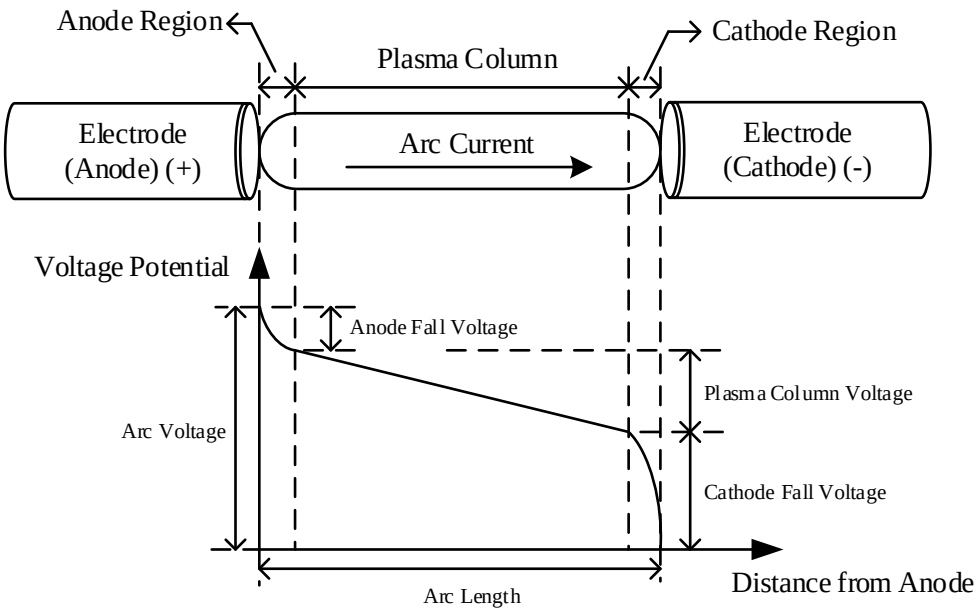

Figure 3-5 Arc Regions and Arc Voltage Distribution

The cathode, plasma column, and anode region can be subdivided as in Figure 3-5. Generally, the temperature in cathode region is between the temperature of the plasma column region and the cathode-fall region, however, when the density of charge carries increased, the cathode region's temperature will exceed the temperature of plasma column region [33].

At the end of the cathode region exists a high luminosity zone, where vapor atoms become excited because of electron collisions. A positive ion is generated and the atom emits a photon and keeps in the unstable state due to the collision of electrons. Compared to the positive ions, the electrons are much lighter and move faster through the cathode-fall region than positive ions traversing in the opposite direction, which let the positive space charge establishes a strong electric field. The strong electric field not only forces

electron emission from the cathode region but also accelerates the movement of electron [33].

Differing with the cathode region, the anode region is populated by electrons, not positive ions. The voltage fall of anode depends upon the energy required for electrons to ionize the atoms of anode vapor. The number of positive ions increases in the anode region toward the plasma column, so the electric field in anode region is weaker than the electric field in cathode region, which causes the current density of the anode is less than at the cathode.

Considering the energy conservation theory, the energy must be balance at the electrodes and at plasma column region. After the ion bombardment and electron emission, the remaining of cathodic spot energy is primarily released by vaporizing the material of cathode [36]. Generally, electrodes only takes 1 μs to reach vaporization temperatures [37]. Similarly, the energy conservation theory can also be applied to anode region. Once the arcing current is greater than 30 amps, the electrodes will loss energy due to the radiation outward from the surface. Additionally, the radiation losses for non-refractory (copper, steel) electrodes are more significant than refractory (carbon) electrodes [38].

3.1.1.3.1 Cathode

Naturally, air is a good insulator, and an arc may not ignite even if the voltage drop across the cathode region is capable of supplying the minimum ionization potential. Generally, there are two conditions at cathode that distinguish arc from other discharges: a high current density at cathode surface and a high concentration of neutral and charged particles at cathode region [39].

Cathode deliver the electrons to the arc column, mostly, the cathode can be divided into two categories: refractory (thermionic) cathode and non-refractory (non-thermionic) cathode, and the boiling points of non-refractory cathode is lower than

refractory's. The refractory cathode are heated to 3500 K or higher temperature in thermionic emission process, and the current density of refractor cathode is on the order of 10^4 A/cm^2 [34]. At the temperatures lower than the temperature of thermionic emission the significant evaporation will happen for non-refractory cathode, the electron emission for non-refractory cathode probably involves a combination of thermionic and field emission, which is called as TF emission [34]. In the field emission process, the electrical field is enhanced by local surface imperfections, which becomes sufficiently high to draw electrons from the metal, so the current density of non-refractory cathode is greater than the current density of refractory cathode. Typically, the current density of non-refractory cathode is 10^6 to 10^8 A/cm^2 [34].

In TF emission process, the strength of electric field at the cathode let cathodic spots augment the number of electrons released. These high electric fields are generated by the positive ions. The positive ions compensate for the energy lost caused by electron emission through bombarding the cathode surface. However, the TF emission theory cannot explain electrons carrying more than 99% of the current in the plasma. The major part of the current in cathode region are carried by the positive ions, but these positive ions only carry less than 1% of the current at plasma region. Therefore, more electrons must be generated between the plasma and the cathode surface through electron-ion or ion-ion collisions [35]. In addition, the high electron velocity caused by low electron mass may explain the extremely large percentage of plasma current carried by electrons. Besides, the positive ions are limited by their own kinetic energy (0.5 mass velocity^2) [40].

Surface irregularities contributes more significant influence on the formation of cathode spot than material properties [41]. The delay time of cathodic spot formation has been correlated with surface variations. Smooth surfaces emit relatively small pre-currents

across the plasma sheath, but rough surfaces emit extremely high pre-currents [42]. Those pre-currents will assist the transition from a glow to an arc discharge.

Actually, the cathodic spot is comprised of numerous little spots, tiny cathodic spots are forming simultaneously and extinguishing. Along with the increase of arcing current, the power supplied to the cathode increased simultaneously, which results the severer erosion of cathode material due to the temperature distribution over the cathode increases with the total number of emitting sites.

According to the energy conservation theory, the energy must be balance at the cathode region. Energy is supplied by joule heating and ion bombardment, and energy is lost through electron cooling, heat conduction, and neutral particle loss. Generally, the magnitude of current density at cathode is two or more orders higher than in plasma column region, which results in a magnetic pressure gradient from the changing self-magnetic field. The gas flow away from the cathode is accelerated by this pressure gradient.

3.1.1.3.2 Anode

Similar to cathode region, a magnetic pressure gradient also exists at the anode region, which draws cold gas into the anode region. The material of anode can be vaporized and entrained into the plasma.

The fall voltage of anode is caused by a space charge over a small distance adjacent to the surface of electrode. The magnitude of the anode fall voltage depends on the energy required to liberate the atoms in the anode vapor. Positive ions generated by collisions move in the cathode direction.

The anode collects electrons carrying current from the arc column. Also, the evaporated material from anode may provide ions to the plasma. The amount of the heat fluxes radiated and conducted from the plasma are the power supplying to the anode. The heat flux associated with the electron current, comprised of the electron enthalpy, supplies

energy to the anode. Also, energy is lost from large particles [33]. The surface of anode loses heat by heat conduction into the bulk of the material, material evaporation, and heat radiated by the surface or convected away from the surface.

3.1.1.3.3 Plasma Column

The plasma column can be characterized as a "small intensely brilliant core surrounded by a cooler region of flaming gases called the aureole [43]," for high pressure gases. For an electric arc, the changing current magnitude causes changes in the arc temperature and ionization level, the gasses around the arc will expand, which will generate the pressure waves from around the arc and radiate outward [44].

The plasma temperature range for high pressure gases is from 5,000 K [45] to 20,000 K [38] depended on the magnitude of arcing current. Figure 3-6 indicates the theoretical and experimental plasma temperatures at arcing point for a vertical arc burning in air under 1 atmosphere [38].

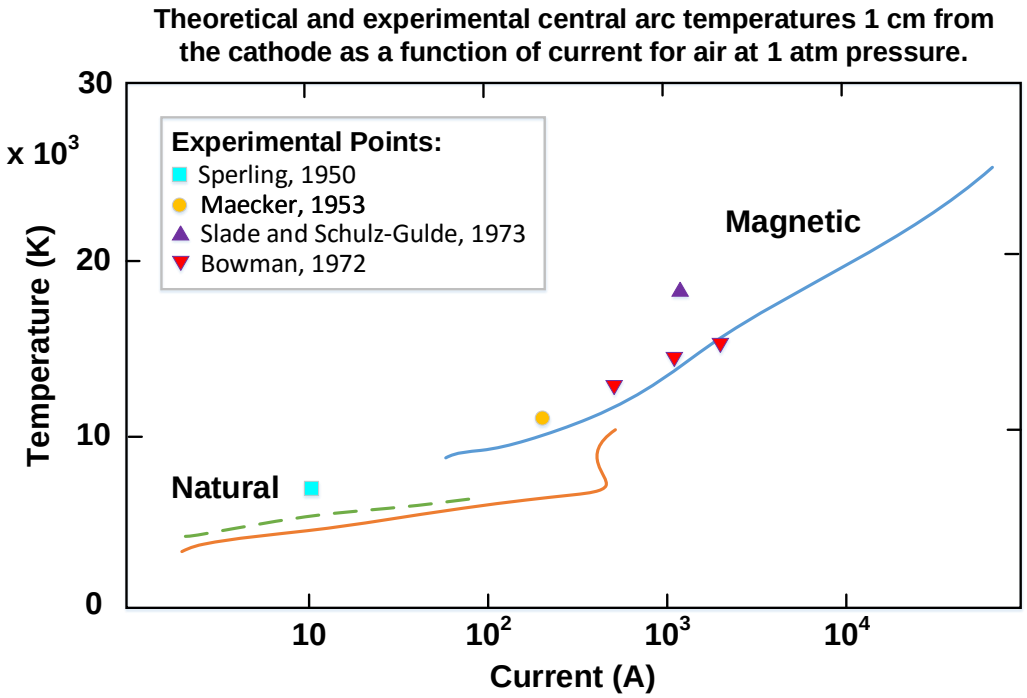

Figure 3-6 Arc Temperature as a function of Current

According to Figure 3-6, once the current is greater than 30 A, the convection induced from the magnetic field of arcing current contributes significant influence on arc properties, which means the arc properties are largely determined by the convection [14]. The density and conductivity of plasma may be determined by Saha's equation which estimates the thermal ionization level at particular temperature regarding the equilibrium conditions. Saha's equation is given as (3-2), where *f* is the fraction of the total number of ionized molecules, *p* is the gas pressure in mmHg, *T* is the temperature in Kevin, E_i is the potential of ionization of the gas, *q* is the charge associated with an electron, and *k* is Boltzman's constant [29].

$$\frac{f^2}{1-f^2}\,p = 2.4\cdot 10^{-4} T^{2.5} \varepsilon^{-\frac{qE_i}{kT}} \tag{3-2}$$

Generally, the electrical power supplied to the arc plasma is dissipated as radiation, conduction, and convection, which is shown as Figure 3-7 [31].

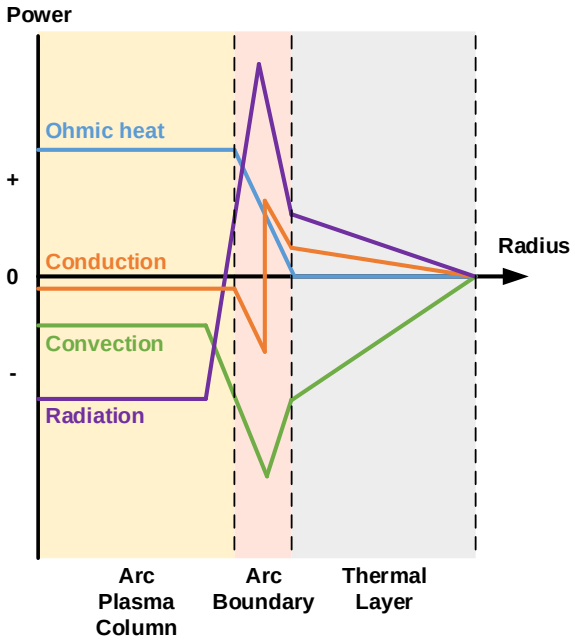

Figure 3-7 Radial Arc Energy Release

Mostly, the high pressure arc columns, owning a radial structure, can be modeled as two zones, “consist of a high temperature, low density and low thermal storage core surrounded by a lower temperature, high density and high thermal storage annulus [31].”

Usually, compared with the thermal constant of the arc, the electrode’s thermal constant is much longer. Figure 3-8 shows the “arc is therefore able to move through a succession of quasi-steady states whilst following the thermal evolution of the electrode [31].”

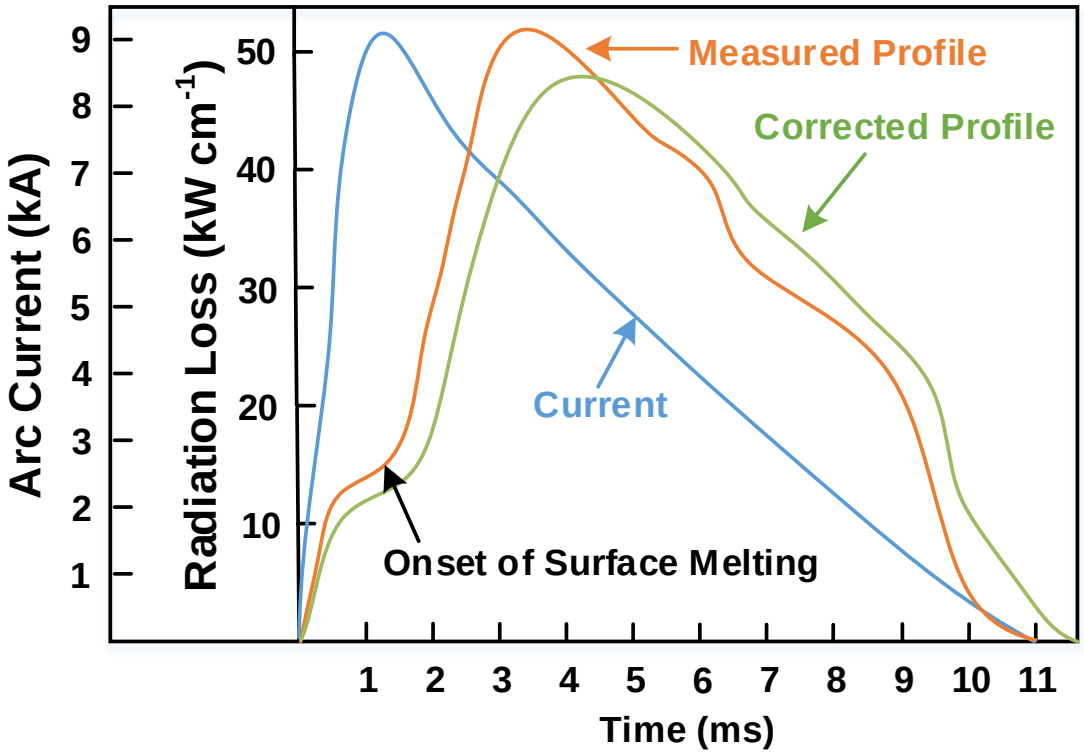

Figure 3-8 Time Delay between Arc Current and Radiation Loss (5 mm above a cathode of a free burning arc)

Approximately, the direction of the plasma jet is normal to the surface of arc root attachment. However, the plasma column is not always linear. If the plasma jet direction does not correspond with the path of the shortest distance between the electrodes, the

actual arc path will be normal to these points for a short distance and then bridge between these two jets. The complex dynamics, driven by the interplay between plasma and airflow and the wandering of the arc roots, prevent the arc from staying entirely stable conditions [46].

3.1.2 Historical DC Arc Models

It is very difficult to develop theoretical models by using arc physics because the physical processes of an electric arc are chaotic and complex in nature. Currently, there are two main methods addressing the DC arc power in power systems. The first method is the theoretical arc model based on the maximum power transfer theory, and second method is semi-empirical models based on the results of some early DC arc tests.

Figure 3-9 shows a typical DC arc test set-up and its equivalent circuit. In reality, the gap between two electrodes (*L* in Figure 3-9) is not equal to the actual arc length. Since the precise measurement of arc length is difficult to achieve, most of the early DC-arc models assume that an arc length is equal to the gap width [47].

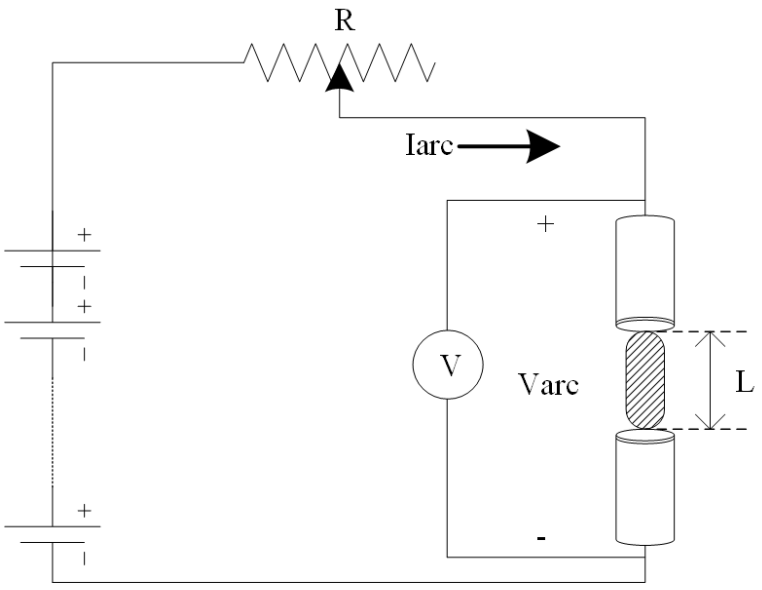

(a) DC arc test circuit

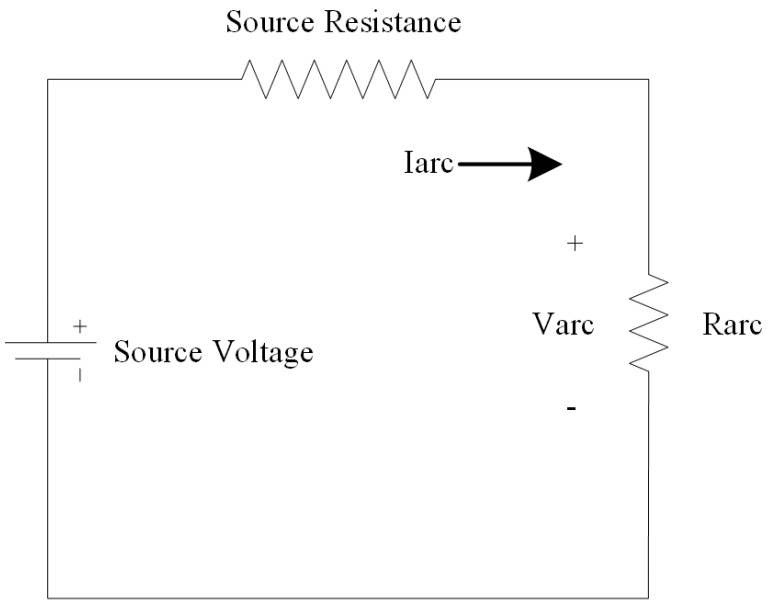

(b) DC equivalent circuit

Figure 3-9 DC Arc Test Circuit and Equivalent Circuit

3.1.2.1 Theoretical DC Arc Model

Currently, the most widely used model to estimate DC arc is based on Ralph Lee's arc model, which assumes that the arc is a spherical radiant source and the entire electrical energy of the arc converts to heat energy. The electrical arc power in this model is determined based on the maximum power transfer theorem [48]. The maximum electrical arc power is 25% of the bolted fault when the arc resistance is equal to the source resistance, as illustrated as Figure 3-10.

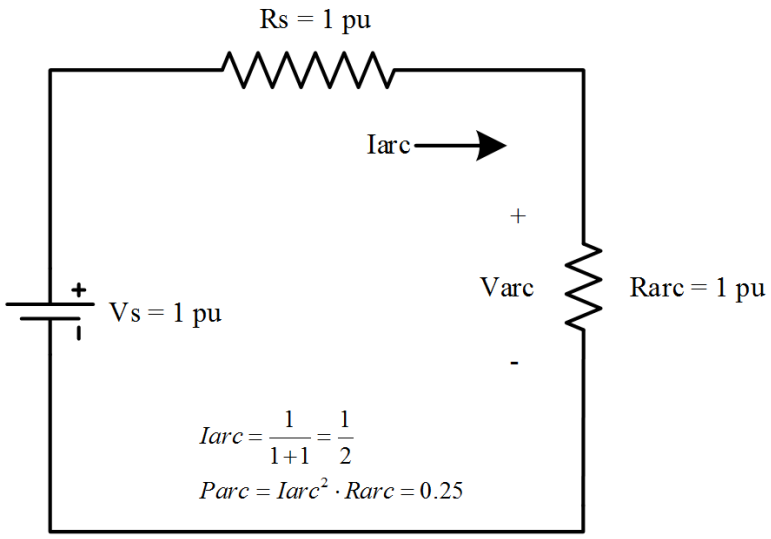

Figure 3-10 Maximum Power Transfer to DC Circuit

3.1.2.2 Ayrton Equation

In 1902, Ayrton presented the steady-state arc model, as in (3-3), where constant *A* describes the voltage fall of carbon electrodes, constant *B* represents the voltage gradient of the plasma column, whose arc length is equal to *L*, expressed in millimeters, and the constants *C* and *D* model the nonlinear characteristics of the electric arc. The V_{arc} and I_{arc} represent arcing voltage in volts and arcing current in amperes, respectively [26]. Typically, Ayrton Equation can be represented as (3-4).

$$V_{arc} = A + BL + \frac{C + DL}{I_{arc}} \tag{3-3}$$

$$V_{arc} = 38.88 + 2.074L + \frac{11.66 + 10.54L}{I_{arc}} \tag{3-4}$$

3.1.2.3 Steinmetz Equation

Steinmetz provided another arc model based on carbon electrodes in 1906, as in (3-5). The constants *A, C, D* are dependent on the material of electrodes, where *L*, V_{arc}, I_{arc} are the arc length in inches, arcing voltage in volts and arcing current in amperes, respectively [49]. Equation (3-6) shows the arcing voltage for 1 inch gap width with carbon electrodes.

$$V_{arc} = A + \frac{C(L+D)}{I_{arc}^{0.5}} \tag{3-5}$$

$$V_{arc} = 36 + \frac{130(1+0.33)}{I_{arc}^{0.5}} \tag{3-6}$$

3.1.2.4 Nottingham Equation

In 1923, Nottingham produced his arc model based on his arc research, as in (3-7). The power *n* varies as a function of the electrode material, and the constant *A* and *B* are determined by the arc length and electrode material. V_{arc} and I_{arc} are arcing voltage in volts and arcing current in amperes, respectively [50]. For cooper electrodes and arc lengths ranging from 1mm to 10mm, the Nottingham equation can be represented as (3-8).

$$V_{arc} = A + \frac{B}{I_{arc}^{n}} \tag{3-7}$$

$$V_{arc} = 27.5 + \frac{44}{I_{arc}^{0.67}} \tag{3-8}$$

3.1.2.5 Hall, Myers, and Vilicheck

A research group published over 100 DC arc test results of DC trolley systems in 1978 [52]. A 325V DC power supply was used in these arc tests, the arcing current ranged from 300 to 2400A, and the gap widths between two electrodes ranged from 4.8 to 152mm. Some test results are listed as Table 3-1, which are matched with the estimation from the equation (3-5).

Table 3-1 Hall's Arcing Fault Data (9.525 mm Gap)

System Voltage (Volts)	***System Resistance (Ohms)***	***Bolted Fault Current (Amps)***	***Arc Current (Amps)***	***Arc Voltage (Volts)***
325	0.6	500	375	75
325	0.2	1380	1200	58
325	0.15	1800	1500	80

3.1.2.6 Stokes and Oppenlander Equation

In 1991, Stokes and Oppenlander conducted over 200 open air single phase AC and DC arc tests, which can be considered as the most complete study of free-burning arcs between series electrodes in open air [46]. They used a 6kV DC power supply, and produced 0.1 to 20kA arcing current between series copper and aluminum electrodes, with gap widths of 5, 20, 100, and 500mm respectively. The model is shown as (3-9), where L is the gap width between two electrodes in millimeters. V_{arc} and I_{arc} are arcing voltage in volts and arcing current in amperes, respectively. This DC arc model has been cited by the NFPA 70E 2015 edition to estimate the DC arc.

$$V_{arc} = (20 + 0.534L)I_{arc}^{0.12} \quad (3\text{-}9)$$

3.1.2.7 Bruce Power DC Arc Flash Tests

In 2007, recognizing the lack of available references of DC arc hazards, Bruce Power contracted Kinetrics laboratory to perform a review of the DC arc hazards present at battery rooms and the plant DC distribution system [52]. The DC arc flash tests from Bruce Power are shown as Table 3-2 and Figure 3-11.

Table 3-2 Bruce Power Arcing Fault Data

System Voltage (Volts)	***Gap (Inch)***	***Bolted Fault Current (Amps)***	***Arc Voltage (Volts)***
260	1	2370	95
260	1	10100	154
260	1	11600	140
260	2	1985	137
260	2	6700	183
260	2	9550	205

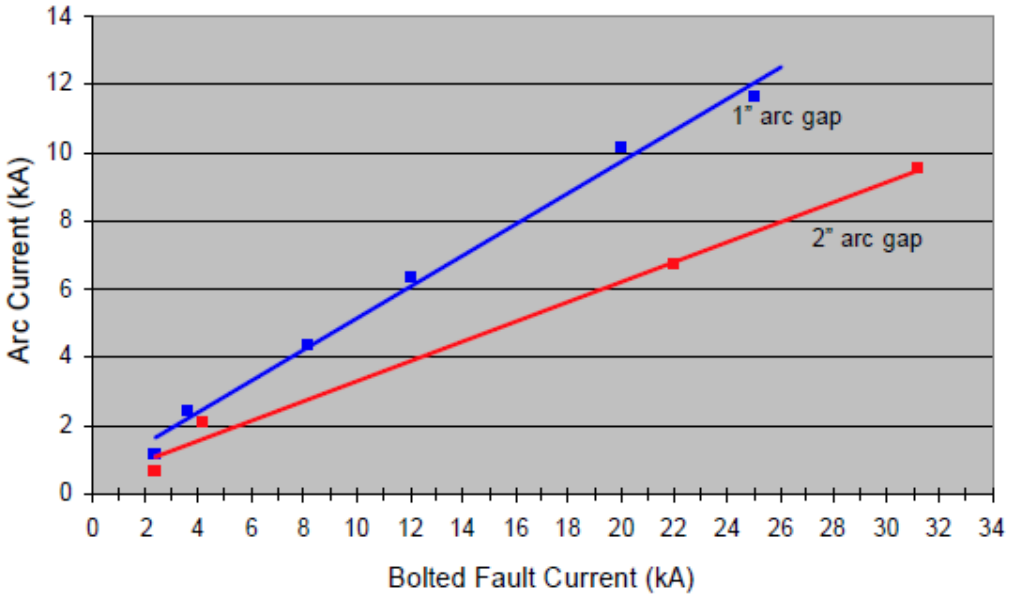

Figure 3-11 Bruce Power DC Arc Test Bolted Fault Current vs. Arc Current

3.2 MHD Modeling of DC Arc

Unlike the historical semi-empirical DC arc models, this dissertation studies and models the DC arc in the power system from the physical point of view. This section presents the assumptions, numerical model, simulation flow chart, computational grids, relevant boundary conditions of a DC electric arc numerical MHD model, and simulation results.

3.2.1 Model Assumptions

This dissertation utilized the computational fluid dynamic software *Code Saturne*® *v. 3.0,* electric arc module [58], developed by the Electricity of France (EDF), to simulate the DC electric arc. The model assumptions provided in this section are based on the theory guide of the *Code Saturne*® [74], these assumptions are commonly used in MHD modeling [55].

This model is based on a magnetohydrodynamic approach (MHD) and coupled with the Navier-Stokes equations for a non-isothermal fluid (air) with the Maxwell equations of electromagnetic fields. Recently, the MHD approach has been considered as one of the best methods to simulate the electric arc burn in the open air [53-54]. The three dimensional model of the DC electric arc is based on the following commonly used assumptions [55]. First, the plasma is considered as a continuous fluid (air) and at Local Thermodynamic Equilibrium (LTE) to reduce the computational burden. Second, the gas is incompressible. In fluid dynamics, the Mach number is a dimensionless quantity representing the ratio of flow velocity past a boundary to local speed of sound. Since the Mach number is a posteriori confirmed always less than 0.3, the gas can be considered as incompressible. Third, the gas flow is laminar and time dependent. This dissertation simulates the electric arc burns in open air, so the Reynolds number is less than 2000 and laminar flow is commonly assumed for the electric arc zone [54-57]. Fourth, the magnitude of gas pressure

is much higher than the magnetic pressure after electric is generated [75-77], so the plasma beta, the ratio of gas pressure to magnetic pressure, is much greater than 1. Fifth, the inductive currents are neglected since there is no power frequency in DC and its ripple is relative small.

3.2.2 Numerical Model

The fluid equations are expressed in a conservative form as a balance of accumulation, net flux by convection, diffusion and net production. The time dependent fluid conservation set of equations can be described as below. The mass conservation equation is represented in (3-10), where ρ and $\vec{u}$ are the mass density in kg/m^3 and the velocity vector in m/s, respectively.

$$\frac{\partial \rho}{\partial t} + \vec{\nabla} \bullet \rho \vec{u} = 0 \tag{3-10}$$

The momentum conservation equation is given as in (3-11), where p, τ , $\vec{J}$, and $\vec{B}$ are pressure in Pa, shear stress tensor, current density vector in A/m^2, and magnetic field vector in Tesla. The term $\vec{J} \wedge \vec{B}$ indicates the Lorentz force induced by the circulation of the electric current in the plasma flow.

$$\frac{\partial \rho \vec{u}}{\partial t} + \vec{\nabla} \bullet \left(\rho \vec{u} \otimes \vec{u} - p + \bar{\bar{\tau}} \right) = \vec{J} \wedge \vec{B} \tag{3-11}$$

The energy conservation equation is listed as in (3-12), where h, λ, C_P, and $\vec{E}$ are gas enthalpy in Joule, thermal conductivity in W/m/K, specific heat in J/kg/K, electric field vector in V/m, respectively. The term $\vec{J} \bullet \vec{E}$ represents the Joule effect resulted from the passage of the electric current through the resistive plasma.

$$\frac{\partial \rho h}{\partial t} + \vec{\nabla} \bullet \left(\rho \vec{u} h - \frac{\lambda}{C_P} \vec{\nabla} h \right) = \vec{J} \bullet \vec{E} \tag{3-12}$$

The ideal gas law and the relationship between enthalpy and temperature for ideal gas are provided as in (3-13 to 3-14), where *p, ρ, R, T* are the pressure of gas in Pa, the mass density in kg/m3, specific gas constant for air in J/kg/K, and temperature in K.

$$p = \rho RT \tag{3-13}$$

$$h = C_P T \tag{3-14}$$

With the simplified Ohm's law approximation and electrical global neutrality, the set of Maxwell's equation is shown in (3-15 to 3-19), where *σ, φ, μ_0*, and $\vec{A}$ are electrical conductivity in S/m, electrical potential in J, vacuum permeability, and vector potential in V·s/m, respectively.

$$\vec{J} = \sigma \vec{E} \tag{3-15}$$

$$\vec{E} = -\vec{\nabla}\varphi \tag{3-16}$$

$$\vec{\nabla} \bullet \vec{J} = \vec{\nabla} \bullet \left(\sigma \vec{\nabla} \varphi \right) = 0 \tag{3-17}$$

$$\vec{B} = \vec{\nabla} \wedge \vec{A} \tag{3-18}$$

$$\vec{\nabla} \bullet \vec{\nabla} \vec{A} = -\mu_0 \vec{J} \tag{3-19}$$

3.2.3 Simulation Flow Chart

The DC electric arc simulation described in this dissertation is based on the computational fluid dynamic software *Code Saturne® v. 3.0,* electric arc module, which is developed by the Electricity of France (EDF) [58]. The summary of the electric arc module simulation flow chart is illustrated in Figure 3-12, and the variables for *Code Saturne* are listed in Table 3-3. The calculation procedure is illustrated as follows:

- Form the file of the physical properties which serves as the basis for calculating the entire field at the beginning of each time step.

- Solve the physical equations based on the imposed boundary of the computational domain. Then, the software begins by solving the equation of the amount of movement, the speed and the pressure are deduced with the conservation of mass.
- Solve the energy conservation equation to obtain the mass enthalpy.
- Obtain the electric potential by solving the current conservation.
- Acquire the electric physical properties, electric field, current density, magnetic vector potential, and magnetic field through Maxwell equations and Ohm's law

This software can also simulate some physical phenomena of plasma, such as the Lorentz force exerted on plasma and the Joule effect.

Table 3-3 Variables for *Code Saturne*

Variable	***Definition***	***Variable***	***Definition***
ρ	Mass density	$\vec{u}$	Velocity vector
p	Pressure	τ	Shear stress tensor
h	Gas enthalpy	$\vec{J}$	Current density
λ	Thermal conductivity	$\vec{B}$	Magnetic Field
C_P	Specific heat	$\vec{E}$	Electric field
σ	Electrical conductivity	$\vec{A}$	Vector potential
φ	Electrical potential	μ_0	Vacuum permeability

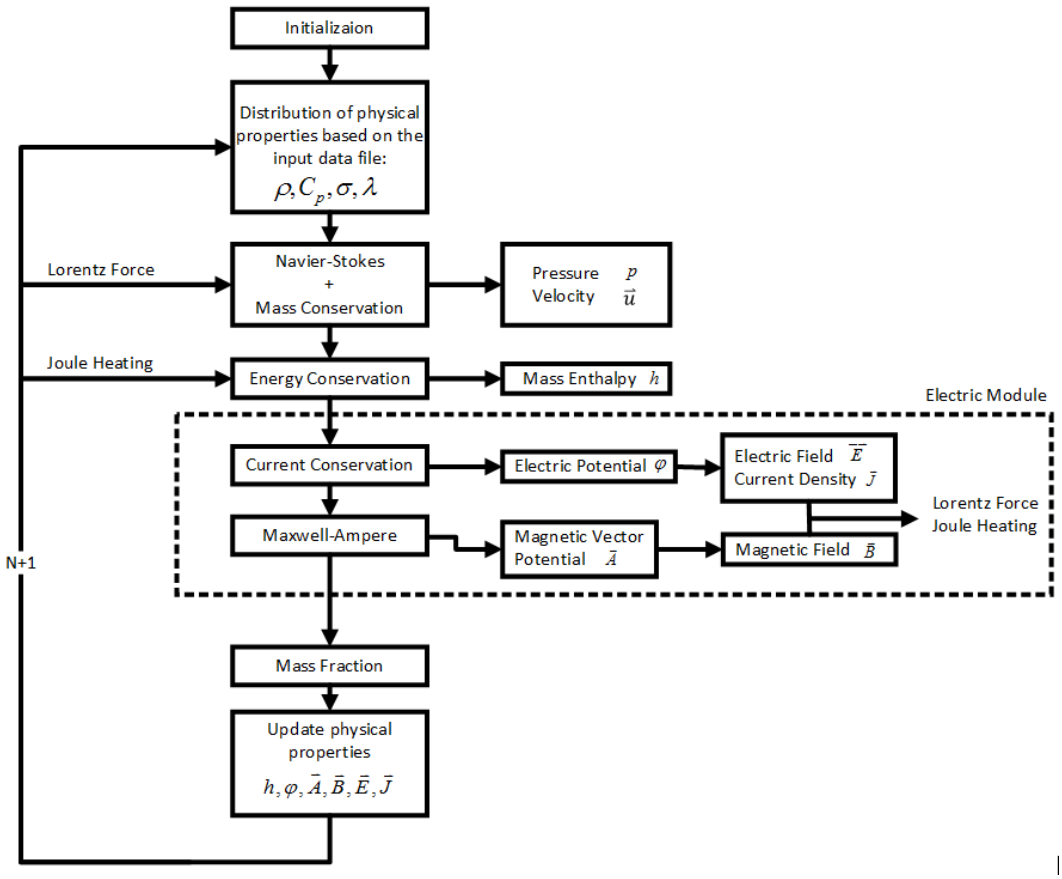

Figure 3-12 Simulation Flow for *Code Saturne*

3.2.4 Computational Grid

A typical example of a DC electric arc computational grid is shown in Figure 3-13. Similar procedures can be applied on other configurations and fault conditions. The grid mesh is created by the software *Salome 6*©. The computational domain refers to the functional fluid area of the arc's evolution. Since the simulation of the entire 3D reactor is computationally taxing, a non-uniform hexahedral mesh is used for all the areas of the computational domain, and the mesh is refined in the vicinity of the electrodes gap to balance between the accuracy and the computational burden. The gap between two

electrodes is 1 inch; the length and radius of the electrode are 4 inches and 0.5 inches, respectively. The depth and width of the computational domain are both 10 inches.

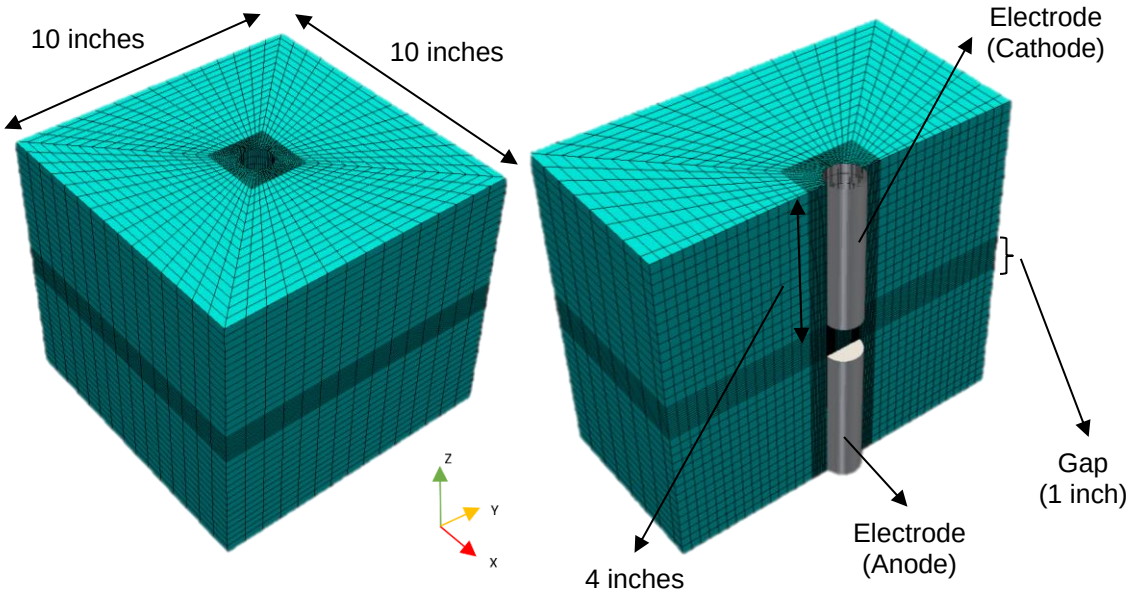

Figure 3-13 Computational Grid Example (Entire View and Cross Section View)

3.2.5 Boundary Conditions

The boundary conditions of this example are detailed and shown in Figure 3-14 and Table 3-4. Since this example simulates the free burning of the vertical arc in open air, there is no inlet velocity, and atmospheric pressure is imposed at the outlet. Regarding the thermal conditions, the sublimation temperature of the electrodes is imposed at the electrodes tip as the initial conditions for the simulation (4000K for graphite electrodes and 2900K for copper electrodes) [59-60]. The boundary conditions for copper electrodes are shown in Table 3-4.

Table 3-4 Boundary Conditions

Zone	***Pressure (atm)***	***Temperature (K)***	***Velocity (m/s)***	***φ (V)***	***$\vec{A}$ (T.m)***
Outlets (AB, CD, EF, GH, AE, DH)	1	$\frac{\partial T}{\partial n}=0$	$\frac{\partial u}{\partial n}=0$	$\frac{\partial \varphi}{\partial n}=0$	0
Electrode (Cathode) (BCIJ)	$\frac{\partial P}{\partial n}=0$	2900K on the tip, else $\frac{\partial T}{\partial n}=0$	0	0	$\frac{\partial \vec{A}}{\partial n}=0$
Electrode (Anode) (KLFG)	$\frac{\partial P}{\partial n}=0$	2900K on the tip, else $\frac{\partial T}{\partial n}=0$	0	System Voltage	$\frac{\partial \vec{A}}{\partial n}=0$

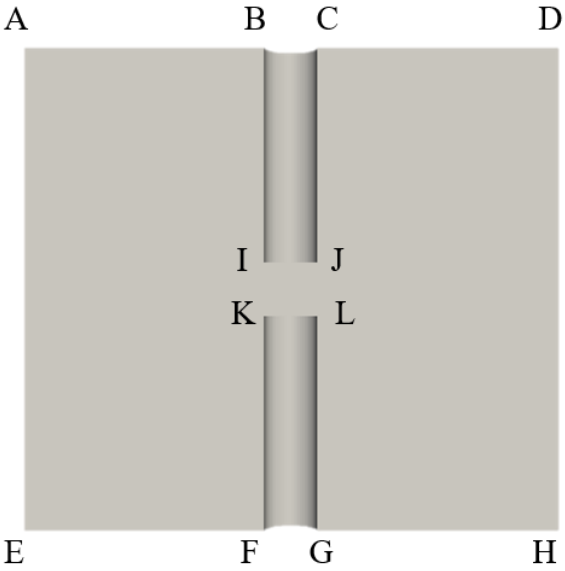

Figure 3-14 Cross Section View of the Computational Domain and Boundaries

3.2.6 Simulation Results

The 3D transient model of the DC electric arc was simulated by using the software *Code Saturne*® v. 3.0, electric arc module [58]. The time step of the simulation is 5μs, which has been shown to be a reasonable computation time for the electric arc modeling [61-62].

3.2.6.1 Case 1: System Voltage: 260V, Bolted Faulted Current: 11600A, Gap: 25.4mm

The simulation results provided in this section considered system voltage and arc current to be 260V and 5900A, respectively to match the conditions of the high current DC arc test from Kinetrics laboratory [52]. The total simulation time is 100ms, and the initialization of the simulation takes the first 1000 iterations (5ms). In order to ignite the first arcs at the first time step, a hot zone at 6000K is artificially implemented between the electrodes, and the current is set ramping from 5A to the target current (6010A) in 5ms.

The dynamic evolution of the post-discharge electric arc flow is shown as from Figure 3-15 to Figure 3-18. The arcs are represented with three different temperature iso-surfaces (2000, 6000, and 13000K) colored according to the temperature level in the color map. In the beginning, due to the surrounding gas pressure, the initial hot zone moves toward the torch outlet, as shown in the Figure 3-15. The temperature in this hot region is a privileged area for arc discharge; the initial hot zone shape is similar to Figure 3-5. The arc is generated as shown in Figure 3-16. Once the arc is generated, as shown in Figure 3-17, the Lorentz force will produce arc curvature. The Figure 3-18 shows the arc behavior at 100ms, which also illustrates the hot air expansion of the vertical arc burning in the open air.

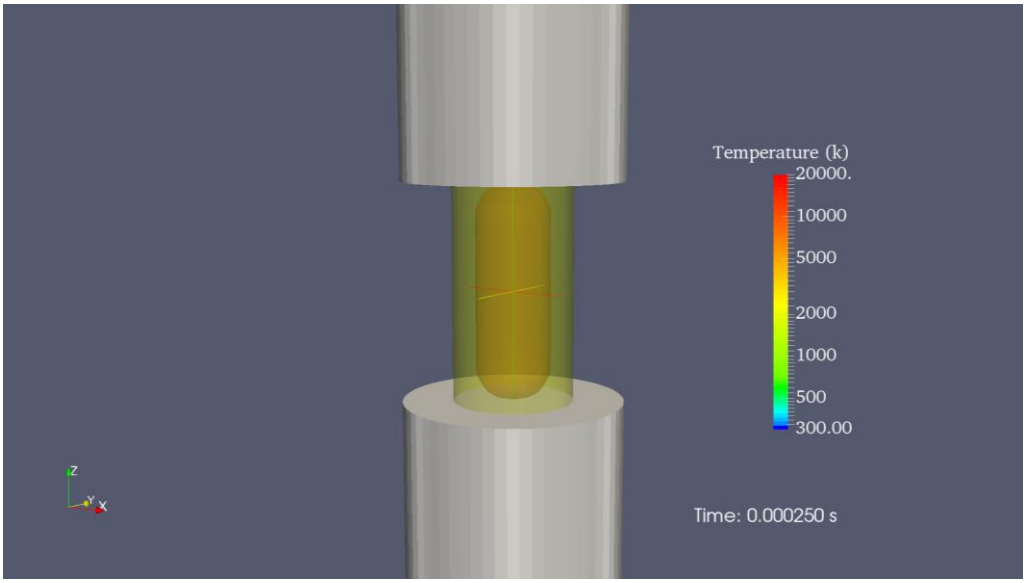

Figure 3-15 Electric Arc Evolution Moment (t=0.25ms)

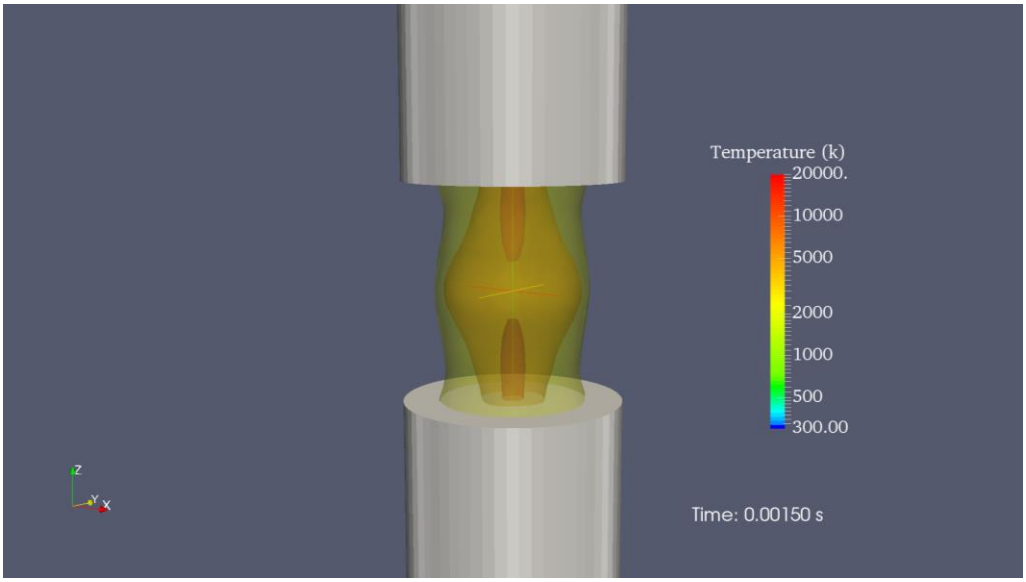

Figure 3-16 Electric Arc Evolution Moment (t=1.5ms)

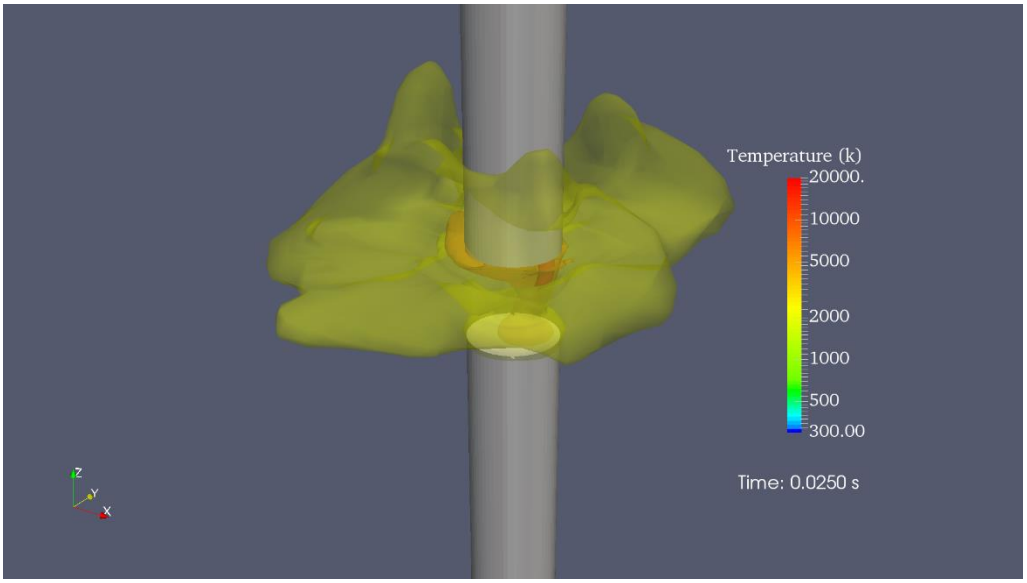

Figure 3-17 Electric Arc Evolution Moment (t=25ms)

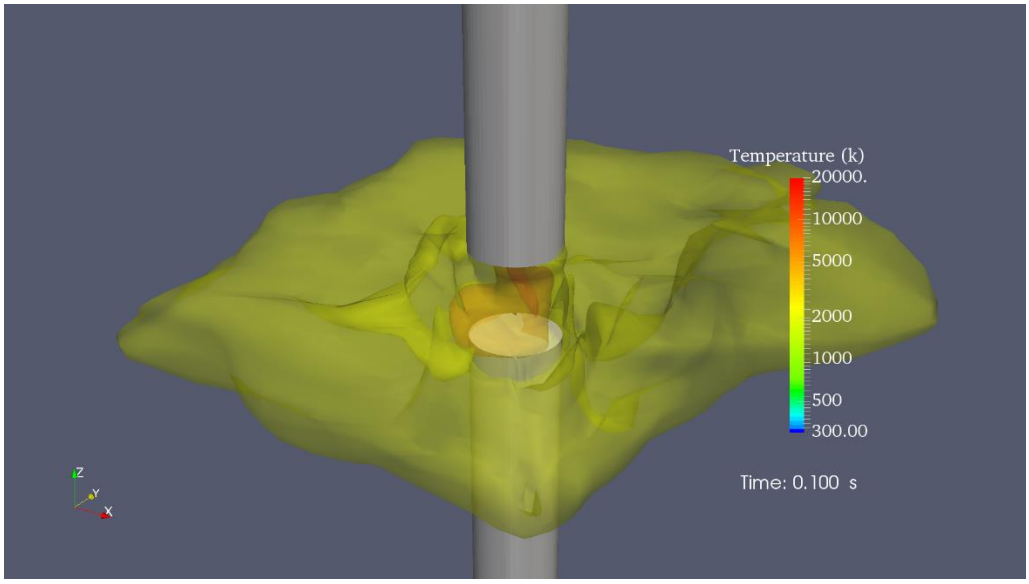

Figure 3-18 Electric Arc Evolution Moment (t=100ms)

The origin of the arc motion is due to the combination of magnetic and hydrodynamic forces. Figure 3-19 shows the jet interaction producing a radial mass expulsion in all directions. The Lorentz force will have a strong influence on the arc motion.

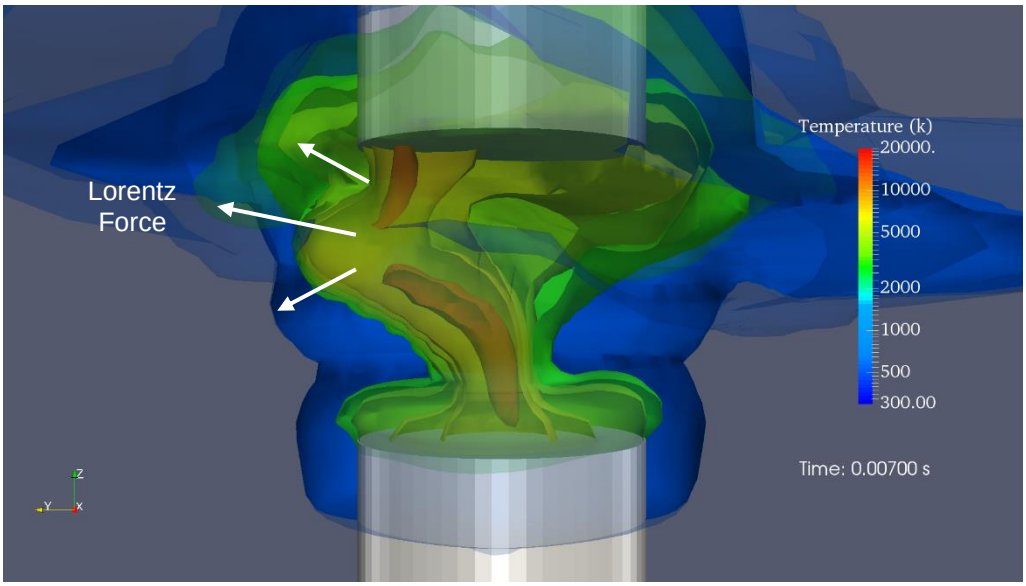

Figure 3-19 Temperature Iso-surface of an Electric Arc between Two Electrodes

The simulation results have been verified by comparing with previous experiment results, as shown in Table 3-5.

Table 3-5 Arcing Fault Data (Vs=260V, Bolted Fault Current=11600A, Gap=25.4mm)

Description	***Arc Current (Amps)***	***Arc Voltage (Volts)***	***Arc Power (kW)***
Bruce Power DC Arc Test [52]	5354	140.7	749.54
Theoretical Method [63] (Maximum Power Method)	5800	130	754
Iterative Method [46] (Stokes and Oppendlander)	7249	97.52	706.92
MHD Simulation	6010	121.6	730.82

3.2.6.2 Case 2: System Voltage: 480V, Bolted Faulted Current: 21744A, Gap: 1 inch

The simulation provided in this section comparing the simulation results with the high current arc test from KEMA high current laboratory [64]. The system voltage, the gap between two electrodes and bolted fault current are 480V, 1 inch, and 21.74kA respectively. Though the test performed in the KEMA high current laboratory is an AC arc flash test and it is not exactly the same as DC arc testing, the arc discharge between single phase AC and DC are quite similar in the arc initialization stage.

Figure 3-20 shows the arc test with vertical metal electrodes performed in the open configuration. This configuration is usually described as Faraday Cage or Faraday Shield Structure, the 3-D view of Faraday Cage is shown as Figure 3-21. Using the Faraday Cage in the testing provides the bench mark results of the arc flash phenomena which will be the base for model development. The assumption of the proposed 3D DC arc simulation matches the arc discharge within the Faraday cage and will be beneficial to improve the accuracy of model development

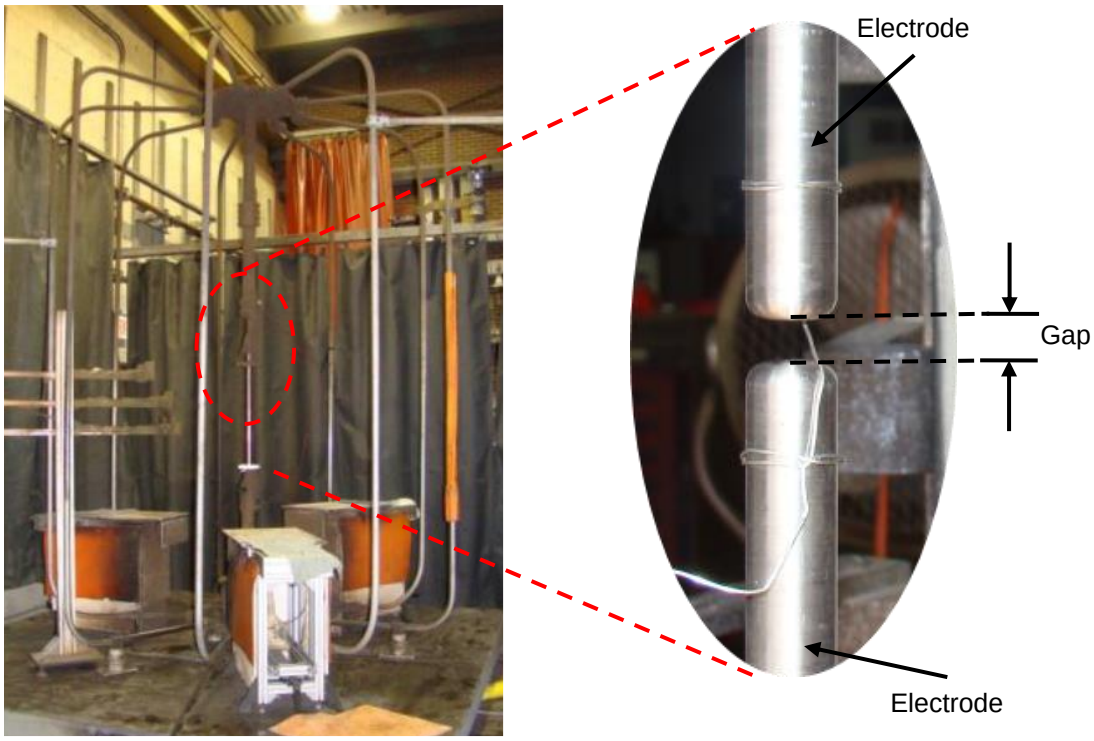

Figure 3-20 Faraday Cage Arc Flash Test

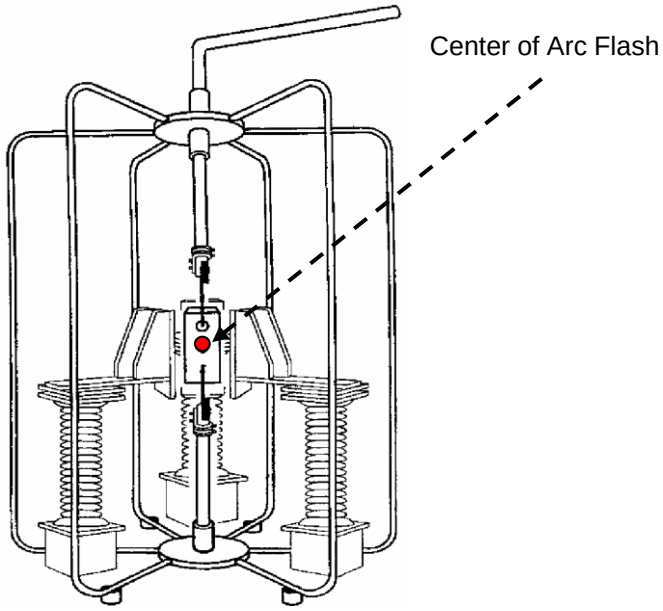

Figure 3-21 3-D View of Faraday Cage

Figure 3-22 compares the dynamic evolution of the post-discharge electric arc flow between the real arc flash test and the simulation, and the comparison between simulations and real arc flash test is given in Table 3-6.

Table 3-6 Arcing Fault Data (Vs=480V, Bolted Fault Current=21744A, Gap=1 inch)

Description	***Arc Current (Amps)***	***Arc Voltage (Volts)***	***Arc Power (kW)***
KEMA Arc Test [64]	15.81	131	2.071
Theoretical Method [63] (Maximum Power Method)	10.872	240	2.609
Iterative Method [46] (Stokes and Oppendlander)	16.89	107.25	1.811
MHD Simulation	16.00	126.76	2.028

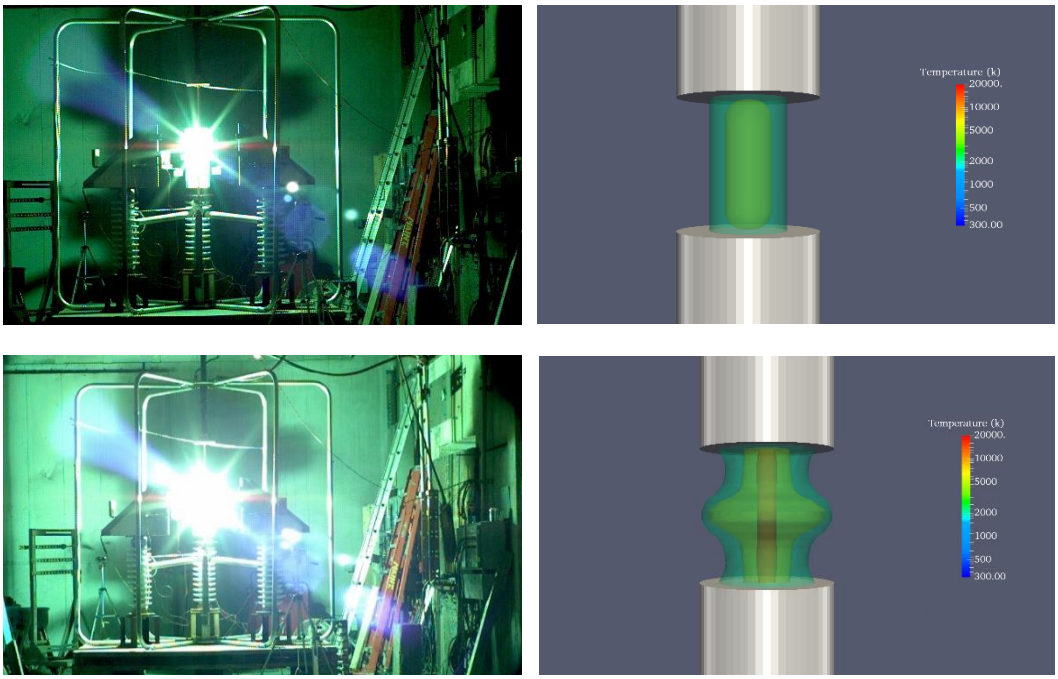

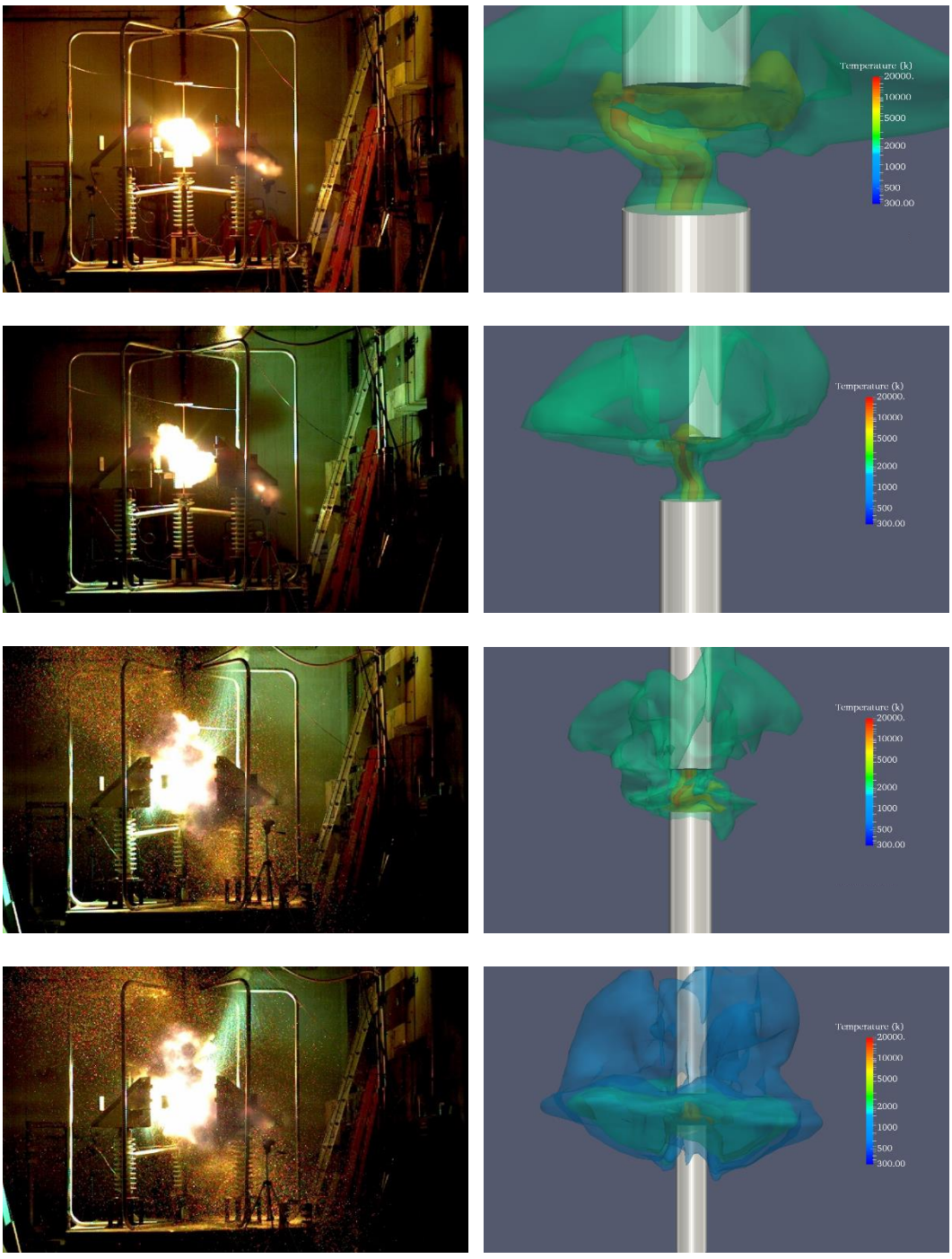

Figure 3-22 Arc Evolution for Different Moments

3.3 Summary

Historically, DC arc energy predictions are obtained through either the theoretical method or the semi-empirical method. The estimation results obtained from theoretical approaches overall produce the estimation on the conservative side, sometime it may overestimate the DC arc energy. Semi-empirical models based on early works have limited test results that depend on electrode materials, the gap width, gas specifics, etc. Thus the semi-empirical models may not be suitable to estimate all DC arcs in a power system.

This dissertation presents a MHD numerical model to simulate DC electric arc by using the CFD software *Code Saturne*® that uses the SOLU (Second Order Linear Upwind) scheme and a fractional step method. The example of the simulation results show that the proposed approach in this dissertation provides an innovative method to study the DC arc energy in power system.

Chapter 4

DC Arc Model Based on 3D DC Arc Simulation

4.1 Literature Reviews

The possibility for DC arc flash events has increased with the broader application of photovoltaic arrays and DC buses in power systems. However, modeling and testing for DC arc hazard assessment are limited. There are four common DC arc models used to estimate the DC arc flash in power systems, which are summarized in Table 4-1, where I_{bf} and I_{arc} are the bolted fault current and arcing current in kilo-amperes for equation (4-3), and in amperes for equation (4-2) and *L* and *G* is the gap width in millimeters and inches respectively. The detail review of these DC arc models is provided in [65].

The theoretical model, referred by the latest NFPA 70E [16], is derived based on the maximum power transfer theorem, which may provide an arc flash estimation on the relative conservative side. Besides, this model cannot be used with nonlinear systems such as photovoltaic (PV) systems due to its nonlinear *I-V* characteristics [66].

Table 4-1 Commonly Used DC Arc Models

DC Arc Model	***Description***
Theoretical Model [48,63]	$V_{arc} = 0.5V_s$ $I_{arc} = 0.5I_{bf}$ (4-1)
Ammerman's Model [67]	$V_{arc} = (20 + 0.534L)I_{arc}^{0.12}$ (4-2)
Commercial Software [68]	A commercial software, verified by Bruce Power arc flash tests [52]
600-V open air [69]	$I_{arc} = 0.9063 \bullet I_{bf}^{0.8927} - 0.1051 \bullet e^{0.1093 I_{bf}} \bullet (G-1)$ (4-3)

Ammerman's DC arc model, the mathematical model of Stoke and Oppenlander [46], is cited by the latest NFPA 70E 2015 edition [16]. It can be considered as the most complete DC arc model, because it covers broader ranges and provides more accurate estimations than other DC arc models. Similarly with other DC arc models, Ammerman's DC arc model considers arcing voltage to have almost linear relationship with gap width; however, practically, the arcing voltage is determined by the arc length [26,35,49]. A commercial software package [68], mainly for AC arc analysis, has been modified to include DC arc study based upon the assumption that it exists 1D temperature field inside the arc and using finite difference method to solve electric field and temperature. Its results were verified based on arc flash tests performed in Bruce Power [52]. The 600-V open air DC arc model is derived based on 125V and 250V DC systems [69].

In order to provide more accurate estimations of DC arc flash in modern power systems, a new DC arc model is necessary to overcome the limitations of previous models. This dissertation proposes a new DC arc model based on the 3D Magnetohydrodynamic (MHD) modeling of a DC electric arc mentioned in Chapter 3.

4.2 Proposed New DC Arc Model

From the system protection point of view, the accurate estimation of arcing current is very important because the arcing current determines the operating time of the protective device, which will have significant influences on the incident energy estimation, because both the arcing current and arc duration time are critical components of the incident energy during arc flash event.

Currently, most of the DC arc models are derived from a few available DC arc tests, which may not be adequate to estimate arc flash in the commonly used DC power system. In order to provide a more accurate DC arc model, conducting more DC arc tests is necessary; however, performing real DC arc tests is not only time consuming but also

limited by the scale of the laboratories. Thus, this section presents a new DC arc model based on the simulations that can provide comparable results with the available lab testing. The new DC arc model provided in this dissertation covers the system voltage range from 100V to 1500V, bolted fault currents range from 0.5 to 25kA, and the gaps range from 0.25 to 3 inch.

4.2.1 Modeling Parameters Sensitivity Analysis

The first step of DC arc model development is to study the correlation between dependent and independent variables through parameter identification. The 325V DC arc simulation results are provided in Figure 4-1 and Figure 4-2. Figure 4-1 reveals that along with the increase of the arc current, the amount of arc voltage change in large gap is greater than the small gap. Apparently, the arc voltage increases consistently in different arc currents while the gap width increases, because all the lines have the similar shape in Figure 4-2. According to Figure 4-1 and Figure 4-2, gap width contributes more significantly to arc voltage than arc current.

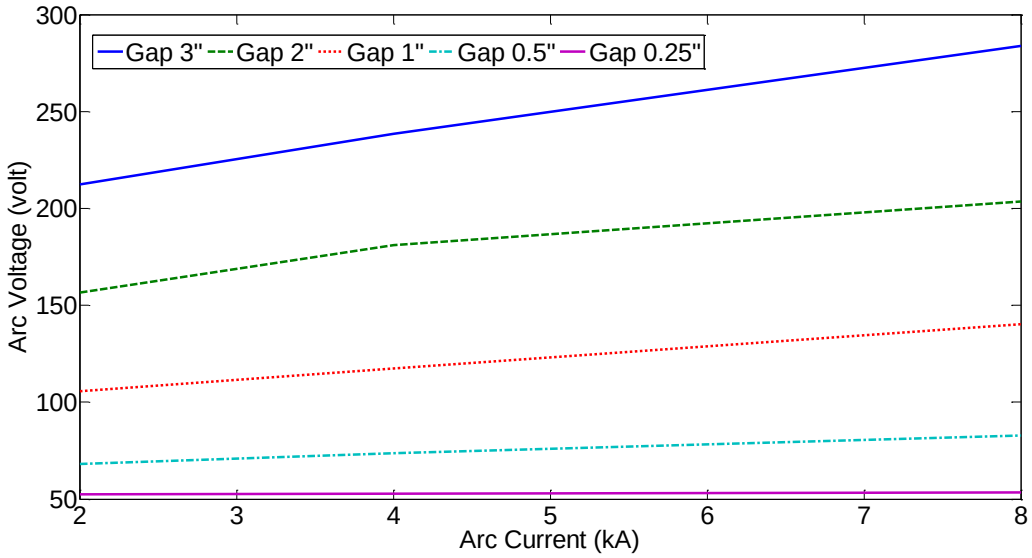

Figure 4-1 DC Arc Simulation Results (325V, V_{arc} vs. I_{arc})

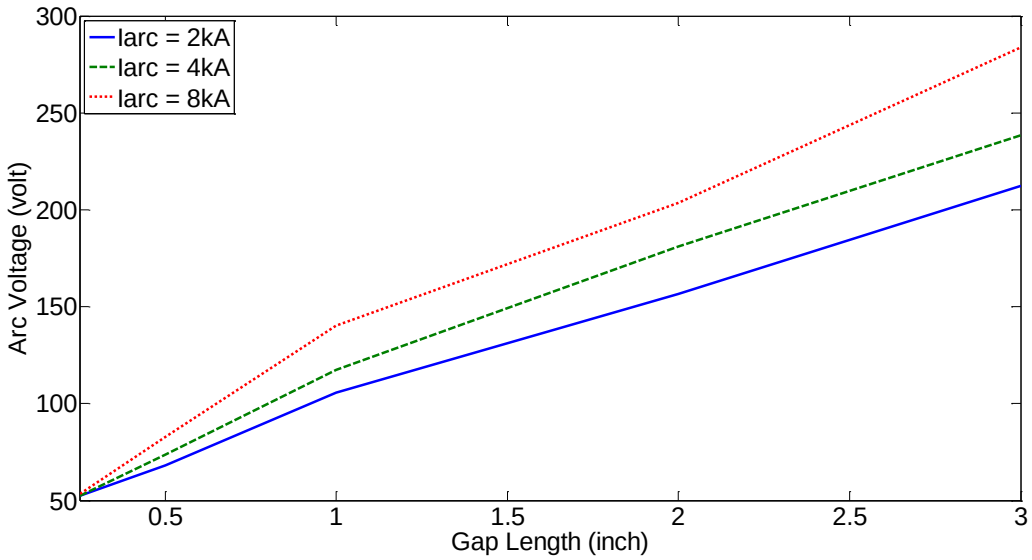

Figure 4-2 DC Arc Simulation Results (325V, V_{arc} vs. *Gap*)

Statistical approaches have been utilized in this dissertation to analyze parameter sensitivity to arc voltage. The single variable linear regression is capable of providing the response indication of the nature of the relationship between a dependent variable and independent variables; however, multiple independent variables may interact with each other to affect the dependent variable and complicate the analysis. Thus, this dissertation applies partial regression analysis to study the impact of adding a variable to a model including independent variables due to consider the effect among other independent variables in model [21]. Figure 4-3 and Figure 4-4 are the partial regression plots on arc voltage modeling process. Figure 4-3 and Figure 4-4 indicate the dependence between gap width and arc current with arc voltage respectively.

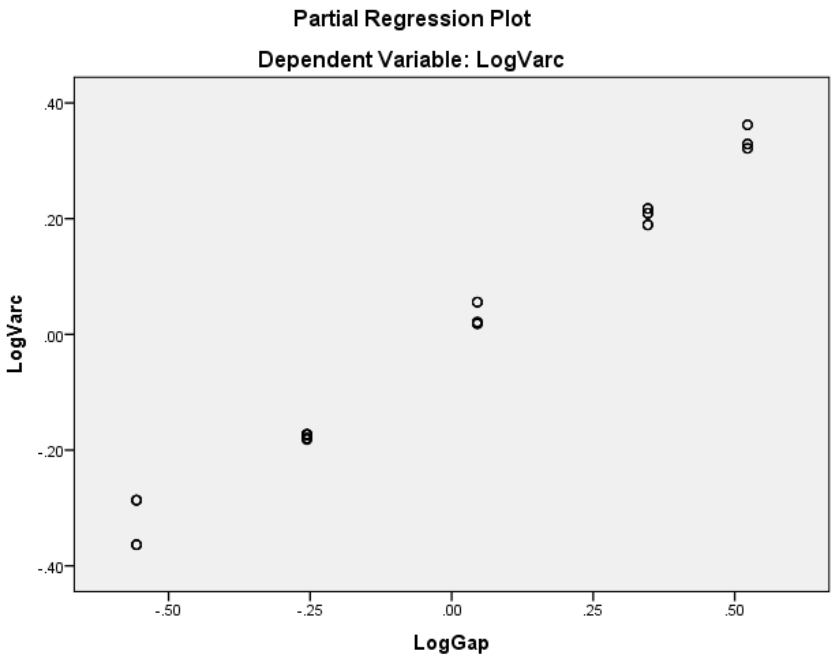

Figure 4-3 Partial Regression Plot (V_{arc} vs. *Gap*)

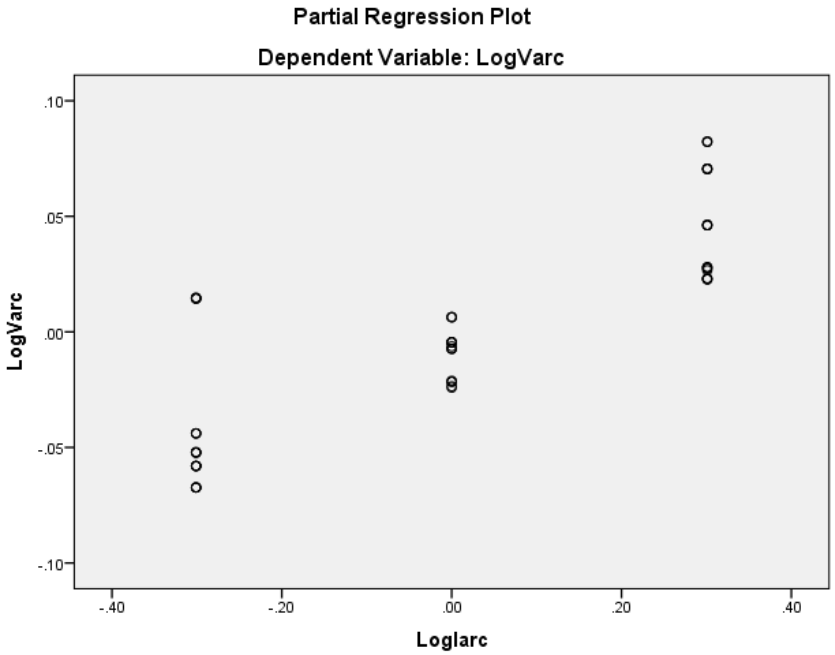

Figure 4-4 Partial Regression Plot (V_{arc} vs. I_{arc})

Observably, the plots illustrate good linearization performance between dependent variables (I_{arc}, and *Gap*) and independent variable (V_{arc}), which means that the dependent variables are influenced by partial regression coefficients significantly. The increasing trend indicates the positive correlation between independent variable and dependent variables. In addition, by comparing with Figure 4-3 and Figure 4-4, it is revealed that the gap width has a stronger positive correlation with arc voltage than arc current.

4.2.2 New DC Arc Model

According to Table 4-1, currently, all available DC arc models consider the arcing voltage for DC arc owning the nonlinear relationship with arcing current but almost linear relationship with the gap. However, in reality, the arcing voltage should be determined by the length of electric arc, and the arc length will be affected by the Lorentz force during the electric discharge flow. Thus, the accuracy of arcing voltage estimation can be improved significantly by imposing its nonlinear relationship with the gap width.

In the DC arc test, the precise measurement of arc length is difficult to achieve, so it has been historically difficult to consider the arc length while deriving DC arc models. Fortunately, the 3D MHD modeling of DC electric is able to simulate the arc length in different fault conditions, which provides an innovative method to study the DC electric arc by considering the arc length instead of gap width while developing the new DC arc model. Figure 4-5 and Figure 4-6 show the arc length in the DC arc simulation under different fault conditions, where Figure 4-5 simulation the DC arc at system voltage, bolted fault current, and the gap width are equal to 1500V, 10kA, and 3inchs, respectively. Figure 4-6 shows the arc length under the arcing fault condition, system voltage is 1500V, bolted fault current is 11.6kA, and the gap between two electrodes is 1 inch.

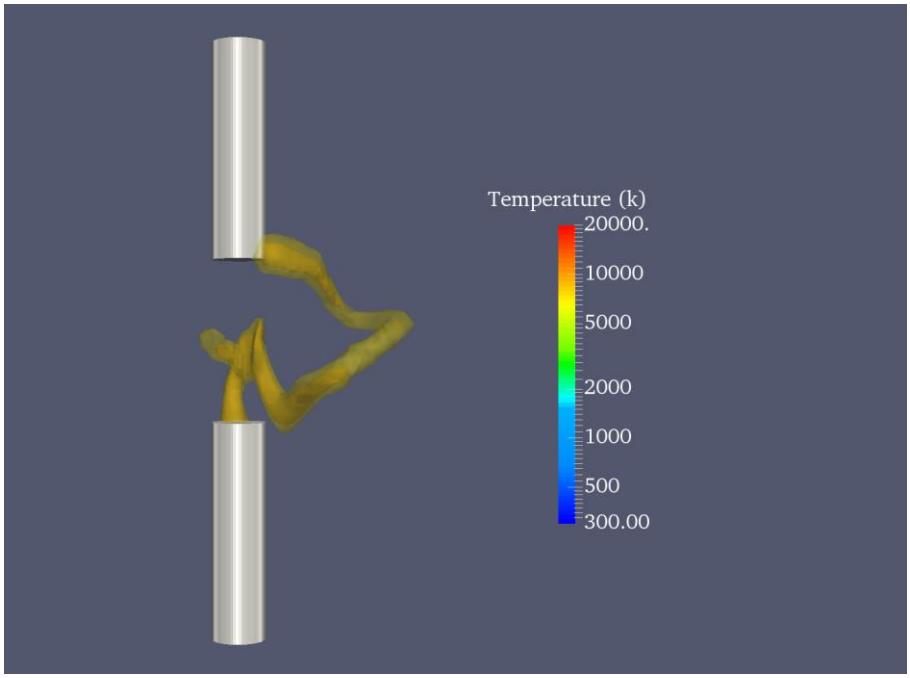

Figure 4-5 Arc Length in DC Arc Simulation (3” Gap)

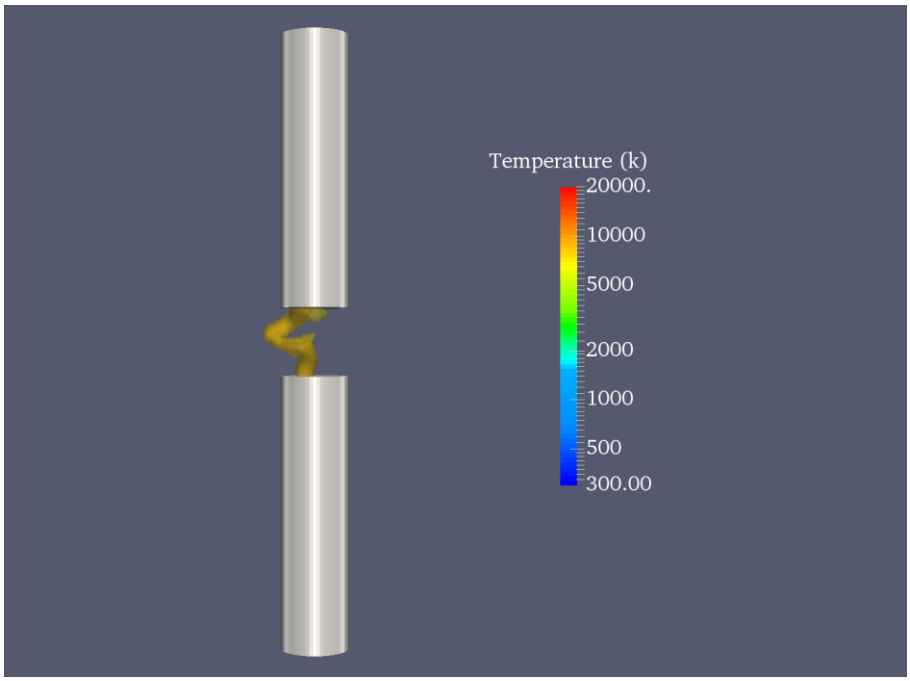

Figure 4-6 Arc Length in DC Arc Simulation (1” Gap)

The new DC arc model based on the 3D MHD electric arc simulation results. Since the electric arc owns the inverse *V-I* characteristic when the arc current is below the transition current, similar with Ammerman's model, the proposed new DC arc model is only valid when the arc current is above the transition current. The transition current is defined by Stokes & Oppenlander paper [46] and also described in Ammerman DC's model [67]. The transition current is given in (4-4), where I_t is the transition current in ampere, L is gap width in millimeters.

$$I_t = 10 + 0.2L \tag{4-4}$$

For the arc current above the transition point, the arc voltage is provided in (4-5), where V_{arc} is the arcing voltage in volt, L is the gap width in millimeters, and I_{arc} is the arcing current in ampere, and the arc resistance and corresponding arc power are given in (4-6) and (4-7), repressively.

$$V_{arc} = (13.11 + 0.287L^{1.238})I_{arc}^{0.154} \tag{4-5}$$

$$R_{arc} = (13.11 + 0.287L^{1.238})I_{arc}^{-0.846} \tag{4-6}$$

$$P_{arc} = I_{arc}^2 \times R_{arc} \tag{4-7}$$

Differing with previous DC arc models, the new DC arc model considers the arcing voltage to have a nonlinear relationship with both arcing current and the gap width. The DC arc model proposed in this dissertation uses the nonlinear term of gap width to represent the influence of real arc length on arcing voltage. The constant term in (4-5) expresses the voltage drop at the electrodes. According to the early DC arc studies, the voltage drop at the electrode remained practically constant and measured 20 to 40 volts

for different material of electrodes [70-71]. Besides, the equation (4-5) indicates that both the gap width and arc current have positive correlation with arc voltage.

The comparison between the estimation results from different DC arc models and DC arc tests are listed as from Table 4-2 to Table 4-4, which reveals that the new DC arc model provides more accurate estimation results than historical DC arc model.

Table 4-2 Bruce Power DC Arc Test (Vs=260V, Bolted Fault Current=2370A, Gap=25.4mm)

Description	***Arc Current (Amps)***	***Arc Voltage (Volts)***	***Arc Power (kW)***
DC Arc Test [52]	1504	95	143
Theoretical Method [63]	1185	130	154
Ammerman's Model [67]	1627	81.51	133
600-V DC Arc Model [69]	1958	45.20	89
New DC Arc Model	1554	89.47	139

Table 4-3 Bruce Power DC Arc Test (Vs=260V, Bolted Fault Current=11600A, Gap=25.4mm)

Description	***Arc Current (Amps)***	***Arc Voltage (Volts)***	***Arc Power (kW)***
DC Arc Test [52]	5354	140	750
Theoretical Method [63]	5800	130	754
Ammerman's Model [67]	7249	97.52	707
600-V DC Arc Model [69]	8082	78.85	637
New DC Arc Model	6611	111.82	739

Table 4-4 Dr. Hall's Arc Test (Vs=325V, Bolted Fault Current=1800A, Gap=9.525mm)

Description	***Arc Current (Amps)***	***Arc Voltage (Volts)***	***Arc Power (kW)***
DC Arc Test [51]	1500	50	75
Theoretical Method [63]	900	162.5	146
Ammerman's Model [67]	1467	60.17	88
600-V DC Arc Model [69]	1612	83.26	134
New DC Arc Model	1496	54.83	82

Figure 4-7 to Figure 4-9 and Table 4-5 provide more comparison between DC arc models and DC arc testing performed in two voltages, 130 volts and 260 volts [52, 80]. The proposed new DC arc model improve the predicting arc currents specifically for higher arc currents.

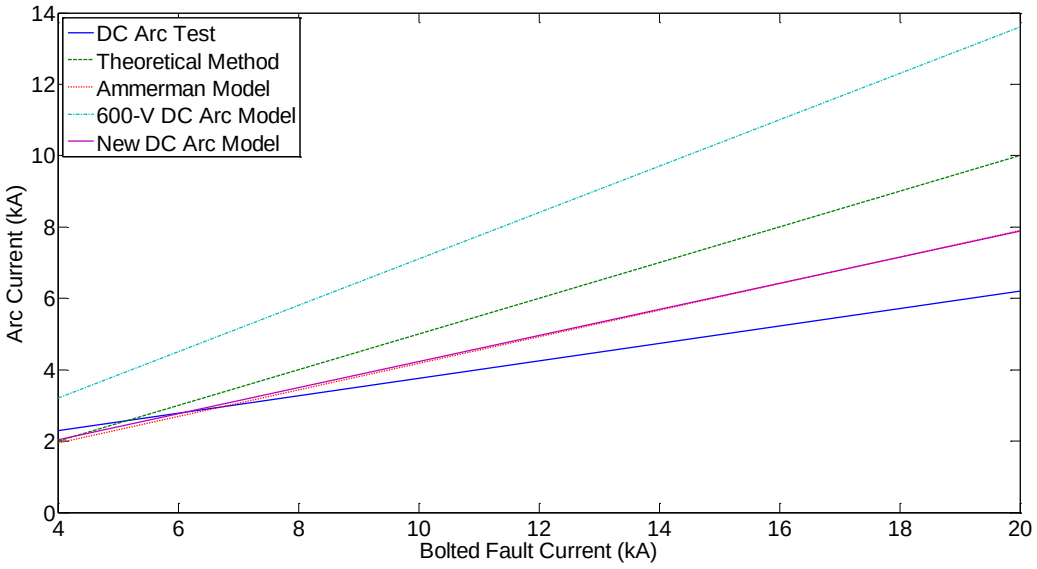

Figure 4-7 130 Volt Testing (0.5" Gap)

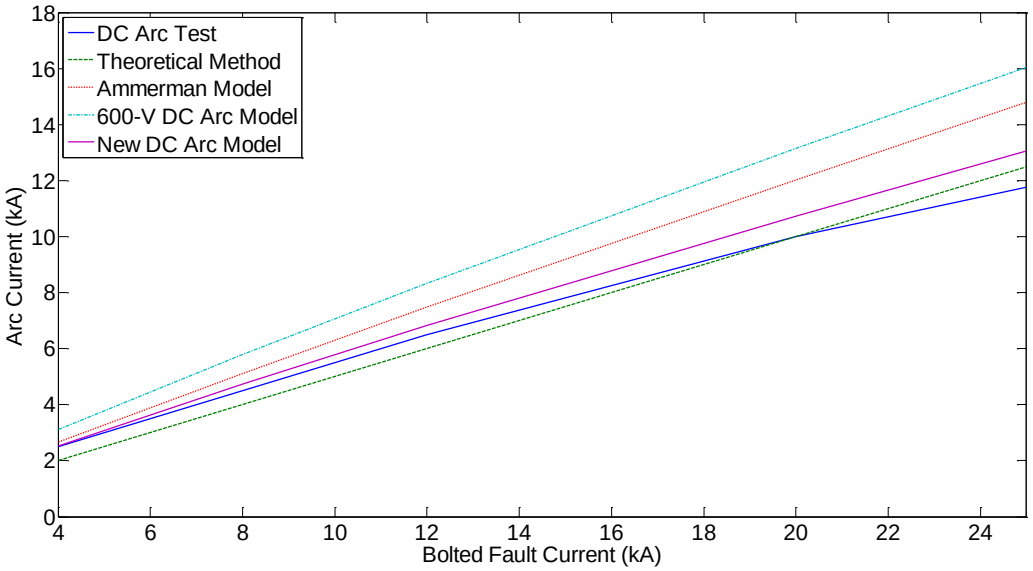

Figure 4-8 260 Volt Testing (1” Gap)

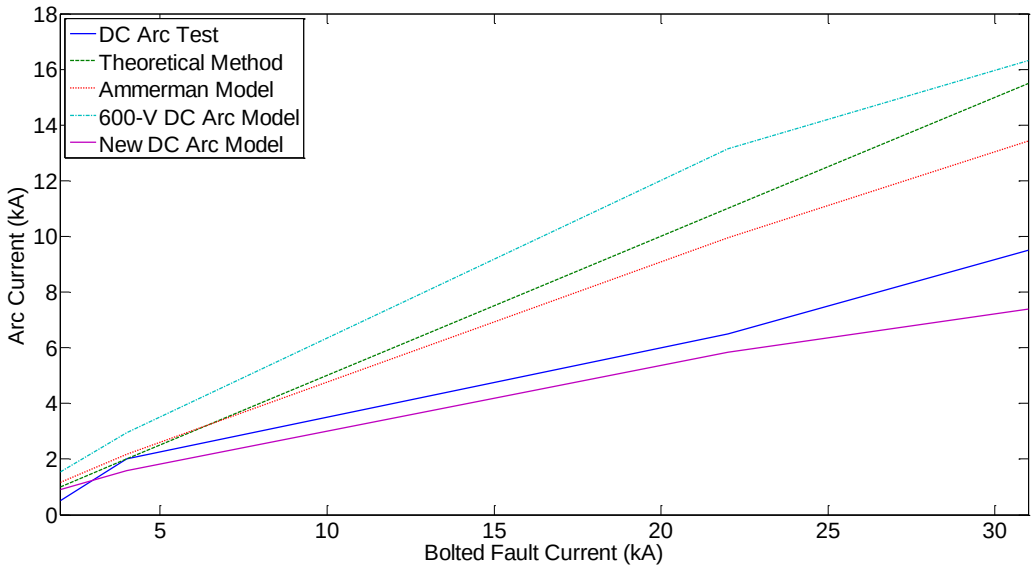

Figure 4-9 260 Volt Testing (2” Gap)

Table 4-5 Test Data VS. Calculated Arc Current

System Voltage (V)	*Bolted Fault Current (kA)*	*Gap (inch)*	*Iarc[1] (kA)*	*Iarc[2] (kA)*	*Iarc[3] (kA)*	*Iarc[4] (kA)*	*Iarc[5] (kA)*
130	4	0.5	2.3	2	1.95	3.21	2.03
130	20	0.5	6.2	10	7.90	13.61	7.88
260	2	1	1	1	1.38	1.68	1.33
260	4	1	2.5	2	2.67	3.12	2.52
260	8	1	4.5	4	5.12	5.80	4.73
260	12	1	6.5	6	7.48	8.33	6.82
260	20	1	10	10	12.03	13.14	10.73
260	25	1	11.75	12.5	14.79	16.04	13.06
260	2	2	0.5	1	1.16	1.55	0.90
260	4	2	2	2	2.18	2.96	1.59
260	22	2	6.5	11	9.96	13.15	5.84
260	31	2	9.5	15.5	13.42	16.32	7.39

[1]DC Arc Test

[2]Theoretical Method

[3]Ammerman’s Model

[4]600-V DC Arc Model

[5]New DC Arc Model

4.2.3 Incident Energy Estimation

According to the 3D DC arc simulation results, the heat energy released during electric arc discharge is similar to a spherical radiant source with uniform heat transmission in all directions. Figure 4-10 uses different temperature iso-surfaces to represent the heat energy transmission. Hence, it is reasonable to use Wilkins' work [72] to determine the DC incident energy density, which is also applied in Ammerman's DC arc model. Therefore, the incident energy of DC arc can be determined by doing an iterative process in (4-5) to (4-7) calculate the arcing voltage, arcing resistance, and arcing power, and then estimate the incident energy through (4-8 to 4-10), where *t* is the arcing duration time in seconds, *d* is the distance from the arc in millimeters, E_s and E_1 represent the incident energy in open-air and enclosures, respectively. Three typical equipment described in IEEE 1584 are provided in Table 4-6 including the optimum values of *a* and *k* [17].

Table 4-6 IEEE Std. 1584 Optimum Values of *a* and *k*

Enclosure	*Width (mm)*	*Height (mm)*	*Depth (mm)*	*a*	*k*
Panelboard	305	356	191	100	0.127
LV Switchgear	508	508	508	400	0.312
MV Switchgear	1143	762	762	950	0.416

$$W_{arc} = P_{arc} \bullet t \tag{4-8}$$

$$E_s = \frac{W_{arc}}{4\pi d^2} \tag{4-9}$$

$$E_1 = k\frac{W_{arc}}{a^2 + d^2} \tag{4-10}$$

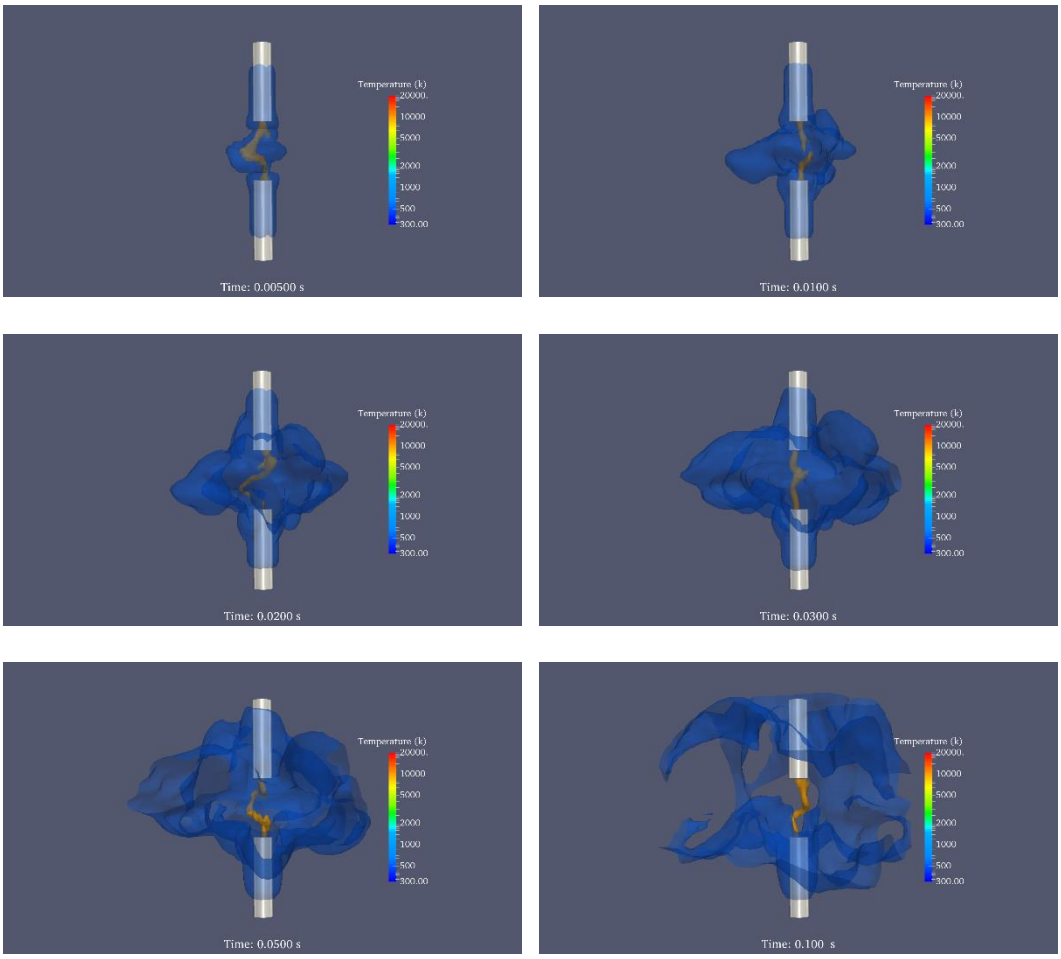

Figure 4-10 Heat Energy Transmission during DC Electric Arc Discharge

4.2.4 Two-Seconds Rule

Owing to the different characteristic of AC arcs, DC arcs do not have zero-current times and do not require re-ignition in each half cycle. Once the DC arc is generated, the arc will be sustained until the arc is cleared by the protective devices; in other words, the arcing duration will be infinity if all the protective devices fail to clear the DC arc.

According to the equation (4-7), the total arcing energy is affected by arcing duration time t proportionally. The arcing energy will be infinite when the arcing duration is

infinite. In this situation, if the incident energy of DC arc is determined by equation (4-7), the estimation result is not reasonable.

IEEE 1584-2002 Amendment 2 Section IV-F states that 2s is usually a reasonable maximum time for incident energy calculation because 2s is the length of time that a person will remain in the location of an arc flash before moving away to safety. Therefore, the maximum arcing duration time should be considered as 2s while using equation (4-7) to determine the incident energy of DC arc flash events.

4.3 Summary

Regarding DC arc flash calculations, this dissertation proposes a new DC arc model based on the DC electric arc simulation, which have been verified by the available real arc tests data. In comparison with the real DC arc tests, the new proposed DC arc model provides more accurate estimation results than historical DC arc models.

Similarly with the Ammerman's DC arc model, this dissertation uses Wilkins' work to determines the DC incident energy density. Besides, the two second rule is applied while predicting the incident energy of DC arc due to provide more reasonable estimations. The new DC arc model provides a reference to future DC arc hazard analysis and industry standard development.

Chapter 5

Conclusions and Future Work Directions

5.1 Conclusions

In order to provide more comprehensive protection for arc flash hazards in the workplace, regarding the lack of research on light intensity in AC power system and the estimations of DC arc flash, this dissertation proposed an AC arc flash light intensity model and DC arc model for arc flash hazards analysis.

Currently, the personal protective equipment (PPE) required by NFPA 70E focuses upon mitigating the thermal hazard in an arc flash event. According to the PPE requirements in NFPA 70E 2015 edition, the safety glasses or goggles are the only protection for human eyes. However, these required PPE can only provide the protection for ultraviolet spectrums during an arc flash event, which is not capable of providing the protection for the extremely high intensity visible light emitted in an arc flash event.

Thus, in order to estimate the arc flash hazard caused by the intense light, this dissertation proposes an AC arc flash light intensity estimation model based on approximate 1500 recording data from three phase real arc tests. The light intensity data is recorded by an arc flash light intensity measurement system through ambient light sensors. Three measurement devices were set at different distances from the arcing point, the typical distances are 3m, 4.5m, and 6m respectively. The laser pointers were applied into the measurement system to avoid the misalignment errors. In order to analyze the parameter sensitivity of arc flash light intensity model, the statistical approaches have been utilized in the modeling process. Additionally, the enclosure size correlation analysis is performed in this dissertation due to studying the impact of enclosure size on the light intensity emitted in an arc flash event. Finally, this dissertation proposes AC arc flash light intensity estimation models of five different configurations. An auto darkening welding lens

were applied in some tests to explore its ability to provide necessary protection for human eyes from the extremely high intensity of light emitted in an arc flash event.

Recently, the application of large scale PV and DC buses have grown substantially in industry, however, the latest study regarding DC arc flash still halted in 1900s. Considering the lack of research addressing to the DC arc flash, this dissertation utilizes the MHD approach to simulate the electric arc in DC power system through a CFD software, *Code Saturne® v. 3.0*, and proposes a new DC arc model based on 3D DC arc simulation.

From the physical point of view, the electric arc physics are introduced briefly in this dissertation, including arc discharge, arc types, arc regions and voltage distribution. Then, the magnetohydrodynamic (MHD) approach DC electric model is presented in this dissertation, which couples the Navier-Stokes equations for air with the Maxwell equations of electromagnetic fields. The detail information about MHD modeling of DC arc is given in this dissertation, such as model assumptions, numerical model, simulation flow chart, computational grid, and boundary conditions. Finally, this dissertation provides two simulation cases, similar procedures can be applied on other configurations and fault conditions.

Currently, there are limited testing addressing to DC, the recent IEEE/NFPA collaborative arc flash research project focuses on AC arc testing. It plans to start to perform DC arc testing after the revision of IEEE P1584. The proposed 3D MHD modeling provides greatly compatible results with currently available lab testing and can be double verified with future DC arc testing and improve the accuracy of DC arc model development. The modeling method proposed in this paper is not only a complement for future DC arc testing parameters setup but also beneficial for future model development, which will assist IEEE or NFPA to establish the theoretical and empirical combination DC arc model.

Similar with the AC arc flash light intensity modeling, the statistic approaches were also applied into the DC arc modeling. Compared with real arc flash tests data, the proposed new DC arc model can predict more accurate estimations than recent commonly used DC arc models.

5.2 Future Work Directions

Nowadays, the emphasis on the electrical safety in the workplace has become a great concern, thus, it is important to improve the recognition of the potential risks and hazards of an arc flash event. The research presented in this dissertation provides deeper insight into arc flash phenomena and the hazards.

This dissertation presents a light intensity model to estimate the potential intense light emitted in an arc flash event, which provides a foundation for light hazard analysis and industry standards development. The auto darkening welding lens gives a method to mitigate the light hazard during arc flash events, and other protection method may be provided by the PPE manufactories in the future.

Compared with the available DC arc test results, although the proposed new DC arc model in this dissertation is capable of providing more accurate estimations for the arcing current and arcing voltage than recent commonly used DC arc models, the new DC arc model still need to be verified by more DC arc tests, because the arc phenomena in reality is really dynamic, which is difficult to simulate comprehensively from physical point of views. Besides, the incident energy estimation in this dissertation still assumes that the heat energy released during electric arc discharge is similar to a spherical radiant source with uniform heat transmission in all directions. Therefore, more tests are needed in the future to address the verification for proposed new DC arc model and estimation of incident energy during a DC arc flash event.

References

[1] Richard B. Cambell, David A. Dini, “Occupational Injuries from Electrical Shock and Arc Flash Events,” *Fire Protection Research Foundation*, March 2015.

[2] Gavin F. Burdge, H. Landis Floyd, “ Electrical Fatalities Reported by Federal OSHA for Calendar Year 2014 with a Consideration of Design Interventions,” *Electrical Safety Workshop (ESW), 2015 IEEE IAS*, March 2016.

[3] The Liberty Mutual Research Institute for Safety from Research to Reality®, 2014 Workplace Safety Index

[4] Fordyca T. A, Kelsh M, Lu E. T., Sahl J. D., Yager J. W., “Thermal Burn and Electrical Injuries among Electric Utility Workers, 1995-2004” *Burns*, 33(2), pp. 209-220, March 2007.

[5] Floyd A. H. L., *Advances in the Practice of Electrical Safety.* IEEE Alberta section meeting, May 2013.

[6] Wyzga, R. E., Lindros W., New York Academy of Sciences, Occupational Electrical Injury an International Symposium, *Health Implications of Global Electrification*. vol. 888, pp. 1-7, November 1999.

[7] Washington State Department of Labor and Industry, *Burn Injury Facts*, April 2006.

[8] ABB, “Protection against electric arc,” *ABB*, 2011.

[9] J. C. Das, *Arc Flash Hazard Analysis and Mitigation*, Hoboken, NJ, USA, Wiley, 2012

[10] D. Leibovici, J. Shemer, SC Shapra, “Electrical Injuries: Current Concepts,” *Injury* 26:623-627, 1995.

[11] “NFPA/IEEE Research and Testing Planning Committee (RTPC),” NETAWORLD, Portage, MI, USA, Jau. 28, 2005.

[12] T. Gammon, Unpublished Analysis of OSHA Records, “electric arc” Key Term, released between Mar. 2005 and Sep. 2008.

[13] “Eye protection in the workplace,” *U.S. Department of Labor, Program highlights*, Fact Sheet No. OSHA 92-93.

[14] T.E. Neal and R.E. Parry, “Sharpnel, pressure and noise,*” IEEE Industry Applications Magazine*, vol. 11, no. 3, 49 – 54, June 2005.

[15] R.L. Doughty, T.E. Neal, T.A. Dear , and A.H. Bingham, “ Testing Update on Protective Clothing and equipment for arc exposure *,” IEEE Industry Applications Magazine* , vol. 5 , no. 1 , 37 – 49 , Jan./Feb. 1999 .

[16] *Standard for Electrical Safety in the Workplace*, National Fire Protection Association Standard 70E, 2015.

[17] *IEEE Guide for Performing Arc Flash Hazard Calculations*, IEEE Standard 1584-2002, 2002.

[18] M. Yanoff, J. S. Duker, Ophthalmology, Elsevier Health Sciences, p. 50, 2009.

[19] C. Rüth and A. Vogler, “Application Note for High accuracy Ambient Light Sensor,” OSRAM Opto Semiconductors GmbH, Regensburg, Germany, Aug. 2006.

[19] W.J. Lee, Z. Zhang, S.H. Rau, T. Gammon, B.C. Johnson, J. Beyreis, “Arc Flash Light Intensity Measurement System Design,” *IEEE Trans. Ind. Appl.*, vol. 51, No. 5, pp. 4267-4274, Sep./Oct. 2015.

[20] “Camera Lens Filters,” [Online]. Available: http://www.cambridgeincolour.com/tutorials/camera-lens-filters.htm

[21] C. S. P. D. C. R. L. S. S. Chet Davis, “Practical Solution Guide to Arc Flash Hazards,” ESA, Inc., 2003.

[22] W.D. Dupont, Statistical Modeling for Biomedical Researchers: *A Simple Introduction to the Analysis of Complex Data*, Cambridge University Press, Oct. 2009.

[23] S.M. Ross, *Introduction to Probability and Statistics for Engineers and Scientists*, Academic Press, Aug. 2014.

[24] David Smith, “Arc Flash Hazards on Photovoltaic Arrays,” Spring 2013. [Online] Available: http://projects-web.engr.colostate.edu/ece-sr-design/AY12/arc/DaveSmith_ECE402_Report_5%205%2013.pdf

[25] Kenneth H. Kingdon, “The Arc Cathode Spot and its Relation to the Diffusion of Ions within the Cathode Metal,” *Journal of Applied Physics*, vol. 36, no. 4, pp. 1351-1360, Apr. 1965.

[26] J. M. Somerville, *The Electric Arc*. London, U.K.: Wiley, 1959. [Online]. Available: https://archive.org/details/electricarc00ayrtrich

[27] William Louis Beasley, *An Investigation of the Radiated Signals Produced by Small Sparks on Power Lines*. Dissertation at Texas A and M University, Jan. 1970.

[28] Leonard B. Loeb, *Fundamental Processes of Electrical Discharge in Gases*. New York: John Wiley & Sons, 1939.

[29] F. A. Maxfield and R. R. Benedict. *Theory of Gaseous Conduction and Electronics*, New York: McGraw-Hill Book Company, 1941.

[30] "Paschen’s law," Wikipedia: The Free Encyclopedia, updated June 14, 2008. [Online]. Available: http://en.wikipedia.org/wiki/Paschen%27s_law.

[31] G. R. Jones, *High Pressure Arcs in Industrial Devices*. London: Cambridge University Press, 1988.

[32] J. D. Cobine, Gaseous Conductors. New York: Dover Publications, 1958.

[33] A. E. Guile, “Arc-Electrode Phenomena,” Proceeding of IEE, IEE Reviews, vol. 118, no. 9R, pp. 1131-1154, Sept. 1971.

[34] T. E.Browne, ed., *Circuit Interruption*. New York: Marcel Dekker, Inc., 1984.

[35] T. H. Lee, “Plasma Physics and the Interruption of an Electric Circuit,” Proceedings of the IEEE, vol. 57, no. 3, pp. 307-323, Mar. 1969.

[36] Ragnar Holm, “The Vaporization of the Cathode in the Electric Arc,” *Journal of Applied Physics,* vol. 20, pp. 715-716, July 1949.

[37] W. R. Wilson, “High-Current Arc Erosion of Electric Contact Materials,” *AIEE Transactions*, pp. 657-664, Aug. 1955.

[38] J. J. Lowke, “Simple Theory of Free-Burning Arcs,” *Journal of Physics D: Applied Physics*, vol. 12, pp. 1873-1886, 1979.

[39] I. G. Kesaev, *Cathode Processes in the Mercury Arc*. New York: Consultants Bureau, 1964.

[40] R. L. Longini, “A Note Concerning the Motion of the Arc Cathode Spots in Magnetic Fields,” *Physical Review*, pp. 642-643, Feb. 1947.

[41] H. Edels, “Properties and Theory of the Electric Arc,” *Proceedings of the Institute of Electrical Engineers*, vol. 108A, pp. 55-69, IEEE paper no. 3498, Feb. 1961.

[42] J. Schein, M. Schumann and J. Mentel, “Analysis of Arc Spot Ignition on Cold Lamp Electrodes,” *1996 Conference Record of the IEEE IAS Annual Meeting*, San Diego, California, pp. 2155-2161, Oct. 6-10, 1996.

[43] K. J. Tseng, Y. Wang, and D. M. Vilathgamuwa, “Development of a dynamic model of electric arc for power electronics simulations,” *1996 Conference Record of the IEEE IAS Annual Meeting*, San Diego, California, pp. 2173-2179, Oct. 6-10, 1996.

[44] Jackson F. Fuller, William J. Hanna and Gene A. Kallenbach, “Arcing faults in metallic conduit at 120 and 240 V,” *IEEE Trans. on Ind. Appl.*, vol. IA-21, no. 4, pp. 820-825, May/June 1985.

[45] James Dillon Cobine, Gaseous Conductors. New York: McGraw-Hill Book Company, 1941.

[46] A. D. Stokes and W. T. Oppenlander, “Electric arcs in open air,” *Journal of Physics D*, vol. 24, no. 1, pp. 26-35, Jan. 14, 1991.

[47] W. B. Nottingham, “Normal arc characteristic curves: Dependence on absolute temperature of anode,” *Phys. Rev*., vol. 28, no. 4, pp. 764-768, Oct. 1926.

[48] R. Lee, “The other electrical hazard: Electrical arc blast burns,” *IEEE Trans. Ind. Appl.*, vol. IA-18, no. 3, pp. 246-251, May/Jun. 1982.

[49] C. P. Steinmetz, “Electric power into light, Section VI. The Arc,” *Trans. Amer. Inst. Elect. Eng.*, vol. 25, p. 802, 1906.

[50] W.B. Nottingham, “A New Equation for the Static Characteristic of the Normal Electric Arc", *Trans. Amer. Inst. Elect. Eng.*, vol. 42, p. 302, 1923.

[51] P. M. Hall, K. Myers, and S. W. Vilcheck, “Arcing faults on direct current trolley systems,” in *Proc. 50th WVU Conf. Coal Mine Electrotechnol*., Morgantown, WV, pp. 1-19, 1978.

[52] C. Keyes, C. Maurice, “DC arc hazard assessment phase II,” *Kinetrics Inc. Report No*., K-012623-RA-0002-R00, 2007.

[53] L. Chemartin, P. Lalande, E. Montreuil, C. Delalondre, B.G. Cheron, F. Lago, “Three dimensional simulation of a DC free burning arc,” *Appl. Light. Phys. Atoms. Res.* 91, pp. 371-380, 2009.

[54] A. Lebouvier, C. Delalondre, F. Fresnet, V. Boch, V. Rohani, F. Cauneau, L. Fulcheri, “Three-dimensional unsteady MHD modeling of a low-current high-voltage nontransferred DC plasma torch operating with air,” *IEEE Trans. Plasma Sci.* 39, pp. 1889-1899, 2011.

[55] C. Rehmet, V. Rohani, F. Cauneau, L. Fulcheri, “ 3D Unsteady State MHD Modeling of a 3-Phase AC Hot Graphite Electrodes Plasma Torch,” *Plasma Chemistry and Plasma Processing*, vol. 33, Issue 2, pp. 491-515, Apr. 2013.

[56] A. Lebouvier, C. Delalondre, F. Fresnet, F. Cauneau, L. Fulcheri, “3D MHD modelling of low current-high voltage DC plasma torch under restrike mode,” *J. Phys. D. Appl. Phys*. 45:025204, 2012.

[57] B. Selvan, K. Ramchandran, KP. Sreekumar, TK. Thiyagarajan, PV. Ananthapadmanabhan, “Three-dimensional numerical modeling of an Ar-N2 plasma arc inside a non-transferred torch,” *Plasma Sci. Techno.* 11:679, 2009.

[58] F. Archambeau, N. Mechitoua, M. Sakiz, “Code Saturne: a finite volume code for the computation of turbulent incompressible flows industrial applications,” *Int. J. Finite*, vol. 1, pp. 1-62, 2004.

[59] H. Larsen, “AC electric arc models for a laboratory set-up and a silicon metal furnace,” NTH, Univ. of Tron., Dep. of metal. Norway, 1996.

[60] G. W. C. Kaye, D. Ewen, “The sublimation of metals at low pressure,” Proceedings of the Royal Society of London. Series A, *Containing Papers of a Mathematical and Physical Character*, vol. 89, No. 607, pp. 58-67, 1913.

[61] P. Freton, J. Gonzalez, A. Gleizes, “Comparison between a two- and a three-dimensional arc plasma configuration,” *J. Phys. D. Appl. Phys.*33, 2000.

[62] J. Park, J. Heberlein, E. Pfender, G. Candler, C. Chang, “Two-dimensional numerical modeling of direct-current electric arcs in nonequlibrium,” *Plasma Chem. Plasma Process* 28(2), pp. 213-231, 2008.

[63] D. Doan, “Arc flash calculations for exposures to dc systems,” *IEEE Trans. Ind. Appl.*, vol. 46, no. 6, pp. 2299–2302, Nov./Dec. 2010.

[64] IEEE/NFPA Arc Flash Phenomena Collaborative Research Project, KEMA-Powertest, LLC, May 12-22, 2009.

[65] T. Gammon, W. J. Lee, Z. Zhang, B. C. Johnson, “A review of commonly used DC arc models,” *IEEE Trans. Ind. Appl.*, vol. 51, no. 2, pp. 1398-1407, Mar./Apr. 2015.

[66] K. Klement, “DC arc flash studies for solar photovoltaic systems: Challenges and recommendations,” *IEEE Trans. Ind. Appl*., vol. 51, no. 5, pp. 4239-4244, Sep./Oct. 2015.

[67] R. F. Ammerman, T. Gammon, P. K. Sen, J. P. Nelson, “DC-Arc Models and Incident-Energy Calculations,” *IEEE Trans. Ind. Appl.*, vol. 46, No. 5, pp. 1810-1819, Sep./Oct. 2010.

[68] *User’s Guide for ARCPRO*, Kinetrics, Toronto, ON, Canada, 2000.

[69] K. S. Y. Cheng, S. L. Cress, and D. J. Minini, “Arc hazard assessment for DC applications in the transit industry,” in *Proc. APTA Rail Conf*., Boston, MA, USA, Jun. 12–15, 2011, pp. 1–7.

[70] V. P. Ignatko, “Electric characteristics of ac open heavy-current arcs,” *Proc. 3rd Int. Symp. Switching Arc Phenom*, pp. 98-102, 1977.

[71] T. E. Browne, Jr., “The electric arcs as a circuit element,” *J. Electrochem. Soc*., vol. 102, no. 1, pp. 27-37, Jan. 1955.

[72] R. Wilkins, “Simple improved equations for arc flash hazard analysis,” *Proc. IEEE Elect. Safety Forum,* pp. 1-12, Aug. 30, 2004.

[73] “Victim of an Arc Flash at an Electric Meter,” [Online]. Available: https://www.nachi.org/bbsystem/viewtopic.php?t=5145&PHPSESSID=68ded59e609759dc8b34a0034a55af1e.

[74] “*Code_Saturne* 3.0.0 Theory Guide,” [Online]. Available: http://code-saturne.org/cms/sites/default/files/docs/3.0/theory.pdf

[75] R. Amrollahi, M. Habibi, “Theoretical Study of Magnetic and Shock Wave Pressure Effects on the Rail Gap Switch Surface used at the Amirkabir Mather Type Plasma Focus Facility,” *IEEE 35th International Conference on Plasma Science*, June 2008.

[76] S.I. Braabinskii, "Theory of the Development of Spark Channel," *J. of Experimental and theoretical physics*, vol. 34, 1958

[77] T. G. Engel, "Expansion of Hydrogen Arcs Driven by Oscillating Currents," *IEEE Transaction on Plasma Science*, vol. 19, no. 5, 1991.

[78] D. R. Doan, R. M. Derer, “Arc Flash Calculations for a 1.3-MW Photovoltaic System,” *IEEE Trans. Ind. Appl*., vol. 51, issue 1, Jan./Feb. 2015.

[79] E. H. Enrique, P. N. Haub, T. P. Bailey, “DC Arc Flash Calculations for Solar Farms,” *1st IEEE Conference on Technologies for Sustainability (SusTech)*, pp. 97-102, 2013.

[80] W. Cantor, P. Zakielarz, M. Spina, “DC arc flash: The implications of NFPA 70E 2012 on battery maintenance,” *International Sationary Battery Conference*, 2012.

[81] Z. Zhang, “Arc flash hazard analysis,” *Proquest,* 2016.

[82] S.H. Rau, Z. Zhang, W.J. Lee, “3D Magnetohydrodynamic Modeling of DC Arc in Power System," *Industrial & Commercial Power System Conference (I&CPS),* 2016 IEEE/IAS 52th, May 2016.

[83] S.H. Rau, W.J. Lee, “DC Arc Model Based on 3D DC Arc Simulation,” *Electrical Safety Workshop (ESW)*, IEEE IAS, 2016

Biographical Information

Shiuan-Hau Rau received the B.S. and M.S. degrees from Tatung University, Taipei, Taiwan, in 2006 and 2008, respectively. He is currently working toward the Ph.D. degree in energy systems at The University of Texas at Arlington, Arlington, TX, USA. He is also currently a member of the Energy Systems Research Center, The University of Texas at Arlington. His areas of interest are arc flash analysis, electrical safety analysis, computational fluid dynamics, and magnetohydrodynamics for arc flash simulation. Also, he has been involved in renewable energy, power systems analysis, and power market researches. He has associated IEEE/NFPA Arc Flash Research Project since 2011.